A STUDY OF FILAMENT WINDING

by

Richard D. Gordon

Thesis presented for the degree of

M.Sc. to the Faculty of Engineering

The University of Glasgow

Department of Aeronautics
and Fluid Mechanics.

April, 1970

ProQuest LLC.
789 East Eisenhower Parkway
P.O. Box 1346
Ann Arbor, MI 48106 – 1346

Acknowledgements

The author wishes to express his gratitude to Professor T.R.F. Nonweiler of the Department of Aeronautics and Fluid Mechanics for providing the author with the opportunity to pursue work towards a higher degree.

The author is deeply grateful for the close interest, support and encouragement of Dr. H.Y.Wong of the above department throughout the course of this work and wishes to state how deeply he values the help and friendship received.

To the many members of the technical staff of the Engineering Faculty who have worked for the author, with especial mention of the members of the departmental workshop, the author expresses his thanks.

Finally, though he knows she does not wish to be mentioned, the author expresses his loving gratitude to his wife for her patience and for her hard work in typing the manuscript.

List of Contents

Introduction

In this work, a study has been made of the particular example of a composite material formed by the filament winding process from filamentary glass reinforcement and epoxy resin matrix.

Mankind has made use from the earliest times of composite materials where enhanced properties of some kind were required. Straw was certainly used by the Israelites in 800 B.C. to make bricks which at a compressive strength of 1000 lb/in^2 are about a quarter of the strength of modern fired bricks. The use of glass fibres is nearly as old as glass itself. In Egyptian times in a manner curiously anticipating filament winding, glass vessels were made by winding fibres onto a suitable core, heating so that the fibres melted into one another and after cooling, removing the core. The use of circumferential wrappings to increase the strength of certain structures too is not new. Wrappings of wire were used around cannon barrels in the early days of weaponry to prevent them from bursting, a use that is paralleled today by the wrapping of glass filament windings around lightweight shotgun barrels. The acceptance of composite structures for applications requiring ultimate structural performance is however recent and unique.

The impetus for the development of the filament winding process may be said to stem from the field of aerospace research. The development of new structures is always of particular importance to aerospace applications, where the requirement to minimise structural weight is always present. Filament wound pressure vessels for space applications have been shown to be highly efficient structures but

their potential as structural members for general application has not been widely appreciated. As a result of the evolution of this process, however, filament wound structures which possess very high specific strength among their other attractive features are currently being considered for wider application.

Normally, the strong reinforcement fibres are embedded in a softer matrix so that the fibres become the major load carrying element and the matrix acts as a load transmitting medium. High strength levels are possible if continuous fibres are employed, eliminating the stress concentrations that would occur at the cut ends of the fibres. The efficiency of the structure may be increased by the appropriate orientation of the fibres along the direction in which maximum strength is required. In structures where this is not possible, placing the fibres at some angle to the principal stress and varying the angle between layers permits a balanced structure to be achieved.

Technically, the complexity of multi-phase systems only became apparent with time and meanwhile, investigations were carried out which in retrospect often were seen to lack control over variables. Over a large range of properties, the short term behaviour of glass-resin composites can be accounted for in terms of the properties, relative quantities and geometry or orientation of the reinforcement. The long term properties are complicated by the creep behaviour of the resin. At the present stage of development, a large range of desirable mechanical, electrical, chemical and other properties can be obtained, however the very existence of a

large range of possible ways of combining glass fibres and resins, the available choice of glass fibre compositions and reinforcing materials and the large number of resins, makes a clear understanding of the design requirements and how to obtain them more crucial than with traditional materials.

Filament winding then, is a process for forming reinforced plastic parts of high strength and light weight and is carried out on a specially designed machine where the precise control of the winding pattern and orientation of the filaments required for maximum strength can be achieved. The design of such a machine has formed part of the present work.

Filament winding has the advantage that a fibre can be oriented to give the component both high strength and stiffness in the directions required and is of particular use for surfaces of revolution. Design analysis dictates the winding pattern employed and a review of the method of analysis of filament wound structures is made. Winding procedures exercise great importance in the final strength of the end item. Attention is paid to this as part of winding and a special study is made of the problem of winding in the vicinity of the ends of a cylindrical tube without disruption of the winding pattern.

As the filament wound vessel may consist of many layers of different filament orientation and is in general anisotropic and heterogeneous, the measurement of strain therefore presents a problem. Since the load carrying ability of a filamentary structure depends to a large extent on the loading conditions in

the fibres, a knowledge of the strain in the structure in the direction of the fibres would be desirable. A study has been made of the use of fine resistance wire integrally wound with the glass reinforcement during manufacture of the member for this purpose.

Internal pressure tests were performed on three hoop wound tubes using test apparatus designed for the purpose to assess experimentally the use of this resistance wire and to determine some elastic property data for this E-glass - epoxy resin filament wound composite material.

Notation

A	cross sectional area
C	contiguity factor
D	flexural rigidity
	circumferential distance defined in Appendix 2
E	Young's Modulus
G	shear modulus
I	moment of inertia
L	length
M	resultant moment
N	resultant force
Q	ratio of stress defined in Appendix 3
R	electrical resistance
S	allowable shearing strength
T	delay time
W	applied load
X	allowable longitudinal strength
Y	allowable transverse strength
c	crack length
l	length
l,m	direction cosines
n	number of layers, rotational speed
p	internal pressure
	pitch
p''	equivalent pressure
r	radius

t	thickness
v	volume fraction
w	width
$[A]$	transformed compliance matrix defined in equation (2.16)
$[A^*]$	defined in equation (2.21)
$[A^{**}]$	defined in equation (2.44)
$[B]$	flexibility matrix
$[C]$	stiffness matrix
$[H]$	strain transformation matrix
$[K]$	defined in equation (2.35)
$[L]$	stress transformation matrix
α_o	angle of wind (NB. denoted as α only for clarity in Chap.2)
γ	shear strain
δ	distance
Δ	increment
ε	strain
η	coefficient of shear distortion
μ	quantity defined in Appendix 3
μ_1, μ_2, β	non-dimensional modular ratios defined in equation (2.18)
ν	surface energy
	Poisson's ratio
ρ	density
	electrical resistivity
σ	stress
τ	shear stress
	time

ϕ_1	rotational angle defined in Appendix 2
χ	change of curvature

Subscripts

a	axial
c	circumferential
f	fibre
h	helical
i	i^{th} layer
l	longitudinal
ls	leadscrew
m	matrix
	mandrel
o,e	odd, even layers
x,y	component directions
w	wire
L,T	directional components along and transverse to fibre
I,II	components in the principal directions of a helical layer.

CHAPTER I Filament Winding

Filament winding is a fabrication technique for forming reinforced plastic parts of high strength and light weight, the construction and properties of which can be controlled to very fine limits. The structures so formed are a particular example of the new class of materials in the field of materials science broadly termed Composite Materials. A composite material may be defined as a solid which is made by physically combining two or more existing materials to produce a multiphase system with different physical properties from the constituent materials. In the case of filament windings, the composite structure is made by exploiting the remarkable strength properties exhibited by continuous fibres or filaments of reinforcement materials encased in a matrix of some other material.

This system thus is one of two continuous phases i.e. matrix and reinforcement, unlike for example the other end of the spectrum where the matrix provides a continuous phase and the reinforcement a dispersed phase, as in resins incorporating chopped strand glass mats. The high strength to weight ratio of filament wound structures is attributable largely to the reinforcement while the matrix is very important in defining the response of the composite material to applied load conditions.

Of the potential reinforcing elements of interest that can be expected to be available as fibres in at least experimental quantities in the future, the majority have values of Young's

Modulus E in the range 40-60 x 10^6 lb/in^2 although values of E greater than 100x10^6 lb/in^2 are possible. The most available and proven reinforcements, tungsten, steel, glass and carbon, are also the least efficient in specific terms with values of E/ρ of less than 100 where ρ is the density. The highest ratios are for the currently available fibres of elements such as boron, graphite and beryllium and some refractories such as alumina, silicon carbide and beryllium oxide. Although E/ρ ratios of over 1,000 are possible, the problems of reliability and consistency of properties have to be recognised. Elastic property data quoted in references are based on some specific test conditions and must be viewed with caution. Aside from tungsten and steel, the densities of most fibres fall in the range 0.067 - 0.145 lb/in^3. In general terms, the variation of strength values for wire may be 5 - 10% for any one diameter which are fairly consistent and reliable properties compared to the surface and structural defects found in many whiskers. (Ref: 1)

Glass and boron are the two strongest common fibres available in large quantities. Glass is inexpensive and low in density, stiff, chemically resistant and capable of modification in composition. Glass however does suffer from static fatigue i.e. loss of strength when stressed for long intervals of time. Boron matches glass in strength properties but is five times stiffer, only being equalled by beryllium whose tensile strength is however much less.

Steel wire has been studied and ultimate tensile strengths of 6 x 10^5 lb/in^2 with a value for Young's Modulus of 26-30 x 10^6 lb/in^2

for a 0.003" wire have been obtained. These wires are not unusually brittle nor prone to abrasive damage and so may be more easily processed for filament winding than glass for example. With careful choice of matching matrix system 70% of the U.T.S. of the fibre has been realised by the composite so formed. (Ref: 2).

In the course of this study, use only has been made of E-glass fibres as reinforcement and epoxy resin as a binder and each phase of the composite material formed by the winding process will now be considered with special reference to an E-glass - epoxy resin system.

In reality, glass resin systems must be considered to be a multiphase system since they incorporate not only the two main phases (glass and resin) but also the "interphase" consisting of the glass and resin surfaces and the keying agent (also known as the "finish" or "size") between them.

The Individual Phases (Ref: 3)

Reinforcement

Nearly all materials in the form of fibres exhibit the increased strength and the same dependence of strength on size. However there may be several different reasons for this and a clear distinction must be made between brittle and ductile materials. Ductile solids show an increase in yield strength with decreasing size, drawn wires exhibiting very high strengths and showing a marked size effect. In this case, this is associated with the degree of cold work that can be achieved and the shape of precipitate particles produced by the wire during the drawing process. Annealing markedly

reduces this strength. The yield and flow stresses are determined by the density and distribution of dislocations. As the density of the dislocations increases, their interactions become greater and the yield or flow stress rises. Yield stresses of 0.01E to 0.03E have been reported for extremely cold worked wires which had 10^{11} - 10^{13} dislocations per cm^2. (Ref: 1)

In brittle solids, however, such as glass, it is well established that the strength is governed by the distribution and severity of surface defects. The size effect in glass fibres has been demonstrated many times and is attributed to the decreasing number of surface defects as the surface area is decreased. (It is now recognised that brittle materials in bulk form can be made to sustain similar stresses to thin fibres if surface defects are carefully etched and polished away). In brittle solids, therefore, internal perfection is not necessary for high strength. Griffiths ascribed the fracture strengths of a solid to stress distributions round a flaw or crack estimated of the order of 5 μin. long under plane strain and plane stress conditions. If σ is the applied stress and 2c is the major axis of the crack, then the stress value for growth of the crack in tension was given by $\sigma = \sqrt{\frac{2\nu E}{\pi c}} \approx \sqrt{\frac{\nu E}{c}}$ where ν is the surface energy. Thus it should be possible to obtain higher strengths for glass fibres (where c is small) than for bulk glass.

The important consequence of this theory is that fracture strength depends on probability that for any given applied stress a flaw of sufficient size is already present - hence implying the very

large scatter of observed strengths of ceramics, and some polymeric materials, is an inherent property of the material and is not due to experimental variations. Attempts have been made to develop a statistical theory of strength based upon the assumption that the number of dangerous flaws is a function of specimen volume or surface area, but as this relation depends on such factors as fabrication and handling history, etc., it is unlikely any generalised theory can be made to hold for all materials.

The origin of these flaws is doubtful; but it is clear that at the glass surface the inter-atomic forces, at approximate equilibrium within the solid, tend to rearrange to reduce surface free energy to a minimum and owing to the nature of glass-making the extent to which this will take place is a time and temperature function.

To explain this it is necessary to consider what glass is. A glass may be defined as an inorganic substance in a condition which is continuous with and analogous to, the liquid state of that substance, but which, as a result of a reversible change in viscosity during cooling has attained so high a degree of viscosity as to be for all practical purposes rigid. The structure of glass is therefore comparable to that of a liquid in that it possesses short-term but no long-term order and corresponds to the structure of the liquid at some elevated temperature. This "configuration" temperature depends on the rate of cooling from the liquid state and the structure of glasses and therefore their properties cannot be defined by chemical composition alone, the thermal history has to be included.

Fibres are quenched from the liquid state to a temperature where the structure is fixed in approximately 10^{-5} seconds; making it probable therefore that the fibre structure is more homogeneous on the atomic scale than that of bulk glass. This will reduce the size of and more evenly distribute the surface flaws. Thus surface conditions are of dominant importance both for the fibre itself and for the multiphase system since they will influence the adhesion between fibres and resin matrix, and therefore, the transfer of stresses from one fibre to another. Studies have shown that fibre surfaces indeed have different composition than that of the bulk glass from which it was drawn, -- for E glass the Na, Al and Si cations being at the surface at the expense of the Ca ions. The residual bonding forces of the ions in the surface are satisfied by the adsorption of hydrogen and hyroxyl ions at the surface and adsorption of additional water molecules by hydrogen bonding further away from the surface.

The theoretical tensile strength of glass based on interatomic forces is 4×10^6 lb/in^2. Under normal ambient conditions glasses other than in fibrous form possess strengths between 5,000 and 30,000 lb/in^2 with measurements showing large scatter. Tested in liquid nitrogen at -196°C E-glass fibres have exhibited strengths approaching 10^6 lb/in^2 but under ambient conditions immediately after fibre-drawing the strength measured has been 530,000 lb/in^2 with a 1% coefficient of variation. While the strength figure appears to be independent of the diameter of the fibre and the glass drawing temperature, this initial fibre strength decreases

instantaneously if the fibre contacts any other body - the strength drops to about half with a large degree of scatter. Exposure to elevated temperatures reduces the strength and raises the density indicating structural changes taking place. It is held that glass always breaks in tension and there is no reason why this should not apply to glass fibres. Studies show that for undamaged fibres, a stress corrosion mechanism will account for the relationship between fibre tensile strength, temperature and time to failure. The apparent activation energy of the failure process of 18.8 Kcal/mole corresponds to the activation energy for Na^+ diffusion in the glass.

The behaviour of glass fibres obeys Hooke's Law and creep is negligible. For all practical purposes glass is a perfectly elastic material. The value of modulus is lower than that of bulk glass for the same composition and increasing the configuration temperature decreases Young's Modulus progressively.

Density of fibres of glass drawn from the melt at 1100° - 1300°C is 2% below that for annealed bulk glass but is approximately the same if fibres are drawn by softening and attenuation at about 700° - 800°C from glass rods. This further indicates the importance of the configuration temperature in influencing the properties.

Matrix

Since the available surface forces on glass fibres are reduced by adsorption of water, linking between resin and glass must proceed either by the displacement of the adsorbed water layer and

direct contact between the resin and glass, or alternatively, by adhesion via the layers of adsorbed water. The field of resins has been well documented and only a brief comment is required here. Basically a linear polymer is formed which contains the ethylene oxide group which because of its reactivity with water is responsible for the excellent adhesion of epoxides to the glass surfaces. They may also contain double bonds. The polymers also contain hydroxy groups, which upon reaction with the necessary chemical hardeners initiate the cross linking between the chains.

The strength of resins is a function of temperature and curing schedule. Below a certain temperature for each system (the "transformation" temperature), resins are brittle solids and, similar to glasses, the failure mechanism is flaw initiated. Above the transformation temperature, time dependant elastic and viscous deformation play significant parts, initially increasing strength as they relieve areas of high stress. At even higher temperatures, the strength decreases due to residual intermolecular forces.

Keying Agents

These agents (also known as coupling agents or finishes) are organo-metallic or organo-silicon compounds applied to the fibres to improve the strength properties. They all are characterised by possessing i) an organic group which is, at least theoretically, capable of reacting with the resin during cure and ii) an alkoxide group or chloride ions which react with OH groups in the glass surface.

Investigations have shown that keying agents are not deposited on the fibres as a film but are disposed as discrete globules attached to reactive sites on the surface, often a micron apart. This leaves areas of glass exposed for attack by the surrounding medium which could reduce the fibre strength. The actual mechanics of their effect on bond strength is not clear except that the keying agents most likely adhere to the glass surface via the hydrogen bonds of the adsorbed water.

Composite Material

The filament winding process constitutes a technique for combining these phases to make a composite material. Failure of this material depends on the ability of the matrix to limit the perturbation of the local stress field produced by the random breakage of fibres occuring well below the ultimate composite strength and on the frequency of these fibre breaks. When failure occurs finally, the resin matrix fails in shear between layers of the reinforcing fibres, followed by the fracture of individual fibres.

Filament Wound Composites

Filament wound composites have been successful in the provision of ultra high strength materials. The potential mechanical advantages offered are related to composites with i) a high elastic modulus especially for light, thin-wall structures ii) a high tensile strength. The realisation of even higher translation efficiencies of the fibre properties to the reinforced composite,

will provide even more in the future the real encouragement to apply these materials to high strength structural applications.

Development

Reliable working strength of materials at present employed in structures for their high strength properties are limited by the inherent toughness or notch sensitivity of the materials. Reduced weight (increased strength) and improved reliability (increased toughness) are opposing properties. The small improvements achievable by better fabrication are not sufficient to satisfy requirements for vessels of still lower weight, and it is here that filament wound structures are valuable in providing a solution. What is required is an improvement in the specific strength and stiffness ratios.

Material	ρ lb/in^3	E lb/in^2	UTS lb/in^2	E/ρ in.	UTS/ρ in.
Aluminium Alloy	0.097	10.0×10^6	6.00×10^4	1.03×10^8	0.62×10^6
Titanium Alloy	0.160	17.0×10^6	9.00×10^4	1.06×10^8	0.56×10^6
Steel	0.280	30.0×10^6	18.00×10^4	1.07×10^8	0.64×10^6
Nickel Alloy	0.280	31.0×10^6	16.00×10^4	1.11×10^8	0.57×10^6
E glass	0.092	10.5×10^6	32.50×10^4	1.18×10^8	3.54×10^6
HTS-E glass	0.092	10.5×10^6	35.20×10^4	1.18×10^8	3.82×10^6
Glass Composite	0.074	7.0×10^6	16.35×10^4	0.95×10^8	2.20×10^6
Boron fibres	0.091	64.0×10^6	50.00×10^4	7.00×10^8	5.50×10^6
Carbon fibres	0.051	29.0×10^6	50.00×10^4	5.70×10^8	9.90×10^6

(Refs: 2, 4, 5).

It will be seen from the table that very little difference exists between the ratios for the more common structural materials used. For any substantial improvement in material properties, it was necessary to consider completely new materials for structural components e.g. composite materials using high strength reinforcements. From the technological aspects, reinforced plastics can compete with steel and titanium on a strength to weight basis.

The combination of E glass and epoxy resin to form a high strength composite is perhaps fortuitous. E glass was developed in the 1920's as a result of a requirement for an electrical insulation tape capable of withstanding high temperatures. Independent of this, patents appeared in the 1930's for thermosetting resins which could be polymerised without heat and pressure. Combined with the glass fibres, a high-strength light weight material was produced. The filament winding process was developed to enable designers to take advantage of the high tensile strength of the reinforcement along the length of the fibre. With the advent of space research programmes where the high performance penalties exacted by even a very small increase in weight of the vehicle made the development of the most efficient strength to weight ratio structures of prime importance, the interest in the possibility of using these high strength properties of filaments in a precise manner to fabricate structures whose properties were essentially tailored to suit, grew.

Filament Winding in Pressure Vessels

The requirement initially was to design and fabricate lightweight high strength pressure vessels, and the basic design method to orient the fibres in the direction of the principal stresses and proportion the number of fibres with respect to the size of the stresses, to take advantage of the orthotropic behaviour of the reinforcement. In structures where it is geometrically impossible to orient the fibres precisely in the direction of the principal stress, they are oriented at some angle with it. The aim is to achieve a balanced structure under load, i.e. one in which the fibres oriented in any direction in the structure have equal stress applied to them under a load. In the analysis of reinforced plastics, it is necessary to assume that the two materials strain equally and thus that a good bond is obtained between glass and resin.

To meet the requirement for filament wound pressure vessels, the netting analysis was developed to enable vessels to be designed according to applied loading. In this approach, several assumptions were made. i) The glass and resin were both homogeneous and elastic.

ii) The glass was anisotropic.

iii) The resin was assumed to have no load carrying ability, acting only as an agent for evenly transmitting the stress throughout the filament wound structure.

iv) The maximum allowable strain of the resin was greater than that of the glass fibre.

The basis of this theory may be shown as follows. (Ref: 6). Consider a system of parallel fibres as shown in the figure.

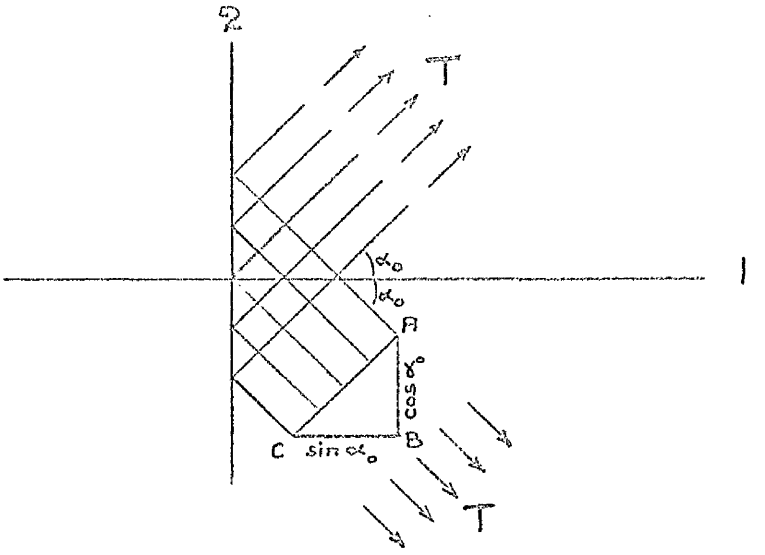

It is required to calculate the force per unit length in the 1 and 2 directions. Let $^{n}/_{2}$ be the number of fibres/unit length normal to the line AC and let T = the tension in each fibre. T may be resolved into components in the 1 and 2 directions.

$T_1 = T\cos\alpha_o$

$T_2 = T\sin\alpha_o$

The number of fibres/unit length crossing the lines AB and BC are $n\cos\alpha_o$ and $n\sin\alpha_o$. Therefore the force per unit length in the 1 and 2 directions is given by

$$N_1 = nT\cos^2\alpha_o \qquad (1.1)$$

$$N_2 = nT\sin^2\alpha_o$$

These equations were the fundamental equations from which the end dome shapes of the vessels and the winding pattern could be obtained. There were three points to note in the use of the netting analysis.

1) The forces N_1 and N_2 were not independent but are related by the winding angle $\frac{N_2}{N_1} = \tan^2 \alpha_o$ (1.2)

This required the shape and filament path in the pressure vessel to be such that this relationship between the principal membrane forces and helix angle was satisfied.

2) Since the tension in each fibre is assumed to be constant and the resin strength is neglected, the filament paths must lie on geodesic paths.

3) Net structures were statically determinate and no elastic constants were necessary to determine stresses.

In a thin-walled circular cylindrical pressure vessel, if directions 1 and 2 represent the longitudinal and hoop directions, under internal pressure loading, the hoop stress is twice the longitudinal stress. Therefore in order to obtain the theoretical maximum strength to weight ratio, $\tan^2 \alpha_o = 2$ i.e. $\alpha_o = 54.75^\circ$, and a winding pattern should be employed using this helix angle. Original vessels were made with this angle of wind employed but, as design models evolved and structural tests were conducted, it was found that in order to achieve the maximum efficiency different winding patterns had to be used. The most serious disadvantage of the netting analysis was that in many practical cases it was impossible to wind on geodesic paths at the desired angle from geometrical considerations, e.g. when the polar openings had different radii. Three methods of winding emerged in the course of developments - polar, circumferential and helical.

Polar winding is in effect a low helix angle wind determined by the end opening dimensions. The rovings are laid down continuously without the crossovers inherent in a helical pattern. The polar winding creates the basic end domes, and provides the longitudinal strength required. In conjunction with polar windings, high angle ($\doteqdot 90^{\circ}$) hoop windings are applied to provide the necessary hoop strength properties. These may also be added as local hoop reinforcement to areas where extremely high hoop strength properties are required. Helical winding at 54.75° can be applied in place of both the hoop and polar winds. The three types of winding are shown diagrammatically below.

POLAR HOOP HELICAL

The actual design pattern to be used is dependent on factors such as overall dimensions, types of end closures, materials of construction, type of winding machine and load requirements. For those applications where integral ends are required or where balanced properties in more than one direction are required helical windings are usually employed. Depending on the ratio of mandrel rotation to feed rate, the reinforcement may be laid down at angles anywhere between approximately 20 and 88 degrees. No extra longitudinal material need be laid down since the low angles of winding possible enable the reinforcement to be laid down to withstand the longitudinal loads.

Filament Winding for other than Pressure Vessels.

The use of the netting analysis for filament wound vessels is limited. With this method it is not possible to determine the elastic constants for the material and hence no accurate analysis of a filament wound structural member can be carried out. For an orthotropic material such as glass f.w. composites the elastic constants vary with the resin-glass ratio and with the orientation of the filaments with respect to a certain coordinate system and in order to determine these constants, the so-called "orthotropic" analysis has been developed.

Utilizing this method the response of the structure to various applied loading systems are predictable and it is possible to so design the laminate that the properties are such as is required by the application, even for example, to the making of an equivalent isotropic material. The parallel development of filament winding techniques with micro-mechanical design concepts has been vital to the increased use of filament wound composites.

Any shape can be filament wound if it can be wound under tension - surfaces of revolution being ideal. Even reverse curvatures can be produced by specialised techniques although not at optimum strength, and flat sheets can be obtained from flattening a large f.w. cylinder. The inner and outer surfaces of a structure need not necessarily have the same configuration, although to minimise interlaminar shearing stress effects which could lead to premature failure, wall thicknesses are normally kept substantially constant.

Since the technique of filament winding allows production of

strong light parts, it has proved of particular application in aerospace, military and hydrospace use and has a number of advantages which makes its use a distinct possibility for the manufacture of aero-engine and airframe components in the future. The application of winding techniques to the design and construction of aircraft lifting surfaces is also under investigation and such research will help to further reduce the whole field of advanced composite materials and processes to production practices.

Outside the aerospace industry, the filament winding process and design capabilities are not yet widely appreciated but the translation of the process and its application in the area of high strength structural composites to many commercial and industrial uses is not improbable. It may be necessary for research efforts to be directed to first of all providing engineering data amenable to statistical analysis resulting from practical fabrication techniques before conceptual use of filament wound composites as a class of material with different fabrication techniques and design becomes commonplace.

Filament Winding Procedures

It is realised that, in order to achieve a satisfactory strength in a filament wound structural member, the procedure of winding is just as important as the choice of the basic materials to form the composite. Essentially, the factors arising out of the winding process which will affect the strength are the maintenance of desired winding pattern, the efficient impregnation of the fibre with resin and control of the fibre volume fraction. It is important, therefore, to acquire a machine

capable of controlling satisfactorily these factors. Part of the present work is the design of such a machine, the details of which are described in Chapter 3.

CHAPTER 2 Strength of Cylindrical Filament-Wound Vessels

A unidirectional layer composed of a reinforcement and a matrix may be considered as a quasi-homogeneous anisotropic material. The reinforcement and the matrix are usually considered to be elastic, isotropic and homogeneous. One of the basic assumptions implied by the application of "distortional energy" conditions to such a quasi-homogeneous anisotropic composite subject to combined stresses, is that there exists within the anisotropy body three mutually perpendicular planes of material symmetry. This implies that the body is really orthotropic rather than generally anisotropic from the point of view of strength.

Where several layers are bonded together, the laminated composite becomes in general anisotropic and heterogeneous. The strength of a composite structure will therefore depend on the strength, thickness and reinforcement orientation of each constituent layer, the strength of which in turn will depend on the properties and distribution of the reinforcement and matrix. The material properties will vary across the thickness of the composite so formed and the stress distribution across the composite will vary according to the relative stiffnesses of each layer. As a result of this, there will be two sets of equivalent elastic constants for the material - one associated with the strain of the middle surface and one set associated with bending analysis - to be considered in the analysis of the response of the composite material to applied stresses.

A filament wound shell is usually binary and composed of n layers

within which homogeneity is assumed. The shape of structure wound in the course of this study has been a circular cylindrical vessel fabricated from E-glass fibres impregnated with an epoxy resin and the detailing of the method of determination of the elastic constants of a composite is now given with this structural configuration and material in mind. Regardless of the winding pattern employed, each layer, whether longitudinally, circumferentially or helically wound, may be considered to be orthotropic. It will be shown that in the case of helical winding, the two interlocking half layers laid on at equal angles + α and - α to the longitudinal axis parallel with the axis of revolution of the surface, are "mirror images" of each other and can be considered to form a "balanced" single orthotropic layer.

When a material is orthotropic, a shear stress applied parallel and perpendicular to the principal axes gives rise to no direct strains in those directions and a normal stress applied along the principal directions produces no shear strains. Thus knowing the properties along the principal axes which constitutes the basic property of a composite shell in its response to external loads, the properties along any other directions may be found.

With known properties of the two consituents of the composite, it is possible to determine the elastic constants of a uni-directional laminate in its principal directions which lie along and transverse to the fibre. Where the fibres are oriented at some angle 'α' to the longitudinal axis, the elastic constants of the layer with reference to a pair of mutually perpendicular axes, one of which coincides with the longitudinal axis may be determined by transformation of the

properties. Where the filaments are laid at angles of + α and - α as occurs in helical winding, the elastic constants of the resulting balanced layer with orthotropic characteristics, whose principal axes in this case coincide with the axial and circumferential directions of the cylinder may be determined in terms of the properties of a single layer with oriented fibres. Finally where the wall thickness of the structure is made up of a number of such orthotropic layers, the overall equivalent elastic constants of the shell may be determined in terms of the constants for each of its constituent layers and their respective thicknesses.

The disadvantage of this so-called "orthotropic" analysis method is its complexity but since, unlike the netting analysis, the effect of the matrix is included, its role in the response of glass fibre filament wound composites to various loading conditions can be determined, and their use for many structural applications where bending, torsion or buckling loads, for example, may be present can be considered on merit.

The resultant forces (N) and the resultant moments (M) per unit length for a thin walled shell of n layers is given by

$$N = \sum_{i=1}^{n} \int \sigma_i \, dz$$

$$M = \sum_{i=1}^{n} \int \sigma_i \, z \, dz \qquad (2.1)$$

It can be shown therefore (Ref: 7) that the structural response to applied external loads is described by the stiffness coefficients according to the governing equations of the generalised Hooke's Law.

$$[\sigma] = [C][\varepsilon] \qquad (2.2)$$

Where $[C]$ is the stiffness matrix which in general contains 36 constants. Applying classical thin shell theory and taking into account the plane of elastic symmetry, the number of constants may be reduced to 6 and equation (2.1) for homogeneous layers may be expressed as

$$\begin{aligned}
[N] &= \sum_{i=1}^{n} (\delta_i - \delta_{i-1})[C]_i[\varepsilon^o]_i - \sum_{i=1}^{n} \tfrac{1}{2}(\delta_i^2 - \delta_{i-1}^2)[C]_i[\chi]_i \\
[M] &= \sum_{i=1}^{n} \tfrac{1}{2}(\delta_i^2 - \delta_{i-1}^2)[C]_i[\varepsilon^o]_i - \sum_{i=1}^{n} \tfrac{1}{3}(\delta_i^3 - \delta_{i-1}^3)[C]_i[\chi]_i
\end{aligned} \qquad (2.3)$$

where δ_i is the distance measured from the coordinate surface to the upper face of the i^{th} layer, and $[\varepsilon]_i = [\varepsilon^o]_i - z[\chi]_i$ where $[\varepsilon^o]_i$ is the strain at the middle surface and $[\chi]_i$ is the change of curvature of the i^{th} layer.

Equation (2.3) represents the elasticity relationships which, used together with the fundamental equilibrium equations or with the energy equations with the appropriate boundary conditions make possible the solution of the response of the shell.

Use of Membrane Theory

In many cases, the deformations in thin shell problems are such that the stresses due to the resultant moments (M) are very small. These conditions, usually applied to isotropic shells, may also be applied to thin anisotropic laminated shells if the layers can be assumed to be symmetrically laid about the middle surfaces. Since walls are usually made of many layers of alternating pattern, this

assumption can provide reasonably good results regardless of whether there are odd or even layers. Thus the analysis of the cylinder is simplified to the solution of the equation

$$[N] = \sum_{i=1}^{n} (\delta_i - \delta_{i-1}) [C]_i [\varepsilon]_i \qquad (2.4)$$

where the total strains $[\varepsilon]_i$ is taken as the strains in the middle surface in place of $[\varepsilon^o]_i$, i.e. it is assumed in effect that the stress is uniformly distributed over the wall thickness

i.e. $N = t\sigma$ (2.5) where t = total wall thickness.

Equation (2.4) becomes

$$t[\sigma] = \sum_{i=1}^{n} t_i [\sigma]_i \qquad (2.6)$$

where t_i is the thickness of the i^{th} layer and $[\sigma]_i = [C]_i [\varepsilon]_i$

Determination of the Elastic Constants

A Unidirectional Layer

It is assumed that this consists of an array of unidirectional fibres uniformly distributed in the binding matrix. The fibres are assumed to be circular in cross section, continuous and both fibres and matrix are assumed isotropic and to have known elastic properties.

Since the layer has orthotropic properties, Hookes Law can be expressed with 'L' denoting the direction along and 'T' the direction transverse to the fibre axes, as

$$\varepsilon_L = \frac{\sigma_L}{E_L} - \frac{\nu_{LT}\sigma_T}{E_T}$$

$$\varepsilon_T = -\frac{\nu_{TL}\sigma_L}{E_L} + \frac{\sigma_T}{E_T} \qquad (2.7)$$

$$\gamma_{LT} = \frac{\tau'_{LT}}{G_{LT}}$$

or in matrix form as $\left[\varepsilon\right]_\alpha = \left[B\right]\left[\sigma\right]_\alpha$ where $\left[B\right]$ is the flexibility matrix and the subscript α is used to indicate the stress and strain in the principal directions of the unidirectional layer which will be assumed presently to be laid at some angle α to the axial direction of the cylinder.

The Longitudinal Modulus E_L has been demonstrated by several experimenters to follow closely the 'law of mixtures'.

$$E_L = v_f E_f + (1 - v_f) E_m \qquad (2.8)$$

where E_f and E_m are the Young's Modulus for the fibre and matrix respectively and v_f is the fibre volume fraction. (It has been assumed here, as is customary, that the misalignment factor introduced by Tsai (Ref: 8) is equal to unity.)

The Transverse Modulus E_T The results of several studies are given in Ref: 7. Good agreement between the expression used here (Ref: 8) and experimental values is reported by Card (Ref: 9) and Tsai (Ref:8) when the value of the contiguity factor "C" is assumed to be 0.2.

$$E_T = 2\left[1 - \nu_m - (\nu_f - \nu_m)\, v_f\right]\left[(1-C)\,\frac{K_f(2K_m + G_m) - G_m(K_f - K_m)(1-v_f)}{(2K_m + G_m) + 2(K_f - K_m)(1-v_f)}\right.$$

$$\left. + C\,\frac{K_f(2K_m + G_f) + G_f(K_m - K_f)(1 - v_f)}{(2K_m + G_f) + 2(K_f - K_m)(1 - v_f)}\right] \qquad (2.9)$$

where $G_f = \frac{E_f}{2(1+\nu_f)}$: $G_m = \frac{E_m}{2(1+\nu_m)}$: $K_f = \frac{E_f}{2(1-\nu_f)}$: $K_m = \frac{E_m}{2(1-\nu_m)}$

and the value of the contiguity factor C varies between 0 for isolated fibres and 1 for contiguous fibres.

Poisson's Ratios The major Poisson's ratio ν_{TL} characterising the elongation in the transverse direction due to normal stress in the longitudinal direction has been found to follow the law of mixtures for the range of material properties and volume fractions used in glass filament wound structures to give results that deviate at most $\pm$ 5% from values calculated using the much more complex relationship derived in (Ref: 8) i.e.

$$\nu_{TL} = v_f \nu_f + (1 - v_f) \nu_m \qquad (2.10)$$

where ν_f and ν_m are the Poisson's ratios for the fibre and matrix respectively.

The minor Poisson's ratio ν_{LT} can be obtained from the reciprocal relation

$$\nu_{LT} = \nu_{TL} \frac{E_T}{E_L} \qquad (2.11)$$

The Shear Modulus G_{LT} may be calculated using the form derived by Hashin and Rosen (Ref: 10) incorporating Tsai's Contiguity Factor C

$$G_{LT} = (1 - C) \frac{\left[(G_f + G_m) + (G_f - G_m) v_f\right]}{\left[(G_f + G_m) - (G_f - G_m) v_f\right]} \cdot G_m + C \frac{\left[2G_m + (G_f - G_m) v_f\right]}{\left[2G_f - (G_f - G_m) v_f\right]} \cdot G_f \qquad (2.12)$$

The Elastic Constants for an Unidirectional Laminate Oriented at an Angle α

If the reference coordinate axes of the externally applied stresses is other than along and transverse to the fibre direction,

the elastic constants will be a function of the elastic constants in the principal directions and the fibre orientation angle α, where for example in the cylinder, α is the angle between the longitudinal direction of the fibres and the direction parallel to the cylinder axis as shown in the diagram.

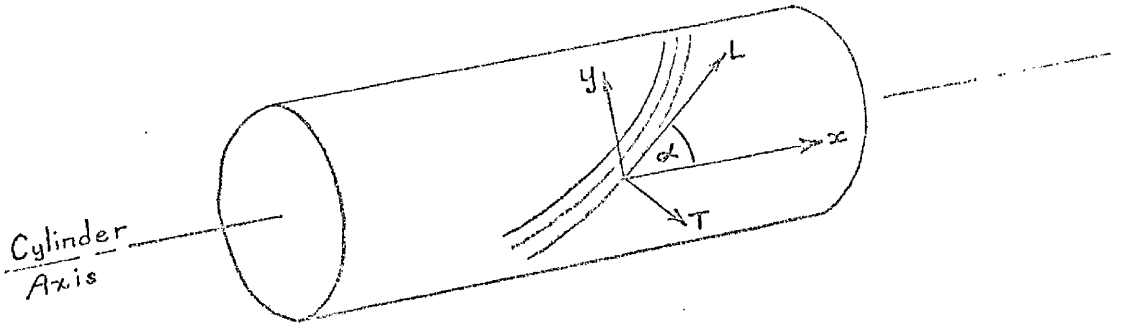

Hooke's Law in this case may be expressed as:-

$$\varepsilon_x = \frac{\sigma_x}{E_x} - \frac{\nu_{xy}}{E_y}\sigma_y - \frac{\eta_{x.xy}}{G_{xy}}\tau_{xy} \qquad (a)$$

$$\varepsilon_y = -\frac{\nu_{yx}}{E_x}\sigma_x + \frac{\sigma_y}{E_y} - \frac{\eta_{y.xy}}{G_{xy}}\tau_{xy} \qquad (b) \qquad (2.13)$$

$$\gamma_{xy} = -\frac{\eta_{xy.x}}{E_x}\sigma_x - \frac{\eta_{xy.y}}{E_y}\sigma_y + \frac{\tau_{xy}}{G_{xy}} \qquad (c)$$

where in this case, since the layer is no longer orthotropic, there is a term involving the coefficient of shear distortion η where $\eta_{x.xy}$ characterises the strain in the x-direction due to a shear stress in the x-y plane and likewise $\eta_{xy.x}$ characterises the shear strain in the x-y plane due to a normal stress in the x-direction, and as before ν_{xy} denotes the Poissons ratio for a strain in the x-direction due to a normal stress in the y-direction.

The transformation of the stresses and strains between the principal directions L and T and the x - y directions are given by

$$\begin{bmatrix}\sigma\end{bmatrix}_\alpha = \begin{bmatrix}L\end{bmatrix}_\alpha \begin{bmatrix}\sigma\end{bmatrix}$$
$$\begin{bmatrix}\varepsilon\end{bmatrix}_\alpha = \begin{bmatrix}H\end{bmatrix}_\alpha \begin{bmatrix}\varepsilon\end{bmatrix} \qquad (2.14)$$

Where the stress transformation matrix $\begin{bmatrix}L\end{bmatrix}_\alpha = \begin{bmatrix} l^2 & m^2 & 2ml \\ m^2 & l^2 & -2ml \\ -ml & lm & l^2-m^2 \end{bmatrix}$ (2.15)

and the strain transformation matrix $\begin{bmatrix}H\end{bmatrix}_\alpha = \begin{bmatrix} l^2 & m^2 & ml \\ m^2 & l^2 & -ml \\ -2ml & 2ml & l^2-m^2 \end{bmatrix}$

where $l = \cos\alpha$ and $m = \sin\alpha$, and α is measured positive as shown in the figure above.

Hence, combining equations (2.7) and (2.14) enables the strains to be expressed in terms of the stresses in the x and y directions, i.e.

$$\begin{bmatrix}\varepsilon\end{bmatrix} = \begin{bmatrix}H\end{bmatrix}_\alpha^{-1}\begin{bmatrix}B\end{bmatrix}\begin{bmatrix}L\end{bmatrix}_\alpha\begin{bmatrix}\sigma\end{bmatrix}$$

and since $\begin{bmatrix}H\end{bmatrix}_\alpha^{-1} = \begin{bmatrix}L\end{bmatrix}_\alpha'$

$$\begin{bmatrix}\varepsilon\end{bmatrix} = \begin{bmatrix}L\end{bmatrix}_\alpha'\begin{bmatrix}B\end{bmatrix}\begin{bmatrix}L\end{bmatrix}_\alpha\begin{bmatrix}\sigma\end{bmatrix}$$

i.e. $$\begin{bmatrix}\varepsilon\end{bmatrix} = \begin{bmatrix}A\end{bmatrix}_\alpha\begin{bmatrix}\sigma\end{bmatrix} \qquad (2.16)$$

From this, the elastic properties in the x, y directions can be expressed, after some computation, in terms of those in the L, T directions.

Hence, expanding the matrices

$$\begin{bmatrix}\varepsilon_x \\ \varepsilon_y \\ \gamma_{xy}\end{bmatrix} = \begin{bmatrix}A_{11} & A_{12} & A_{16} \\ A_{21} & A_{22} & A_{26} \\ A_{61} & A_{62} & A_{66}\end{bmatrix}\begin{bmatrix}\sigma_x \\ \sigma_y \\ \tau_{xy}\end{bmatrix} \qquad (2.17)$$

and, using engineering terms, the matrix $\begin{bmatrix}A\end{bmatrix}_\alpha$ has terms

$$A_{11} = \frac{1}{E_x} = \frac{1}{E_L}\left[l^4 + (\frac{1}{\mu_1} - 2\nu_{TL})l^2m^2 + \frac{m^4}{\beta} \right]$$

$$A_{22} = \frac{1}{E_y} = \frac{1}{E_L}\left[m^4 + (\frac{1}{\mu_1} - 2\nu_{TL})l^2m^2 + \frac{l^4}{\beta} \right]$$

$$A_{66} = \frac{1}{G_{xy}} = \frac{1}{G_{LT}}\left[1 + (\mu_1 + \mu_2 + 2\mu_1\nu_{TL} - 1)4l^2m^2\right]$$

$$\left.\begin{aligned} A_{12} &= -\frac{\nu_{xy}}{E_y} \\ A_{21} &= -\frac{\nu_{yx}}{Ex} \end{aligned}\right\} = \frac{1}{E_L}\left[(1 + \frac{1}{\beta} + 2\nu_{TL} - \frac{1}{\mu_1})l^2m^2 - \nu_{TL} \right]$$

$$\left.\begin{aligned} A_{16} &= -\frac{\eta_{x.xy}}{G_{xy}} \\ A_{61} &= -\frac{\eta_{xy.x}}{E_x} \end{aligned}\right\} = \frac{lm}{E_L}\left[2(\frac{m^2}{\beta} - l^2) + (\frac{1}{\mu_1} - 2\nu_{TL})(l^2 - m^2) \right]$$

$$\left.\begin{aligned} A_{26} &= -\frac{\eta_{y.xy}}{G_{xy}} \\ A_{62} &= -\frac{\eta_{xy.y}}{E_y} \end{aligned}\right\} = \frac{lm}{E_L}\left[2(\frac{l^2}{\beta} - m^2) - (\frac{1}{\mu_1} - 2\nu_{TL})(l^2 - m^2) \right]$$

(2.18)

where $\mu_1 = \frac{G_{LT}}{E_L}$; $\mu_2 = \frac{G_{LT}}{E_T}$; $\beta = \frac{E_T}{E_L}$ and $\eta_{x.xy}$; $\eta_{xy.x}$; $\eta_{y.xy}$; $\eta_{xy.y}$ are the coefficients of mutual influence and shear distortion respectively.

A is known as the transformed compliance matrix and the elastic constants comprising its terms are sometimes known as the 'free' elastic constants of the layer to differentiate from those obtained when two layers are laid at + α and - α to give an equivalent orthotropic layer, as occurs when a helically wound layer is wrapped around a cylinder.

The 'Restrained' Elastic Constants for a Balanced Layer of Equivalent Orthotropic Construction

If two unidirectional layers are bonded together at alternate angles α_o and α_e where subscripts 'o' and 'e' refer to odd and even layers respectively, equation (2.3) gives

$$t_o[\sigma]_o + t_e[\sigma]_e = t[\sigma] \qquad (2.19)$$

and the requirements of consistent deformations demands that

$$[\varepsilon]_o = [\varepsilon]_e = [\varepsilon] \qquad (2.20)$$

Applying equation 2.16 to find the stress components of the odd and even layers in the x and y directions, from equation (2.19) and (2.20) we obtain

$$\begin{aligned} [\sigma]_o &= [A^*]^{-1}[A]_{\alpha e}[\sigma] \\ [\sigma]_e &= [A^*]^{-1}[A]_{\alpha o}[\sigma] \end{aligned} \qquad (2.21)$$

where $[A^*] = \frac{1}{t}\{[A]_{\alpha o}t_e + [A]_{\alpha e}t_o\}$

and $[A]_{\alpha o}$ and $[A]_{\alpha e}$ are of the form given by equation (2.16). Now let us apply equation (2.21), which need not be restricted to unidirectional layers but applies to orthotropic layers in general, to the case of a helically wound layer.

The process of continuous helical winding causes filaments to cross each other to form two interlocking half layers oriented at + α and - α to the x - axis. In this form, the layers are no longer free to undergo shear deformation under normal stresses as the tendency of one half-layer to undergo a shear strain of $\gamma_{I\!I}$ is counteracted by the equal and opposite tendency of the other half-layer to undergo $-\gamma_{I\!I}$. Thus there results a zero shear strain and the two half layers combine to form an equivalent orthotropic layer whose principal

directions I and II coincide with the longitudinal and circumferential directions of the shell respectively, i.e. with directions x and y.

Hooke's Law can then be written as

$$\varepsilon_{I} = \frac{\sigma_{I}}{E_{I}} - \frac{\nu_{III}}{E_{II}}\sigma_{II}$$

$$\varepsilon_{II} = -\frac{\nu_{II1}}{E_{1}}\sigma_{1} + \frac{\sigma_{II}}{E_{II}} \qquad (2.22)$$

$$\gamma_{1II} = \frac{\tau_{1II}}{G_{1II}}$$

or in the form of equation (2.7) $\left[\varepsilon\right] = \left[B\right]\left[\sigma\right]$

The strain in the two half layers is given by equation (2.16) as

$$\left[\varepsilon\right]_{+\alpha} = \left[A\right]_{+\alpha}\left[\sigma\right]_{+\alpha}$$

$$\left[\varepsilon\right]_{-\alpha} = \left[A\right]_{-\alpha}\left[\sigma\right]_{-\alpha} \qquad (2.23)$$

Note that $\left[A\right]_{+\alpha}$ and $\left[A\right]_{-\alpha}$ have similar terms except that $A_{16}{}_{-\alpha} = -A_{16}{}_{\alpha}$ and $A_{26}{}_{-\alpha} = -A_{26}{}_{\alpha}$ and the terms of A are as given in equation (2.18) in terms of engineering constants and direction cosines.

Utilizing the equilibrium and strain compatibility equation for the two half layers of the same thickness we have

$$\left[\sigma\right]_{\alpha} + \left[\sigma\right]_{-\alpha} = 2\left[\sigma\right] \qquad (2.24)$$

$$\left[\varepsilon\right]_{\alpha} = \left[\varepsilon\right]_{-\alpha} = \left[\varepsilon\right] \qquad (2.25)$$

and by substitution in equations (2.22) and (2.23) we obtain the relation $2\left[B\right]^{-1} = \left[A\right]_{\alpha}^{-1} + \left[A\right]_{-\alpha}^{-1}$ (2.26)

and this is the transformation equation defining the elastic constants along the principal axes I and II in terms of the longitudinal and transverse coefficients of the fibres, as given in equation (2.18) Note here that shear forces will act on each half layer but that the

resultant shear force acting on the laminate is zero. The magnitude of this shear force can be determined from equation (2.13c) by setting $\gamma_{xy} = 0$. Hence

$$\tau_{xy} = G_{xy} \cdot \frac{\eta_{xy.x}}{E_x} \cdot \sigma_x + G_{xy} \cdot \frac{\eta_{xy.y}}{E_y} \cdot \sigma_y \qquad (2.27)$$

substituting this in (2.13a) and (2.13b)

$$\begin{aligned}
\varepsilon_x &= \sigma_x \left[\frac{1}{E_x} - \frac{\eta_{xy.x}}{E_x} \cdot \frac{\eta_{x.xy}}{G_{xy}} \cdot G_{xy} \right] - \sigma_y \left[\frac{\nu_{xy}}{E_y} + \frac{\eta_{xy.y}}{E_y} \cdot \frac{\eta_{x.xy}}{G_{xy}} \cdot G_{xy} \right] \\
&= \sigma_x \left[\frac{1 - \eta_{xy.x}\eta_{x.xy}}{E_x} \right] - \sigma_y \left[\frac{\nu_{xy} + \eta_{xy.y}\eta_{x.xy}}{E_y} \right] \\
\varepsilon_y &= -\sigma_x \left[\frac{\nu_{yx}}{E_x} + \frac{\eta_{y.xy}}{G_{xy}} \cdot \frac{\eta_{xy.x}}{E_x} \cdot G_{xy} \right] + \sigma_y \left[\frac{1}{E_y} - \frac{\eta_{xy.y}}{E_y} \cdot \frac{\eta_{y.xy}}{G_{xy}} \cdot G_{xy} \right] \\
&= -\sigma_x \left[\frac{\nu_{yx} + \eta_{xy.x}\eta_{y.xy}}{E_x} \right] + \sigma_y \left[\frac{1 - \eta_{xy.y}\eta_{y.xy}}{E_y} \right]
\end{aligned} \qquad (2.28)$$

These are of form $\varepsilon_a = \frac{\sigma_a}{E_a} - \frac{\nu_{ab}\sigma_b}{E_b}$

Hence, the terms in brackets represent the equivalent elastic constants of the helical layer. From equations (2.28)

$$\frac{1}{E_1} = \frac{1 - \eta_{xy.x}\eta_{x.xy}}{E_x} = A_{11} - \frac{A_{16}^2}{A_{66}} = B_{11}$$

$$\frac{1}{E_{II}} = \frac{1 - \eta_{xy.y}\eta_{y.xy}}{E_y} = A_{22} - \frac{A_{26}^2}{A_{66}} = B_{22}$$

$$\begin{aligned}
\frac{\nu_{1II}}{E_{II}} &= \frac{\nu_{xy} + \eta_{xy.y}\eta_{x.xy}}{E_y} = -A_{12} + \frac{A_{62}A_{16}}{A_{66}} = B_{12} \\
\frac{\nu_{II1}}{E_1} &= \frac{\nu_{yx} + \eta_{xy.x}\eta_{y.xy}}{E_x} = -A_{21} + \frac{A_{61}A_{26}}{A_{66}} = B_{21}
\end{aligned} \qquad (2.29)$$

Hence $\nu_{1II} = \dfrac{A_{16}A_{62} - A_{12}A_{66}}{A_{22}A_{66} - A_{26}^2}$

$$\nu_{II1} = \frac{A_{61}A_{26} - A_{21}A_{66}}{A_{11}A_{66} - A_{16}^2}$$

(Note $\frac{\nu_{12}}{E_2} = \frac{\nu_{21}}{E_1}$)

Similarly, by setting the strain ε_x and $\varepsilon_y = 0$ in equations (2.13a) and (2.13b) the expression for the shear modulus of the balanced layer may be obtained, i.e.

$$\frac{\sigma_x}{E_x} = \left(\frac{\nu_{xy}}{E_y}\sigma_y + \frac{\eta_{x.xy}}{G_{xy}}\tau_{xy}\right)$$

$$\therefore \quad \frac{\sigma_y}{E_y} = \left(\nu_{yx}.\frac{\nu_{xy}}{E_y}\sigma_y + \nu_{yx}.\frac{\eta_{x.xy}}{G_{xy}}\tau_{xy}\right) + \frac{\eta_{y.xy}}{G_{xy}}\tau_{xy}$$

$$\text{i.e.} \quad \frac{\sigma_y}{E_y}\left(1 - \nu_{yx}\nu_{xy}\right) = \frac{\tau_{xy}}{G_{xy}}\left(\eta_{y.xy} + \nu_{yx}\eta_{x.xy}\right)$$

$$\text{i.e.} \quad \frac{\sigma_y}{E_y} = \frac{\tau_{xy}}{G_{xy}}\left(\frac{\eta_{y.xy} + \nu_{yx}\eta_{x.xy}}{1 - \nu_{yx}\nu_{xy}}\right)$$

$$\text{Similarly,} \quad \frac{\sigma_x}{E_x} = \frac{\tau_{xy}}{G_{xy}}\left(\frac{\nu_{xy}\eta_{y.xy} + \eta_{x.xy}}{1 - \nu_{yx}\nu_{xy}}\right)$$

Therefore substituting in equation (2.13c) we obtain

$$\gamma_{xy} = -\eta_{xy.x}\left(\frac{\nu_{xy}\eta_{y.xy} + \eta_{x.xy}}{1 - \nu_{yx}\nu_{xy}}\frac{\tau_{xy}}{G_{xy}}\right) - \eta_{xy.y}\left(\frac{\eta_{y.xy} + \nu_{yx}\eta_{x.xy}}{1 - \nu_{yx}\nu_{xy}}\right)\frac{\tau_{xy}}{G_{xy}} + \frac{\tau_{xy}}{G_{xy}} \qquad (2.30)$$

This is of the form $\gamma_{ab} = \frac{1}{G_{ab}}\tau_{ab}$, therefore the equivalent shearing modulus of the helical layer is represented by

$$\frac{1}{G_{12}} = \frac{1}{G_{xy}} - \frac{\eta_{xy.x}}{G_{xy}}\left(\frac{\eta_{x.xy} + \nu_{xy}\eta_{y.xy}}{1 - \nu_{yx}\nu_{xy}}\right) - \frac{\eta_{xy.y}}{G_{xy}}\left(\frac{\eta_{y.xy} + \nu_{yx}\eta_{x.xy}}{1 - \nu_{yx}\nu_{xy}}\right)$$

or, alternatively, (since $\frac{\eta_{x.xy}}{G_{xy}} = \frac{\eta_{xy.x}}{E_x}$ and $\frac{\eta_{y.xy}}{G_{xy}} = \frac{\eta_{xy.y}}{E_y}$)

$$\frac{1}{G_{12}} = \frac{1}{G_{xy}} - \frac{\eta^2_{xy.x}}{E_x\eta_{x.xy}}\left(\frac{\eta_{x.xy} + \nu_{xy}\eta_{y.xy}}{1 - \nu_{xy}\nu_{yx}}\right) - \frac{\eta^2_{xy.y}}{E_y\eta_{y.xy}}\left(\frac{\eta_{y.xy} + \nu_{yx}\eta_{x.xy}}{1 - \nu_{xy}\nu_{yx}}\right)$$

$$= \frac{|A|}{A_{11}A_{22} - A_{12}A_{21}} = B_{66} \qquad (2.31)$$

It is interesting to note that the elastic constants for a balanced construction such as a helically wound layer are identical to the elastic constants for a single oriented unidirectional layer if $\eta_{xy,x} = \eta_{x,xy} = \eta_{xy,y} = \eta_{y,xy} = 0$. This condition occurs if $\alpha = 0^{\circ}$ or $\alpha = 90^{\circ}$ i.e. for a purely orthotropic construction. A comparison of the elastic constants for the helical layer with those for a single oriented layer shows not surprisingly that the moduli, especially the shear moduli are significantly higher. It follows that for the same thickness, a helically wound layer is much stiffer than a unidirectional laminate.

The Equivalent Elastic Constants of a Multi-Layer Cylindrical Wall

Filament wound shells consist of a number of layers each of which is orthotropic with their elastic principal axes coinciding with the longitudinal and circumferential directions of the cylinder. By approaching the problem in a manner similar to that used for the balanced, helically wound layer, the overall elastic constants for the shell along these directions can be readily determined. The equivalent elastic constants of the shell are a

function of the elastic constants of each orthotropic and equivalent orthotropic (e.g. helically wound) layer together with their thickness.

1 The elastic constants associated with stretching of the middle surface.

The elastic constants associated with stretching of the shell are obtained as for the previous analysis by considering the equilibrium and strain compatibility of the shell. For 'n' layers, the equilibrium and strain compatibility of the shell are expressed by the equations

$$\sum_{i=1}^{n} [\sigma]_i t_i = [\sigma] t \qquad (2.32)$$

$$\text{and } [\varepsilon]_i = [\varepsilon] \text{ for } i = 1, \ldots\ldots n \qquad (2.33)$$

which are of the form of equations (2.24) and (2.25). Since the shell and all the layers are orthotropic, the relation between the stresses and strains is of the form

$$\varepsilon_x = \frac{\sigma_x}{E_x} - \frac{\nu_{xy}\sigma_y}{E_y}$$

$$\varepsilon_y = -\frac{\nu_{yx}\sigma_x}{E_x} + \frac{\sigma_y}{E_y} \qquad \text{i.e. } [\varepsilon] = [B][\sigma]$$

$$\gamma_{xy} = \frac{\tau_{xy}}{G_{xy}}$$

with subscripts i for the i^{th} layer

$$\text{where} \quad [B] = \begin{bmatrix} \frac{1}{E_x} & -\frac{\nu_{xy}}{E_y} & 0 \\ -\frac{\nu_{yx}}{E_x} & \frac{1}{E_y} & 0 \\ 0 & 0 & \frac{1}{G_{xy}} \end{bmatrix}$$

Hence equation (2.26) becomes

$$t \, [B]^{-1} = \sum_{i=1}^{n} t_i \, [B]_i^{-1} \qquad (2.34)$$

$[B]^{-1}$, the inverse flexibility matrix, can be shown to be the stiffness matrix $[C]$, and in the determination of the elastic constants, equation (2.2) appears to be of greater application; hence, with subscript i to denote the i^{th} layer

$$t \, [C] = \sum_{i=1}^{n} t_i \, [C]_i = [K] \qquad (2.35)$$

where $[K]$ has coefficients

$$K_{11} = \sum_{i=1}^{n} t_i \, (C_{11})_i$$

$$K_{12} = \sum_{i=1}^{n} t_i \, (C_{12})_i$$

etc.

where $[C]$ takes the form

$$[C] = \frac{1}{(1-\nu_{xy}\,\nu_{yx})} \begin{bmatrix} E_x & \nu_{xy}E_x & 0 \\ \nu_{yx}E_y & E_y & 0 \\ 0 & 0 & G_{xy}(1-\nu_{xy}\nu_{yx}) \end{bmatrix}$$

(2.36)

Hence $[K]$ has terms

$$\begin{bmatrix} \frac{tE_x}{1-\nu_{xy}\nu_{yx}} & \frac{t\nu_{xy}E_x}{1-\nu_{xy}\nu_{yx}} & 0 \\ \frac{t\nu_{yx}E_y}{1-\nu_{xy}\nu_{yx}} & \frac{tE_y}{1-\nu_{xy}\nu_{yx}} & 0 \\ 0 & 0 & tG_{xy} \end{bmatrix} \qquad (2.37)$$

Hence we can determine the overall elastic constants in terms of $[K]$ from equation (2.37) as

$$E_x = \frac{1}{t}\left(\frac{K_{11}K_{22} - K_{12}K_{21}}{K_{22}}\right)$$

$$E_y = \frac{1}{t}\left(\frac{K_{11}K_{22} - K_{12}K_{21}}{K_{11}}\right) \qquad (2.38)$$

$$\nu_{xy} = \frac{K_{12}}{K_{11}} \; ; \quad \nu_{yx} = \frac{K_{21}}{K_{22}}$$

$$G_{xy} = \frac{1}{t}K_{66} \qquad \text{Note } K_{12} = K_{21}$$

Hence, for example, for a composite cylinder consisting of three layer configurations, one longitudinally wound layer, designated by subscript "l", taken to lie at $\alpha = 0^\circ$; one circumferentially wound layer, designated by subscript "c", taken to lie at $\alpha = 90^\circ$; and one helically wound layer designated by subscript "h", the equivalent composite wall elastic constants are as follows, where t_l, t_c, t_h are the thicknesses of each layer and t is the total wall thickness.

$$tE_x = \frac{E_L t_l}{1-\nu_{TL}\nu_{LT}} + \frac{E_T t_c}{1-\nu_{TL}\nu_{LT}} + \frac{E_l t_h}{1-\nu_{lH}\nu_{Hl}} - \frac{\left(\frac{\nu_{TL}E_T t_l}{1-\nu_{TL}\nu_{LT}} + \frac{\nu_{LT}E_L t_c}{1-\nu_{TL}\nu_{LT}} + \frac{\nu_{Hl}E_H t_h}{1-\nu_{Hl}\nu_{lH}}\right)^2}{\frac{E_T t_l}{1-\nu_{TL}\nu_{LT}} + \frac{E_l t_c}{1-\nu_{TL}\nu_{LT}} + \frac{E_H t_h}{1-\nu_{Hl}\nu_{lH}}}$$

$$tE_y = \frac{E_T t_1}{1-\nu_{TL}\nu_{LT}} + \frac{E_L t_c}{1-\nu_{TL}\nu_{LT}} + \frac{E_{II} t_h}{1-\nu_{1II}\nu_{II1}} - \frac{\left(\frac{\nu_{TL}E_T t_1}{1-\nu_{TL}\nu_{LT}} + \frac{\nu_{LT}E_L t_c}{1-\nu_{TL}\nu_{LT}} + \frac{\nu_{II1}E_{II} t_h}{1-\nu_{II1}\nu_{1II}}\right)^2}{\frac{E_L t_1}{1-\nu_{TL}\nu_{LT}} + \frac{E_L t_c}{1-\nu_{TL}\nu_{LT}} + \frac{E_{II} t_h}{1-\nu_{II1}\nu_{1II}}}$$

$$\nu_{yx} = \frac{\frac{\nu_{TL}E_T t_1}{1-\nu_{LT}\nu_{TL}} + \frac{\nu_{LT}E_L t_c}{1-\nu_{LT}\nu_{TL}} + \frac{\nu_{II1}E_{II} t_h}{1-\nu_{II1}\nu_{1II}}}{\frac{E_T t_1}{1-\nu_{LT}\nu_{TL}} + \frac{E_L t_c}{1-\nu_{TL}\nu_{LT}} + \frac{E_{II} t_h}{1-\nu_{II1}\nu_{1II}}}$$

$$\nu_{xy} = \frac{\frac{\nu_{LT}E_L t_1}{1-\nu_{LT}\nu_{TL}} + \frac{\nu_{TL}E_T t_c}{1-\nu_{LT}\nu_{TL}} + \frac{\nu_{1II}E_1 t_h}{1-\nu_{II1}\nu_{1II}}}{\frac{E_L t_1}{1-\nu_{TL}\nu_{LT}} + \frac{E_T t_c}{1-\nu_{TL}\nu_{LT}} + \frac{E_1 t_h}{1-\nu_{II1}\nu_{1II}}}$$

$$tG_{xy} = G_{LT}t_1 + G_{LT}t_c + G_{1II}t_h \qquad (2.39)$$

2 The equivalent elastic constants due to bending.

The stiffnesses due to bending may be determined in a similar manner to that used for extensional stiffnesses. It has been shown (Ref:11) that the elastic constants associated with bending differ from those for extension for a multi-layer orthotropic shell, and hence the bending stiffness cannot simply be determined from D = E I where E is the extensional constant and I is the moment of inertia of the cross section. The equivalent elastic constants to be used when solving the equations relating bending moments and curvatures.

$$\chi_x = \frac{M_x}{D_x(1-\nu'_{xy}\nu'_{yx})} - \frac{\nu'_{xy}M_y}{D_y(1-\nu'_{xy}\nu'_{yx})}$$

$$\chi_y = -\frac{\nu'_{yx}M_x}{D_y(1-\nu'_{xy}\nu'_{yx})} + \frac{M_y}{D_y(1-\nu'_{xy}\nu'_{yx})}$$

$$\chi_{xy} = \frac{1}{2} \frac{M_{xy}}{D_{xy}} \qquad (2.40)$$

can be determined as functions of the extensional elastic constants as

$$\begin{aligned}
D_x^* &= D_x\left(1 - \nu_{xy}\nu_{yx}\right) \equiv \left(EI\right)_x = E_x'I \\
&= \frac{C_2C_4 - C_1C_3}{A_{21}C_2 - A_{11}C_3} \\
D_y^* &= D_y\left(1 - \nu_{xy}\nu_{yx}\right) \equiv \left(EI\right)_y \equiv E_y'I \\
&= \frac{C_2C_4 - C_1C_3}{A_{12}C_4 - A_{22}C_1} \\
\nu_{yx}' &= \frac{A_{21}C_1 - A_{11}C_4}{A_{21}C_2 - A_{11}C_3} \\
\nu_{xy}' &= \frac{A_{12}C_3 - A_{22}C_2}{A_{12}C_4 - A_{22}C_1} \\
D_{xy} &\equiv \left(GI\right)_{xy} \equiv G_{xy}'I \\
&= \frac{1}{4A_{66}} \sum_{i=1}^{n} \left(t_i\right)^2 + \sum_{i=1}^{n} D_{xy_i}
\end{aligned} \qquad (2.41)$$

where $D_x = \frac{(EI)_x}{1-\nu_{xy}\nu_{yx}}$ is the flexural rigidity of the material corresponding to M_x

$D_y = \frac{(EI)_y}{1-\nu_{xy}\nu_{yx}}$ is the flexural rigidity corresponding to M_y

$D_{xy} = (GI)_{xy}$ is the torsional rigidity corresponding to M_{xy}

and primed constants E_x', E_y', G_{xy}', ν_{xy}', ν_{yx}' are those equivalent constants associated with bending, and the terms A_{jk} and C_j are

defined as follows in terms of the extensional and bending stiffnesses as

$$A_{11} = \sum_{i=1}^{n} \frac{1}{E_{x_i} t_i} \qquad A_{22} = \sum_{i=1}^{n} \frac{1}{E_{y_i} t_i}$$

$$A_{12} = A_{21} = \sum_{i=1}^{n} \left(- \frac{\nu_{xy_i}}{E_{y_i} t_i} \right) \qquad A_{66} = \sum_{i=1}^{n} \frac{1}{G_{xy_i} t_i}$$

$$C_1 = \left[\sum_{i=1}^{n} \left(\frac{t_i}{2} \right)^2 + A_{11} \sum_{i=1}^{n} D_{x_i} + A_{12} \sum_{i=1}^{n} \nu'_{yx_i} D_{y_i} \right]$$

$$C_2 = \left[A_{11} \sum_{i=1}^{n} \nu'_{xy_i} D_{x_i} + A_{12} \sum_{i=1}^{n} D_{y_i} \right]$$

$$C_3 = \left[\sum_{i=1}^{n} \left(\frac{t_i}{2} \right)^2 + A_{22} \sum_{i=1}^{n} D_{y_i} + A_{21} \sum_{i=1}^{n} \nu'_{xy_i} D_{x_i} \right]$$

$$C_4 = \left[A_{22} \sum_{i=1}^{n} \nu'_{yx_i} D_{y_i} + A_{21} \sum_{i=1}^{n} D_{x_i} \right]$$

where in all cases the subscript 'i' denotes the i^{th} layer and the summation is for the 'n' layers of the composite.

Rather simpler approximate expressions for these elastic constants may be derived if the products of the Poisson ratios are small compared to unity and are neglected. Alternatively they may be derived by considering the proportions that each layer contributes to the moment of inertia of the composite section. The following relations are thus derived which might serve to provide values for a preliminary design study of cylinder strengths.

$$D_x^* = \sum_{i=1}^{n} E_{x_i} \left(I_{x_i} + t_i \bar{z}_i^2 \right)$$

$$D_y^* = \sum_{i=1}^{n} E_{y_i}\left(I_{y_i} + t_i \bar{z}_i^2\right)$$

$$\nu'_{yx} = \frac{\sum_{i=1}^{n} \nu'_{yx_i} E_{y_i}\left(I_{y_i} + t_i \bar{z}_i^2\right)}{D_y^*} \qquad (2.42)$$

$$\nu'_{xy} = \frac{\sum_{i=1}^{n} \nu'_{xy_i} E_{x_i}\left(I_{x_i} + t_i \bar{z}_i^2\right)}{D_x^*}$$

$$D_{xy} = \sum_{i=1}^{n} G_{xy_i}\left(I_{x_i} + t_i \bar{z}_i^2\right)$$

where I_{x_i}, I_{y_i} are moments of inertia of i^{th} layer about its own centroidal axis and $\bar{Z}_i$ is the distance of the centroidal axis of the i^{th} layer from that of the laminate.

Failure of a Laminate

Failure in engineering terms implies that the applied loads have caused sufficient deformation of the structure to inhibit its further satisfactory functioning under these loads. With suitable layer thickness ratios and appropriate filament orientation within the layers, a filament wound structure can be expected to resist applied loadings efficiently. To design a structure employing filament winding a knowledge of its strength is desirable and the stresses and strains having been calculated in the layers, the failure of the structure requires some criterion by which its strength may be judged.

The commonly applied anisotropic yield criteria all having the form

$$\left(\frac{\sigma_L}{X}\right)^2 - k\,\frac{\sigma_L \sigma_T}{XY} + \left(\frac{\sigma_T}{Y}\right)^2 + \left(\frac{\tau_{LT}}{S}\right)^2 = 1 \qquad (2.43)$$

where X, Y, and S are the allowable longitudinal, transverse and shearing strengths of a unidirectional layer, has been suggested in various forms by many investigators. (Ref: 12). It is usually assumed that failure by yielding and by ultimate strength are synonymous so that the stress interaction equations of this type may be applied. This assumption has been shown to be reasonable for glass-epoxy resin composites (Ref: 12) and the use of these equations is representative of the present state of the art.

Where k = 1, equation (2.43) reduces to that proposed by several investigators which differs only in the denominator of the second term from that proposed by Tsai where $k = \frac{Y}{X}$ (Ref: 12). Where k = 0, the equation 2.43 reduces to the ellipsoidal expression proposed in ANC - 18 for wooden aircraft structures (Ref: 13). Where both σ_L and σ_T are in tension, the use of k = 0 will predict lower values at failure and therefore is safer to use from the design point of view than the more commonly applied "distortional energy" condition obtained by letting $k = \frac{Y}{X}$. Several investigators have shown this form of the equation to be valid for the prediction of strength of multi-layer plates loaded in tension, and the values obtained thereby to differ little from values calculated by the ANC - 18 method.

Typical values for the strengths X, Y, and S reported in literature are noted in table 1.

Under the basic assumption implied by the use of the "distortional energy" condition of failure strength the yield condition must be applied to the state of stress expressed in the coordinate system coincident with that of material symmetry. Hence, the states of

TABLE I.

Typical values of X, Y and S, the allowable strength in the longitudinal, transverse and shear directions quoted by references for glass/epoxy material.

Type of Load	Allowable Strengths			
	X ksi	Y ksi	S ksi	Reference
Tension	150	4	6	12
Tension	165-178	8	9	16
Compression	207	12	9	"
Compression	400	12	7	15
Compression (S-glass)	210	-	-	22

stress and strain in each layer must first be determined, and for the investigation of its strength, be resolved along the principal directions of the layer. This can be done by a simple transformation using the transformation matrix $[L]$ as defined in equation (2.15). i,e. $[\sigma]_{\alpha_i} = [L]_{\alpha_i}[\sigma]_i$ where $[\sigma]_i$ denotes the stresses in the axial and circumferential directions of the cylinder of the i^{th} layer. $[\sigma]_i$ can be expressed in the generalised form of equation (2.21) for a symmetrically laminated shell of 'n' different orthotropic layers (where each of the 'n' layers comprises all identical layers of the i^{th} configuration in the laminate) as

$$[\sigma]_i = [A]_i^{-1}[A^{**}]^{-1}[\sigma] \qquad (2.44)$$

where $[A^{**}] = \frac{1}{t_i}\sum_{i=1}^{n}(t_k[A]_k^{-1})$

i.e. the stress in the i^{th} layer referred to the axes of material symmetry may be obtained from

$$[\sigma]_{\alpha_i} = [L]_{\alpha_i}[A]_i^{-1}[A^{**}]^{-1}[\sigma] \qquad (2.45)$$

The various combinations of winding patterns employed may now be studied using equations (2.21) or its more general form (2.44). The two most commonly employed combinations comprising circumferential and longitudinal windings or circumferential and helical windings have been detailed in Ref: 7 in terms of the stress ratios referenced to applied stress in the circumferential directions.

It is worth commenting here, that, as is clearly demonstrated in Ref: 7, the stresses in an individual layer of a laminate may reach the level at which failure of the layer will occur while the apparent stress level obtained by dividing the applied load by the

wall thickness is at a "safe" level. The remaining layers may be able to sustain the existing load, but on further increase of the load these, too, may reach the ultimate strength at which failure occurs. This fact would make it seem reasonable that failure of the cylinder would occur between the failure bounds generated by considering the winding pattern used, and determining the strength of each type of layer wound.

As shown earlier, the membrane theory can be reasonably applied to the analysis of shells with high radius to thickness ratios and consisting of a reasonable number of unsymmetrically laid layers. In this case the equivalent elastic constants associated with stretching are applied in the analysis. However, where it is desired to analyse discontinuity stresses and streeses from local loads in fibre glass shells, it is necessary to know the bending solutions. In many cases, as is shown in Ref: 11, the bending solutions for isotropic shells under similar conditions (obtained for example from Ref: 23) may be employed provided that the necessary modifications are made to use where necessary the equivalent elastic constants associated with bending to take account of the fact that the equivalent constants differ for bending and stretching in a multi-layered orthotropic shell.

Where a filament wound cylinder is used as a pressure vessel only, there will be no buckling problem but when it is expected to carry additional loads where either σ_L or σ_T or both are in compression the possibility of buckling rather than material failure occurring exists and prediction of failure strength by use of the

interaction formula is less reliable. The onset of buckling is always difficult to predict and this is hampered even further by the lack of experimental data available. Predictions of strength for even isotropic materials are always much higher than the experimental values obtained. These predictions of buckling strength are usually based on the small deflection theory, and in the case of anisotropic materials, the application of a large deflection theory such as that advanced by Von Karman and Tsien is very complex. (Ref: 14).

A detailed study of the buckling of a filament wound shell is beyond the scope of this present work and the following notes are intended only as a guide to some of the approximate expressions proposed by investigators for the prediction of behaviour of the composite shell under buckling conditions.

Recent work reported in Ref: 15 using a derived equation for small deflection buckling for an orthotropic multi-layered cylinder under applied loads provided predictions for the strength under applied axial compression that compared as favourably with experimental data as would have predictions made for isotropic metal cylinders provided the assumption that the cylinder matrix behaves linearly, holds. This was found to be true for low angles of wind and non-liniarity of behaviour for the matrix was suspected as the cause for less close agreement as the angle of wind was increased. This derived equation took into account coupling and bending stiffnesses as well as extensional stiffnesses and a comparison with the results obtained by ignoring the coupling effect indicated that, for tubes

of the configuration used with a small number of layers laid alternately, coupling effects were small.

Further work on filament wound cylinders under various load conditions has shown that this equation (Ref: 15) provided predictions of strength that gave good agreement with experimental predictions of strength that gave good agreement with experimental values for buckling failure under external pressure load, although results were inconclusive for axial compression loads for the configuration of cylinder employed. (Ref: 16).

The equation employed in Ref: 15 was a Donnell-type stability equation derived from Ref: 17 in which the bending, coupling and extensional stiffnesses of the cylinder wall are included.

Isotropic shell studies have shown that initial wall irregularities from the circular cross section have a marked detrimental effect on buckling strength and as initial deviations are likely to be more severe and present to a larger extent in a filament wound structure, the winding process involved may cause the local wall strength to vary a great deal.

A simpler expression, also based on small deflection theory, for predicting the critical compressive stress than that derived in Ref: 15 has been presented by Dow and Rosen (Ref: 18) for orthotropic shells of radius r and thickness t.

$$\sigma_{cr} = \left(\frac{t}{r}\right)\left[\frac{E_x E_y}{3(1 - \nu_{xy}\nu_{yx})}\right]^{\frac{1}{2}} \phi k \qquad (2.46)$$

where

$$\phi = 1 \text{ or } \left[2G_{xy}\left(1 + (\nu_{xy}\nu_{yx})^{\frac{1}{2}}\right)/(E_x E_y)^{\frac{1}{2}}\right]^{\frac{1}{2}}$$

whichever is the smaller, and K is a coefficient < 1. To allow for the inadequacies of the small deflection theory and the presence of

initial wall deviations, a value much less than 1 should be employed for design purposes.

Although the small deflection theory contends that the presence of internal pressure has no effect on buckling strengths of isotropic cylinders, several investigators have shown interal pressure to be of importance in delaying the onset of bucking in cylinders under compressive loading. However it has been shown that there is an upper limit beyond which the effect of internal pressure in stabilising cylindrical shells becomes negligible. For isotropic shells, the parameter which indicates the limit appears to be at $\frac{p}{E}\left(\frac{r}{t}\right)^2 = 0.160$ and it would seem likely that the larger wall irregularities possible with filament wound vessels would make the value of such a parameter higher.

For the problem of buckling under torsional loads, Donnell et alii showed that the following relation predicted buckling strengths which were in agreement with those experimentally obtained. (Ref:19,20).

$$\tau_{cr} = k_s \frac{\pi^2 D}{L^2 t} \qquad (2.47)$$

where L = length of cylinder

$$D = \frac{Et^3}{12(1-\nu^2)}$$

$$Z = \frac{L^2}{rt}(1-\nu^2)^{\frac{1}{2}}$$

and $k_s = 0.85\, Z^{\frac{3}{4}}$ for simply supported edges

and $k_s = 0.93\, Z^{\frac{3}{4}}$ for clamped edges.

An approximation for an orthotropic cylinder under torsion obtained by assuming that the cylinder is an equivalent isotropic cylinder

would hold if the axis of the cylinder is in line with one of the principal axes. Then the equivalent isotropic elastic constants can be represented by the geometrical mean values of the elastic constants along the principal directions of the material.

i.e. $E = (E_x E_y)^{\frac{1}{2}}$ and $\nu = (\nu_{xy}\ \nu_{yx})^{\frac{1}{2}}$

The application of internal pressure again can delay substantially the onset of buckling. A simple interaction formula was established by Crate, Batdorf and Baab (Ref: 21) which determined the critical shear stress due to torsion under the influence of internal pressure for isotropic cylinders. This has shown good agreement with experiment. Where τ and p are the applied torsional and internal pressure stresses respectively and τ_{cr} and p_{cr} are the critical shear stresses in the absence of pressure and the critical hydrostatic pressure which causes buckling in the absence of torsion respectively the equation derived is:

$$\left(\frac{\tau}{(\tau_{cr})_{p=0}}\right)^2 + \frac{p}{(p_{cr})_{\tau=0}} = 1 \qquad (2.48)$$

This equation could well provide a simpler interaction formula for the determination of the buckling strength of a laminated cylinder under the combined action of torsion and pressure than the complex Donnell - type stability equation derived in Ref: 15.

CHAPTER 3 Machine Design

Introduction

Glass fibres for filament winding are supplied by the manufacturers in the form of roving wound onto a spool to form a package known as a "cheese". Each roving is made up of several "ends", each end consisting of a large number of continuous monofilaments of glass. The process of filament winding starting from the unimpregnated roving as supplied by the manufacturer entails that, with the minimum loss of strength due to handling in their passage from the cheese, the rovings are impregnated with the resin matrix to the required degree and applied under tension in some designed pattern to the surface of a former to fabricate a balanced structure with high strength properties, where the fibres oriented in any direction have equal stress applied to them under load.

Regardless of which method of winding is employed, a winding machine will consist of two basic items, a former, usually known as the "mandrel" on which the part under construction is wound and a reinforcement feeding head or "laying-on guide" which positions the impregnated rovings onto the mandrel surface. These two items move relative to each other in such a manner that the reinforcement is continuously applied to the mandrel at the precise orientation required. To improve the accuracy of directional guidance of the reinforcement, the final laying-on guide should lie close to the mandrel surface.

As stated briefly in Chapter 1, factors such as the maintenance of the desired orientation of reinforcement in the winding pattern, the efficient impregnation of the reinforcement with the matrix and control of the reinforcement volume fraction in the resulting composite material during the process of winding are inter-related and influence greatly the final strength and density of the part that is being wound. Of these, the winding pattern is the most important as it determines the directional strength of the composite material.

The 'ideal' is to orient the fibres in the direction of the principal stresses and proportion the number of fibres with respect to the size of these principal stresses. In most structures, it is geometrically impossible to orient the fibres precisely in the principal stress directions and they are oriented at some angle thereto so that a balanced structure is achieved. As the previous chapter showed, analysis of the strength of a vessel is based on the properties of the constituent materials and the orientation angle at which the fibres in each layer are laid. The importance of close maintenance during winding of the angle of wind dictated by the design is evident on study of equations 2.18, 2.29 and 2.30 for an oriented unidirectional layer and a balanced helical wound layer respectively, where the elastic constants are obtained in terms of the elastic constants along and transverse to the fibres and the fourth power of the direction cosines of the orientation angle.

It is assumed also in the analysis that the fibres are uniformly distributed over the surface of the mandrel. If this is not the case,

the interstices left in the winding pattern will either remain as voids or, if excess resin is present, will become resin-rich areas. As the resin strength is low in comparison with that of the glass, the effect in either case will be to form a weak point in the vessel wall from where failure may be initiated at a value much below design strength. Relatively small stresses in the composite wall may lead to high strain levels in the resin because of the high resistance to deformation of the glass reinforcement and these may cause failure in the resin. A practical effect of non-uniformity of winding pattern is the variation of wall thickness that can occur with overlapping of filament bands in one location and voids elsewhere. This can cause cumulative dislocation of orientation and pattern in subsequent layers.

Of the three types of winding pattern, helical, polar or hoop, it was considered that the first could be the most flexible in application to a study of filament winding. This type of winding, where the roving is applied in interwoven helical paths requires precise control to distribute the material evenly over the mandrel but by varying the angle of wind and/or adding additional hoop windings, any ratio of hoop to longitudinal strength may be obtained. The design for a machine for this type of winding may be more complex than for the polar winding method, especially if the fabrication of filament wound parts of varying cross-section is to be considered. In this work, however, only cylindrical test specimens of uniform cross-section were produced.

In a helical winding machine, the mandrel is rotated about its

longitudinal axis while the laying-on guide is traversed to and fro along the mandrel and the angle of winding is determined by the ratio of the circumferential velocity of the mandrel to the traversing velocity of the guide. It is thus theoretically feasible to perform all three types of winding operation on such a machine provided that a sufficiently large range of relative speeds is available to permit the variation of the angle of wind from that required for hoop windings (determined for a roving band width 'w' and mandrel radius 'r' by the relation $\tan \alpha_o = \frac{2\pi r}{w}$) to the low angles of wind employed for polar windings, determined usually by vessel end dome configurations, although in practice, the wrapping of the filaments around the end of the vessel at very low angles of wind would require special attention in the design of the machine.

In addition to the control of the relative speed ratio of the mandrel and guide, control of the guide at each end of its traverse must be possible to ensure the desired pattern of roving application required to lay each successive band of rovings alongside a previous band is maintained, so that a layer completely covering the mandrel surface to a uniform thickness is built up, free from either overlapping of the filament bands or resin rich areas totally devoid of filaments. This entails applying a delay to the carriage at each end of the traverse. When winding open-ended cylindrical vessels the resulting build-up of wall thickness at each end may be undesirable and cause dislocation of the winding pattern. A study of this problem has been made and is detailed in Appendix 2.

Impregnation of rovings with the resin matrix may be carried

out by the roving supplier in which case the roving is supplied in the form of dry, slightly tacky tape. This is sometimes known as dry pre-impregnated roving. Where impregnation is carried out by the user, there are two possible methods. The roving may either be impregnated on a rig separate from the winding machine and stored until required in airtight containers or it may be impregnated on the winding machine itself. The first of these alternatives, sometimes called the "wet pre-impregnated" technique is claimed to have advantages over the second technique in efficiency of impregnation and cleanliness and ease of handling during winding. It, however, requires careful respooling after impregnation if, during the actual winding process, the spool is to unwind cleanly without the ribbon cutting into the remainder of the spool package. The other alternative, usually known as the "wet-winding" technique, applies a controlled amount of resin to the rovings as they are being drawn from the cheese onto the mandrel.

In the analysis of composite materials, the assumption is made that a good bond exists between the glass and the resin so that they strain equally under load. As stated in Chapter 1, failure of the composite will also depend on the ability of the matrix to act as a binder and limit the perturbation of the local stress field produced by random breakage of the fibres occurring well below the ultimate composite strength and on the frequency of these breaks. The resin is expected to transfer the load from one fibre to the next at discontinuities. Where impregnation of the fibres has not been thoroughly carried out, shear failure in the resin at the point of

discontinuity of the fibre or failure of the interface bond between fibre and matrix may occur. Any impregnation process must thus ensure that adequate resin has been applied to the glass in a manner that ensures as thorough "wetting" of the individual fibres in the roving band as possible consistent with the requirement for minimum degredation of strength due to handling. If the filaments are drawn through the resin bath too rapidly, little, if any, resin will cling to its surface and this reduces the rate at which winding may be performed. Use of a low viscosity resin and means of gently forcing the resin into the fibre allows the process to be speeded up.

In the wet-winding method, efficient impregnation techniques together with a means of applying controlled tension to the roving strand are important in control of the way the glass is laid onto the mandrel. The optimum configuration of the strand at the point of winding is a flat band of parallel fibres and this should be guided onto the mandrel in such a manner that it remains uniform regardless of winding pattern geometry. By placing the continuous strands next to each other in such a parallel arrangement more glass can be placed in a given volume.

The tensioning should be as uniformly distributed as possible over all fibres, and be capable of being controlled. Its function is to ensure that the fibres are pretensioned and properly aligned on the mandrel. In wet-wound systems, tensioning controls also the resin content while, where pre-impregnated systems are employed, tension control helps to produce dense, void free composites by compacting the material on the mandrel. In general a wet impregnated

roving will not stand as much back tension as a dry pre-impregnated roving because the wet resin will not transfer shear and each filament is without assistance from its neighbours.

Tensioning may be achieved by mechanical braking at the spool or by passing the fibre band through a series of stationary rods and braked rollers, adjustable so that variation in tension may be controlled. The use of too many or too small rods can cause fibres to suffer mechanical damage by fraying and bending. It is simplest to apply and control the tension at the spool. This is satisfactory for dry pre-impregnated rovings where the tendency of in-line tensioning devices such as rods to strip and pick up the resin causes trouble. However when wet-winding it is usually considered desirable to tension the roving band after impregnation as near to the mandrel as possible although this may be a more difficult arrangement to control. Tensioning at the spool makes impregnation difficult and use of in line tension devices on the dry glass before impregnation can cause up to 50% loss of strength in the glass by interfilament fraying and abrasion against the rods.

Thus in order to prosecute a study into the strength of glass filament wound parts, it must be possible to satisfy these requirements while retaining the ability to vary easily the part dimensions and winding patterns employed, and it was decided that part of this project would be the design and commission of a winding machine.

Machine Design

Basic Concept

The aim from the outset was to keep the design of the machine simple and compact. General arrangement of the machine may be seen in Figures 1 and 2. The overall dimensions of the machine including the mountings for the glass cheeses are 84" long by 36" wide by 48" high with maximum mandrel dimensions of 8" diameter by 45" long.

The mandrel with its drive system is located at the top of the machine and a moving carriage on which is mounted the final laying-on guide, runs on two rails alongside the mandrel. This carriage is traversed by a leadscrew driven by a separate drive system from that of the mandrel. Separate drives to the mandrel and laying-on guide were incorporated to permit a wide range and easier changes of the winding angle. Control units have been provided for both the motor speeds and automatic control of the carriage traverse including timed delay periods at either end. The cheeses of glass rovings, up to six of which may be used, are mounted horizontally in two vertical banks of three at either end of the machine on the same side of the mandrel as the moving carriage. Each individual cheese shaft has been provided with a braking facility for tension control. In the centre of the machine near floor level, two horizontal PTFE rollers are mounted along with combs to guide the rovings being drawn from the cheeses to the carriage.

The Mandrel

In the design of a mandrel for filament winding, two important points must be borne in mind. Firstly it must be sufficiently

rigid to bear the compressive load accumulated from the many layers of filaments, each of which is pre-tensioned during winding. Secondly, consideration must be given for the removal of the wound part from the mandrel when winding is completed. In the present study, where only open-ended cylinders were fabricated, a collapsible mandrel was adopted. This is shown in Figure 3a and 3b and consists of two cylindrical half shells mounted on detachable end plates located on the mandrel shaft. The chamfered edges of the two half casings are supported on rods to form a cylinder with two narrow longitudinal slits in the surface. The outer surface of the cylinder is smooth and polished. A single layer of Melinex film is wrapped around to form an unbroken surface. (Figure 4)

To remove the winding, the support rods are withdrawn so that the two half cylinders can be brought closer together to allow the winding to be slid off the mandrel leaving the Melinex layer on the inside of the filament wound tube. It has been found that the Melinex film is very easily released from the tube matrix and lining materials used in this study, imparting its own high degree of surface finish to the inner wall of the tubes as may be seen from the reflection of the dial test instrument visible in Figure 16.

The Moving Carriage.

This runs on two guide rails and is driven through two leadnuts by the leadscrew. Figures 5 and 6 show a general view of the carriage arrangement. The limit of the carriage traverse may be controlled by two micro-switches set on a scale alongside the outer rails. These are actuated by the carriage and initiate the delay

sequence at either end of the traverse before engagement of the drive in the opposite direction. The carriage and microswitches are fitted with pointers by which distance of carriage travel and position may be observed.

As with the rest of the machine, simplicity is the basis of design of the carriage framework which consists only of a base plate, on which the roller and lead nut suspensions are mounted and two uprights, onto which, at the side of the carriage remote from the mandrel, a PTFE roller assembly is mounted. This assembly which incorporates six dropper switches as used in the textile industry, is free to pivot longitudinally about its mid point and serves to guide the rovings as they rise from the two lower guide rollers at the base of the machine into the impregnation bath. The dropper switches are used to detect any break in the supply of roving from any of the six available cheeses, when they complete a warning circuit in the control console.

In the wet winding system adopted for use in this machine, the resin impregnation bath and final laying-on guide comprise a single unit on the moving carriage, mounted between the uprights so that the mean path between the PTFE roller assembly and the mandrel is horizontal. (Figure 6)

Above the bath is positioned a resin supply tank which drip feeds the resin through a spreader bar to the resin trough. Beneath this tank provision is made for a reel of fine resistance wire on a free running shaft to be positioned between the uprights to permit the incorporation of the wire into the glass roving being applied to the mandrel. The purpose of this wire is described in subsequent chapters.

The Roving Path

Figures 1, 2, 5 and 6, show the detail of the roving path.

Ideally the roving should have a short straight run from the cheese to the mandrel to minimise the possibility of strength degredation. To achieve this for a carriage traverse along a four foot mandrel would require either that the mandrel traverse past a fixed bath and guide or, where a moving carriage is employed, that the cheeses be mounted either on the carriage in line with the bath or if the associated length of glass run could be tolerated, at as great a distance as possible remote from the winding machine to minimise the angle through which the roving band is swept. None of these alternatives was feasible in this case and the present path was adopted.

The individual cheeses of glass are mounted on freely rotating shafts on which is incorporated a braking facility for tensioning of the roving at the spool. This facility is described in Appendix 1. On leaving the cheeses, each strand of roving travels diagonally downwards before passing through a highly polished guide comb. The rovings immediately thereafter pass around the large diameter PTFE rollers mounted at the base of the machine and travel upwards towards the guide roller and dropper switches on the moving carriage. As described earlier, this upper roller assembly pivots so that its longitudinal axis is perpendicular to the line of the roving path from the lower rollers to the carriage at any instant in its traverse. The three rollers used were all made in PTFE to take advantage of its non-stick and low frictional coefficient properties and were made large in diameter to minimise bending of the filaments in their path

around the roller. The positions of the rollers were selected such that the maximum length of run for each half of the path was obtained so that the arcs swept through by the roving band as it unwound from the cheese or passed up to the moving carriage were minimised. Passage of the rovings over these rollers helps to spread the band into the desired configuration before entry into the impregnation bath.

The bath (Figure 6 and 7) consists of fixed and moveable highly polished rods over and under which the roving alternately passes before finally passing over the laying-on guide. The number of rods is arbitrary but is judged on the basis of the process of impregnation within the space available. In this respect, their vertical relative positions are made adjustable. The first bay between two fixed rods adjacent to the roller is shaped in the form of a trough for the resin and is lined with plastic foam sponge. The remaining two moving rods and two fixed rods are spaced so that within the range of verticle adjustment available in their relative positions, undue bending of the filaments does not take place. These rods by stroking alternate sides of the roving band complete the process of spreading and impregnation of the band while also removing some of the excess resin clinging to the surface of the fibres.

It was found that the speed of winding was causing excessive resin to be carried forward out of the trough by the band, and that this was beyond the capability of the four rods to remove. Three additional perspex scrapers which are also adjustable for vertical position relative to the fixed rods were incorporated, raked in front

of the fixed rods to aid in the removal of this excess resin and further ensure the forcing of resin into the fibre band.

The rovings leaving the bath pass over the final laying-on guide which is machined semicircular to the diameter of the rods and to a concave circular shape in elevation (Figure 7). This shape was designed so that the band of rovings leaving the impregnation bath would be so maintained by the guide while being laid onto the mandrel regardless of the angle of winding that was being employed. This has been successful in use, the roving band sliding around the curve without apparent bunching of the fibres until its new equilibrium position on the curve was reached. A drawback to this system is the offset of the roving band off the centre-line of the bath when winding at low helix angles. This shift of position on the guide at either end of the traverse may affect slightly the pattern of wind and the accuracy of calculation of the time delay required at the vessel ends.

Tension level of the roving band during wet-winding is mainly applied by adjustment of the relative positions of the rods and scrapers, the cheese braking facility being only set at a low level to provide an initial constant back-tension and to prevent overrun of the otherwise freely rotating cheeses during unwinding.

Mandrel and Leadscrew Drive Systems

The layout of the drives to mandrel and leadscrew is shown in Figure 8. Both systems are driven by electric motors whose output speeds are infinitely variable from zero to 100% full speed through

a closed loop speed control system utilizing a tachogenerator output direct from the armature shaft. The accuracy of control will be discussed in the machine control section.

The mandrel drive is transmitted to the mandrel shaft by an electromagnetic clutch unit driving through flexible couplings. The moving carriage is traversed by an Acme thread leadscrew through two leadnuts mounted below the carriage and adjusted against each other to eliminate play on the screw, which might reduce the accuracy of winding at either end of the traverse. The leadscrew is driven through flexible couplings by a mitre gear unit with two contra-rotating driven gears. Each driven gear incorporates the sprocket of an electromagnetic clutch, the housings of which are keyed to the leadscrew shafting. Alternate engagement of each of these clutches provides the means of traversing the carriage in either direction past the mandrel.

At the end of both leadscrew and mandrel shafts remote from the drive systems, electro-magnetic brake units are fitted along with stroboscopic discs so that the motor speed controllers may be checked for accuracy using a photoelectric tachometer unit.

Determination of Winding Angle

Let n_m, n_{ls}, p, and r be respectively the mandrel rpm, the leadscrew rpm, leadscrew pitch (inches) and the mandrel radius (inches). If τ is time in minutes the circumferential distance

travelled on the mandrel = $2\pi r n_m \tau$ inches and the horizontal movement of the carriage = $p n_{ls} \tau$ inches.

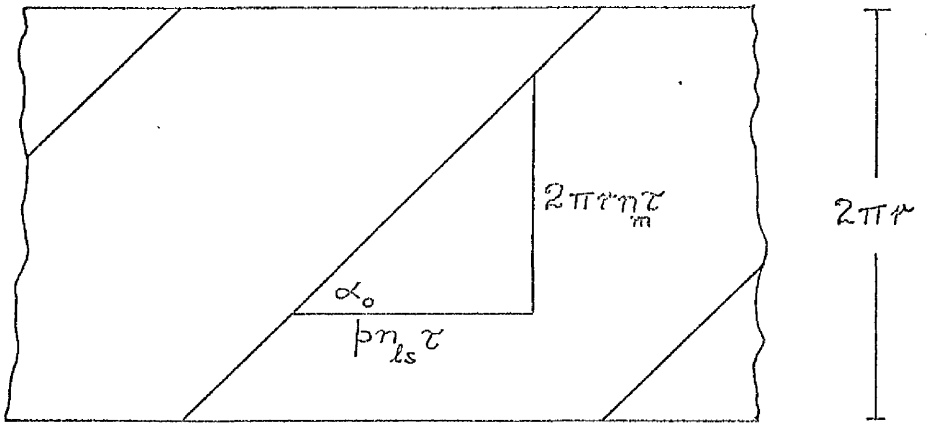

Consideration of the roving path on the mandrel surface gives,

where $\frac{2\pi r}{p}$ is a constant, $\tan \alpha_o = \frac{2\pi r}{p} \cdot \frac{n_m}{n_{ls}}$ (3.1)

α_o, the orientation of the filaments thus depends on the mandrel and leadscrew shaft speed ratio.

In this machine mandrel and leadscrew shaft full speeds are 20 rpm and 270 rpm respectively, leadscrew pitch is $\frac{1}{6}$ inch and the mandrel radius has been 2 inches, therefore the angles that can be wound assuming the minimum possible speed setting of each system to be 1% of full speed, (this is a conservative estimate), may be calculated to be $\alpha_o \geq 3^o$. This range of angles makes feasible the adaption of the machine to all three types of winding configuration if required.

Machine Control

One of the aims in the design of this machine was that it should be possible for a single person to operate it. This, and the desirability of completing without interruption the winding of a tube once the operation has been commenced required that the machine be capable of automatic operation so that the attention of the operator might be solely applied in monitoring the process with especial regard to the impregnation of the resin into the roving. This requires that a) the angle of winding be accurately maintained, b) the traverse to and fro of the laying-on guide be automatically programmed.

A console was designed to house in a compact manner all the units required for the control of the process and supply of power to the winding machine components. Mounted on the front panel of this console are all the control switches and information displays necessary for the operator to be able to see at a glance the status of the winding machine. (Figure 9)

a) Control of the Angle of Winding. As stated earlier, drive shaft speed of each motor is controlled by a closed loop servo system. The accuracy of these systems was claimed as better than 2% for a 50% change in load and a 10% change in voltage at any setting between 0% and 100% full speed. Thus the value of the tangent of the winding angle shown earlier to be dependent on the ratio of mandrel rpm to leadscrew rpm may be controlled to an accuracy of approximately

4% by these systems. The output shaft speed of each motor is directly indicated as a percentage of full speed on a large cirscale meter which may be read to an accuracy of ±0.25%. Thus the speed ratio may be set to an accuracy of 4½% under the worst conditions. A study of the supply voltage indicated no large voltage variations and as the mandrel system loading is constant and the leadscrew system loadings differs only in whatever difference there is in the driving characteristics of two similar clutch units and leadnuts, the accuracy of speed ratio may be maintained to better than 4½%. It may be estimated that a 3% variation in the speed ratio implies a maximum variation in α_o of $< 1^o$ at $\alpha_o = 45^o$.

b) Automatic Control of the Carriage Traverse. Because of the requirement for a delay period at each end of the traverse generated by the problem of maintaining the desired winding pattern to ensure even coverage of the mandrel surface, it is necessary for the carriage to be held stationary at either end of its traverse for a given time by the leadscrew brake units. The length of delay time required may be determined beforehand and the carriage traverse controlled by manual setting or automatically by a time control unit.

To achieve the design aim of one-man operation the provision of automatic traversing control incorporating timed delay periods was undertaken for this winding machine. The design requirements for such a control unit were:-

1. that the carriage would be traversed to and fro in the following

continuous cycle requiring sequential operation of the leadscrew clutch and brake units

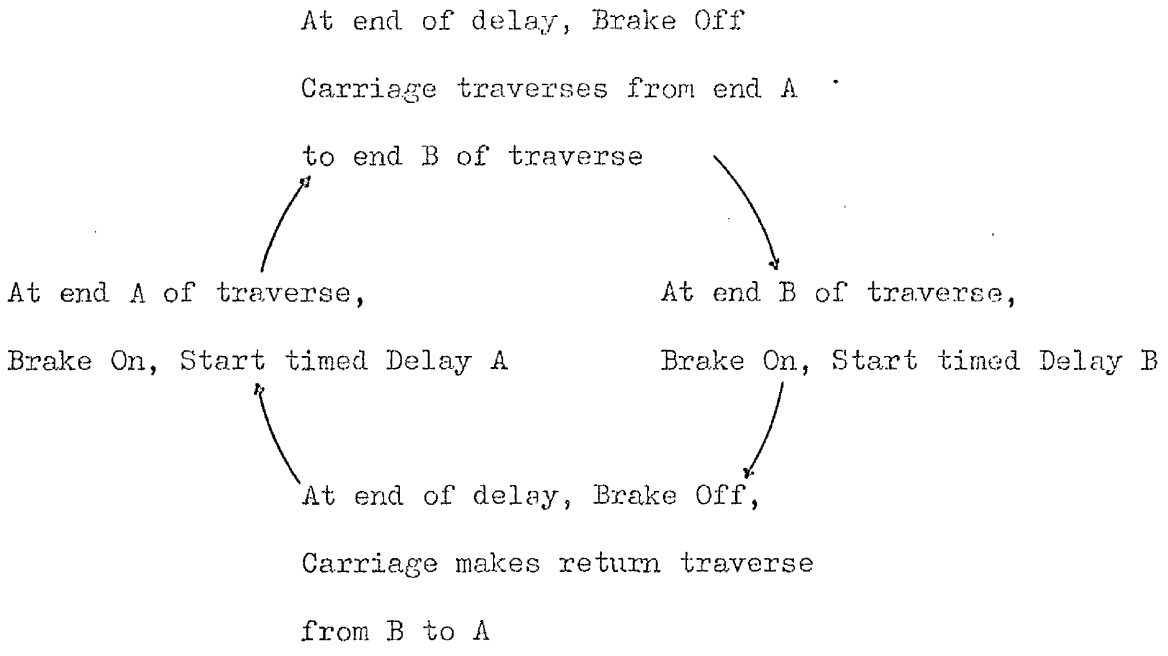

2. that this continuous cycle be capable of interruption and restart at any carriage position in the traverse without loss of winding pattern.

In addition; 3. The timed delay periods at either end of the carriage travel were to be independent of each other in setting and capable of alteration during actual operation of the machine.

4. The delay timers were to reset automatically but were not to reset on failure of the power supply.

5. A counter was to be incorporated into the control system. The installation of an automatic count of the number of traverses of the carriage will be advantageous in the control of the machine, especially in helical winding where it may be desirable to know the number of traverses required for the completion of a whole helical layer.

It was found possible to achieve this by utilizing two single cycle electro-mechanical timers with a dial setting facility which also satisfied the requirements for easy timing period changes, setting accuracy ($\pm \frac{1}{2}$ sec), and fast resetting with a repeat accuracy of 0.25%. These timers used in isolation had a possible switching arrangement of up to six load circuits. The switching arrangements were adjusted and the load circuits inter-connected in a novel way proposed by the author whereby there were four independent load circuits available and in addition one dependent load circuit operating off the timer supply line (240V 50 c/s) Use was made of this one dependent circuit in each unit to reset the other timer while three of the four independent circuits available in each timer were used in pairs, comprising one circuit from each timer, to operate the 24V.D.C. electromagnetic clutch and brake units of the leadscrew drive system in the desired sequence.

The timed delay periods are started at each end of the carriage traverse by the carriage opening a normally closed limit switch. By arranging the one timer to be reset by the second unit when that unit timed out at the end of its timing sequence, the desired continuous cycling arrangement required was achieved. The timer status required at the various stages of the traverse cycle and the resultant drive unit energised is indicated in the table.

Carriage Position	Traverse A - B	Delay at end B	Return traverse B - A	Delay at end A	Unprogrammed hold in winding
Timer A	Timed Out	Timed Out	Reset	Timing	Status maintained
Timer B	Reset	Timing	Timed Out	Timed Out	Status maintained
Clutch A-B	ON	-	-	-	-
Clutch B-A	-	-	ON	-	-
Brake	-	ON	-	ON	ON

In use, this arrangement has performed satisfactorily, the only problem occurring being caused by the fractionally slower decay of the clutch fields compared with the build-up of the brake field on switching. This has been overcome by the addition of a relay in each circuit to the electromagnetic units.

The complete circuit diagram for the winding machine is shown in Figure 10.

The counter, an electromagnetic 24 V.DC unit chosen to be compatible with the drive units, may be connected into either of the clutch circuits, so that it operates once every two traverses, or the brake circuit, if required to count each individual passage of the carriage along the mandrel length.

The ability to override both mandrel and leadscrew shaft drives and apply the brakes similtaneously has been provided. This is of use where alteration to the winding pattern is being made or where items such as strain measuring devices are being incorporated as well as in an emergency halt to the winding process and ensures that the orientation of the filaments is not altered before the winding process can be restarted

Mandrel Curing Oven

As the matrix used in this work is a hot setting epoxy resin system curing at a temperature of not greater than 120°C curing of the wound vessels on the machine with the mandrel rotating has many advantages. For example, when the vessel is kept in rotation, not only is the effective curing temperature more uniform but there is also a chance for the resin to migrate throughout the structure

to areas of lower resin content and to spread out evenly over the outer surface of the vessel, as with the increasing temperature, it initially becomes less viscous.

Accordingly an oven was designed which could be mounted around the rotating mandrel on removal of the carriage. Details of the design are indicated in Figure 11.

The oven is basically a syndanyo box encasing a cylindrical radiation reflector made of aluminium sheet. This reflector, which is of double-wall construction with fibreglass wool insulation between the walls, is in two parts. The lower portion is inserted under the rotating mandrel to fix onto the winding machine frame. The upper portion can be lowered onto this portion to form a closed box around the mandrel. Close to the surface of the upper reflector, electrical heating wires are suspended so that they touch neither reflector nor the vessel. The power input is controlled by means of a variable transformer and the internal temperature of the oven is measured by thermometers placed at two different locations.

Pre-Impregnation Rig

Although wet-winding only has been undertaken in this study it was intended in the design of this machine that it would be of general application to the study of filament-wound vessels and accordingly as an accessory to the winding machine, a rig was designed to permit impregnation and respooling of the roving to be carried out at some stage prior to winding. This rig is shown in Figure 12. The design employs the same impregnation and tensioning principles used in the main machine.

CHAPTER 4 Winding of Vessels

The procedure of winding may be described as follows.

Preparation of Mandrel

The mandrel assembly together with its single wrap of "Melinex" film, as shown in figure 4, is coated with several layers of "Breon 625", PVC latex solution which fuses at 25°C. This forms a thin skin of PVC on which the filament tube is to be wound. The Melinex imparts a smooth finish to this PVC lining, the main purpose of which is to help seal the filament tube under internal pressure. The two PTFE coated rings seen in Figure 4 clamped at either end of the mandrel are used to form the edge of the wound tube square for compression testing purposes.

Calculation of the Timed Delay at End of Traverse.

When helical winding is being performed the roving band requires to be located in position on the mandrel surface at the end of one traverse before the carriage return in the opposite direction commences. At this point, it is essential that the roving should not slip across the mandrel surface. This may be achieved by delaying the carriage at the end of its travel until the roving is held in position by a length of circumferentially wound roving. A consequence of holding the carriage at the end of its travel for a given time is the increase in wall thickness there which may disrupt the orientation of the filaments on their return journey. One way of eliminating this is to wind a tube longer than required and remove, by machining, the end portions in which

the pattern has been disorientated. But this will remove somewhat the advantages of using continuous fibres in a filament wound vessel.

The time delay process appears to be a better proposition provided that the extra thickness built up at the ends of the tube is not too excessive. A time delay that minimises this build-up may be estimated from consideration of the winding pattern on the mandrel at the end of the carriage traverse to be $T = \frac{30}{\pi n_m} (\phi_1 + \frac{D}{r})$ seconds where 'n_m' and 'r' are the mandrel rotational speed and radius respectively and ϕ_1 and D are quantities that depend on the angle of helical winding α_o. (Details of this approach are given in appendix 2).

Setting of Drive Speeds

The motor speed ratio $\frac{n_m}{n_{ls}}$ depends on the angle α_o according to equation (3.1). A plot of the motor speeds for various angles of wind has been made (Figure 13).

For a given motor speed ratio, the winding process may be performed at widely differing rates within the limit of the motor capacities. Choice of the most suitable settings of the shaft speeds is made on the basis of the computed time delay necessary at either end of the carriage traverse for the required winding pattern. The two meters in the control panel, indicating the shaft speed as a percentage of full speed for each drive system, permit the accurate setting and subsequent easy monitoring of the shaft speeds during the winding operation.

The Winding Operation

The time delay initiating limit switches are positioned on the carriage guide rail at either end of the desired traverse length. The resin mixture is introduced into the reservoir on the carriage and fed to the bath. The rovings are drawn from the cheese through the bath and manually wound a turn onto the mandrel to secure the ends. Power is applied simultaneously to both drive systems and unless manually interrupted, winding continues automatically until the desired number of traverses at theat selected angle have been completed. Interruption of the automatic mode may be made at any time, when both systems will be held stàtionary against the roving back tension by the electromagnetic brake units so that the winding pattern is not disturbed. The process may be interrupted for example to enable the angle of wind to be changed or to permit incorporation of the fine diameter resistance wire measurements into the roving band, but as the resin system is of fairly low viscosity, the duration of interruptions should be kept as short as possible to avoid resin migration across the mandrel surface to the lowest point.

Insertion of Resistance Wire During Winding

Since the filament wound tube is considered anisotropic and heterogeneous, the question is whether ordinary strain gauges can accurately measure the strains arising in the fibres. If a fine resistance wire (with a similar diameter to that of the individual glass fibres) is wound along with the roving band, a strain measurement of such a wire may be more representative to that of the fibre.

A study of 0.001" dia.'Advance' wire for use in this way was made and is detailed in appendix 3. To carry this out, a method had to be devised to successfully handle the fragile wire and incorporate it at intervals during the winding of the tube.

From a mounting just above the impregnation bath on the carriage, the wire is drawn through a guide to run along with the roving band onto the mandrel surface, as shown in Figure 6 . Care is also taken to allow the ends of the wire to be accessible when the tube is cured.

Completion of the Winding Operation

After winding is completed, the mandrel is kept rotating while the carriage is removed and the curing oven placed around the mandrel to commence the cure of the resin. After the cure is completed and the oven removed, it is convenient at this juncture to attach any items such as strain gauges before removal of the mandrel from within the tube.

Typical build up of a tube on the mandrel is shown in Figure 14. Examples of wound tubes are seen in Figure 15.

CHAPTER 5 Testing of Vessels

Determination of the Final Composition of the Tube

Since glass does not oxidise at moderately high temperature a common method of determining the composition of the material, where a sample coupon may be obtained for the purpose, is to burn off the resin at a temperature of approximately 550°C until no further weight loss is recorded, when it is assumed that only the glass is left of the sample. By appropriate measurements before and after burn-off, the weight composition of the material may be determined. Where it is not possible to obtain samples of the materials for testing in this way, the ratio of the constituents in a tube may be obtained in the following manner.

The tubes used in the present study contain resin, glass, PVC and resistance wire. The glass weight can be simply obtained by weighing the cheeses before and after winding. In a similar way, the weight of resistance wire inserted may be determined directly from the material used. The weight of PVC deposited on the mandrel can be determined by weight measurement of the mandrel before and after the application of PVC:

Hence knowing the final weight of the cured tube by measurement on removal from the mandrel, the weight of resin in the tube may be obtained by subtraction as follows:-

Weight of resin used = Weight of cured tube

- (the weight of glass used + weight of PVC used + weight of wire used)

Knowing the weight composition, the volume fraction of each constituent and the composite density of the tube can be readily computed knowing the densities of each constituent material.

Determination of the Mean Wall Thickness

The mean wall thickness is required in the analysis of the tube under applied loads. Where the weights and densities of the constituents are known, it is possible to calculate a value for the average wall thickness from the volume of the tube knowing its length and radius. Since the outer surface of the tube is slightly uneven because of the resin surface layer thickness variations, actual measurement of the wall thickness requires to be carried out at several positions around and along the tube to permit the average wall thickness to be obtained with accuracy.

A simple device, incorporating two dial test indicators with scale graduations of 0.0005", which enabled the wall thickness of a wound tube to be measured at any position along its length, was made and can be seen in Figures 15 and 16. The measurement of thickness obtained could be read to an accuracy of $\pm$0.0002".

Both methods were used in the determination of the wall thickness of the tubes used in this study, and yielded results in close agreement with each other.

Tube No.	Mean Wall Thickness	
	a) by weight method	b) by measurement (mean value)
1	0.1175"	0.115"
2	0.1223"	0.121"
3	0.050"	0.0514"

The Use of Integrally Wound Resistance Wire as a Strain Gauge

The wire studied was 0.001" in diameter 'Advance' wire in the bright condition. Advance is a copper nickel alloy containing 55% copper, which has a resistivity of 49 $\mu\Omega$-cm. and was chosen because it has a relatively low temperature coefficient. The first requirement is to determine the gauge factor of such a wire for strain measurement.

Owing to the heterogeneous nature of a filamentary reinforced structure strain measurement cannot be easily carried out with common methods of measurement. As the material may consist of many layers of different filament orientations and is in general anisotropic and heterogeneous, the measurement of strain therefore presents a problem. Although ordinary electrical strain gauges have been used, the strain thus measured, however, can only represent the resultant strain in the binder where the gauge is placed. It bears no exact relationship to the actual strain in the load carrying fibres especially in cases where the fibres interlock with each other to form a composite layer with the binding material. Since the load carrying ability of a filamentary structure depends to a large extent on the loading conditions in the fibres, a knowledge of the strain in the structure in the direction of the fibres is desirable.

If a fine electrical resistance wire is incorporated in a strand of filaments during the winding process, the wire, as an integral part of the structure, will experience the same strain as the filaments under load provided that the size of the wire is small enough not to interfere with the actual loading conditions in the fibres. Thus the wire can be treated in the same manner as an ordinary strain gauge.

It will measure the average strain over the length of the filaments along which the wire runs. The glass filament used in the present work has a diameter of 0.00038". One roving strand consists of 2400 such filaments. With care a number of strain gauge wires can be incorporated into the structure at different locations and depths from the surface leaving a short length from each end of the wire to protrude from the surface for connection to the strain gauge bridge unit.

The gauge factor of a resistance wire used to measure mechanical strain is defined as the ratio of the change in electrical resistance due to the change in mechanical strain i.e. G.F. $= \frac{dR}{R} / \frac{dl}{l}$ where the resistance R may be expressed as $R = \frac{\rho l}{A}$ and ρ is the resistivity, l the length and A the cross-sectional area of the wire. The theoretical derivation of the gauge factor is detailed in Reference 24, where it is shown that G.F. $= 1 + 2\nu + \frac{\partial\rho}{\rho} / \frac{\partial l}{l}$ where ν is the Poisson ratio of the wire. The gauge factor values from three different reference sources quoted in Reference 24 from tests on Advance wire used either in single wire form or as an unbonded gauge are 2.1, and 2.12(bis).

Experiments were carried out on several specimens of wire to verify these figures. The ends of each length of wire were soldered to copper terminals bent in the shape shown in the diagram to provide a facility for tensile loads to be applied.

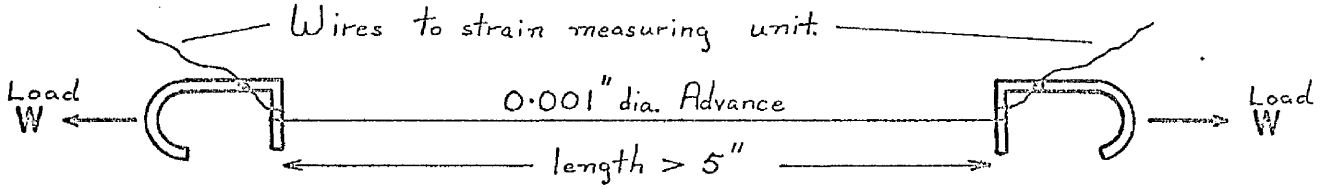

A typical strain gauge circuit using an electronic null point indicator and a bridge unit was set up. For initial balancing of the bridge unit, a wire wound variable resistor was used as the

the dummy gauge. Load was applied by dead weight in increments of 0.5gm. up to a maximum weight of 10.5gms. Choice of such a small weight increment was aimed at eliminating as much as possible any dynamic force during the changing of weights. The maximum load of 10.5gms. was chosen to ensure testing was carried out well within the elastic portion of the stress - strain curve, a test indicating that non-elastic deformation occurred in the region of 18gms. applied load. The test was repeated twice for each of the five specimens of wire and the change in resistance $\frac{\Delta R}{R}\%$ measured for each load increment of 0.5gm. during both the loading and subsequent unloading of the wire, providing 266 observed values in all, with an estimated accuracy of observation of 3.4%. Despite the care taken during loading and unloading, a wide range of scatter existed in these observed values and twelve were rejected on the basis of Chauvenet's criterion as having too large a deviation. The distribution of the remaining 254 is shown in Figure 17. A mean value of $\frac{\Delta R}{R}\%$, was computed for a load increment of 0.5gm. together with the standard deviation, s, of the observations.

From the definition $\frac{\Delta R}{R} = G.F. \times \frac{dl}{l}$

$= G.F. \times \frac{W}{AE}$ where W, A and E are the applied load, the cross-sectional area and Young's Modulus of the wire. Hence the value of the ratio $\frac{E}{G.F.}$ may be determined from the experimental values obtained for the change in resistance for a known load increment, and knowing the modulus value, the G.F. may be deduced.

For the single unbonded wire, for a load increment W of 0.5gm., mean value of $\frac{\Delta R}{R} = 1.43 \times 10^{-4}$. Standard deviation $s = 0.17 \times 10^{-4}$ permits calculation of the probable error of the mean value to be 0.723×10^{-6}. This mean value gives a value for the ratio of Young's Modulus to Gauge Factor of $9.5155 \times 10^{6} lb/in^{2}$ and using the Young's Modulus value quoted by the manufacturer of $E = 20 \times 10^{6}$ lb/in^{2} the Gauge Factor value of the wire is obtained as 2.1018. This value is in good agreement with those quoted in Reference 24.

A further series of tests was carried out in order to observe whether or not a resistance wire can be used to measure strain accurately employing the value of gauge factor thus determined if the wire is bonded to a basic material.

Three lengths of aluminium alloy strip of nominal $\frac{1}{2}$" x $\frac{1}{8}$" cross section were used as basic specimens with one of the faces specially prepared for the bonding of the resistance wire by means of epoxy resin. Three points need be borne in mind. They are the actual length of the wire bonded to the specimen, the total length of the wire including the portion which will not be under strain, and the alignment of the wire with the basic specimen so that the wire will experience the same degree of strain as the specimont under load. The last point can be achieved if the resistance wire is laid under slight tension along the central line of the specimen prior to bonding. A jig was specially made for this purpose.

With the aluminium strips in position in the jig, a thin coat

of the resin system used for tube manufacture was brushed on evenly over the prepared surface and cured to provide insulation of the wire from the aluminium. The ends of the strips were then masked so that only the central portion of length '2l' was left uncovered. Lengths of the 'Advance' wire were laid in position along the centre line of the strips and tensioned slightly before a second application of resin was flowed from a fine brush along the wire. When this coat of resin had been cured, the wires were cut while still under tension to a total length 'L'. The masking and cutting operations were all carried out under magnification. The ends were soldered to electric leads - allowing for the solder junctions, the total length may be taken as 'L_1' instead of 'L'.

Let R_1 and R_2 be respectively the resistance of the total length L_1 of the wire before and after load is applied.

Let R_1' and R_2' be respectively the resistance of the bonded portion of the wire of length "2l" before and after load is applied.

Then $R_1 = R_1' + r$ } where r is the resistance of the two
$R_2 = R_2' + r$ } unstrained portions of the wire of length $1/2(L_1 - 2l)$.

Now from its definition, G.F. $= \frac{\Delta R}{R} \cdot \frac{1}{\varepsilon}$,

Where ε, the strain of the aluminium strip may be determined from

$$\varepsilon = \frac{\text{Tensile Load}}{\text{Cross-sectional area x Young's Modulus}} = \frac{W}{A.E}$$

$$\therefore \text{G.F.} = \frac{R_2' - R_1'}{R_1'} \cdot \frac{1}{\varepsilon} = \frac{R_2 - R_1}{R_1'} \cdot \frac{1}{\varepsilon}$$

$$= \frac{R_2 - R_1}{R_1} \cdot \frac{1}{\varepsilon} \cdot \frac{L_1}{2l} \quad \text{since } R_1' = \frac{\rho 2l}{A} \text{ and } R_1 = \frac{\rho L_1}{A}$$

Now we measure $(\frac{\Delta R}{R})$ observed $= \frac{R_2 - R_1}{R_1}$

$\therefore$ G.F. $= (\frac{\Delta R}{R})$ observed $\cdot \frac{1}{\varepsilon} \cdot \frac{L_1}{21}$

$= (G.F.)_{observed} \times \frac{L_1}{21}$

Therefore the ratio $\frac{L_1}{21}$ must be applied as a correction to the observed G.F. values obtained during testing of the strips.

Testing was carried out by applying tensile load increments of 0.05 ton to the strips while the values of $(\frac{\Delta R}{R}\%)_{observed}$ were recorded by means of a strain bridge unit as described earlier. The tests were repeated several times for each strip, and the results plotted with $(\frac{\Delta R}{R}\%)_{observed}$ against applied load. From the average value of $(\frac{\Delta R}{R}\%)_{observed}$ for a load increment of 0.05 tons throughout the range of loading for each specimen, a value of the gauge factor G.F. $= \frac{\Delta R}{R} \cdot \frac{AE}{W} \cdot \frac{L_1}{21}$ was computed. The estimated accuracy of observations combine to give an accuracy of $\pm 7\%$ for the G.F. value. A much smaller range of scatter is apparent in the observations for this series of tests, only one value of $(\frac{\Delta R}{R}\%)_{observed}$ being rejected. The derived G.F. values calculated are shown below, the different ratios of $\frac{L_1}{21}$ applying to the specimens making direct comparison of observed resistance change meaningless.

Specimen	L_1	21	$\frac{\Delta R}{R}\%_{observed}$ Average	G.F.
1	6.50	4.0	2.50×10^{-4}	2.195
			2.45×10^{-4}	2.150
2	6.54	3.94	2.47×10^{-4}	2.216
			2.44×10^{-4}	2.187

			2.45×10^{-4}	2.198
			2.46×10^{-4}	2.204
			2.44×10^{-4}	2.187
			2.41×10^{-4}	2.160
3	5.57	3.0	2.18×10^{-4}	2.188
			2.19×10^{-4}	2.196
			2.19×10^{-4}	2.196

The mean value obtained was G.F. = 2.189. Standard deviation s = 1.794×10^{-2} permits calculation of the probable error of the mean to be 0.58×10^{-2}.

It is interesting to note the close comparison of the values of the G.F. obtained for the three specimens despite the different ratios of $\frac{L_1}{2l}$ for each specimen.

When a strain gauge is bonded to a basic material, it is assumed that the effect of the bonding material is negligible so that for practical analysis purposes, the gauge experiences the same strain as the material to which it is bonded. The aim of the foregoing tests was to determine whether any significant difference existed between the gauge factors applying 1) to the unbonded wire 2) the wire bonded to the surface of some other material and 3) the wire embedded within the composite material. From the tests, the gauge factor for case 1, the unbonded wire was determined as 2.1018 and that for case 2, the wire bonded to the surface of the aluminium as 2.189, a difference of 4%. There might be three possible explanations for this. Either the wire is being strained to a lesser degree than the aluminium because of

shear strain taking place within the resin layer or the value of the Young's Modulus used for the wire in case 1, is too low
the Young's Modulus used for the wire in case 1, is too low.
It is also possible that the difference may be accounted for by experimental errors in the two series of tests.

Of the three cases, case 2 may be considered to be the least favourable condition for the resin employed as bonding agent to efficiently transfer the strain from the basic material to the resistance wire. When the wire is incorporated within the roving band being wound onto the mandrel, if the assumption of efficient impregnation and alignment of the roving band during the winding process holds, the wire will become completely surrounded by filaments in close proximity to the wire with very thin layers of resin between the individual load-carrying fibres, whereas, the layer of resin between the wire and the surface of the base material in case 2 (the aluminium strip in this study) may be greater than the wire diameter.

Consider the wire bonded to the aluminium surface. A larger gauge factor in this case implies from the definition of gauge factor that the bonded wire is undergoing a lower strain than the aluminium strip. This is possible as the transfer of load from the strip to the wire must have caused a certain amount of shear strain in the resin layer. The investigation given in Appendix 3 is to determine the difference in strain of the strip and the wire under the present conditions.

The ratio of the two strains is given by

$$Q = \frac{\varepsilon_2}{\varepsilon_1} = 1 - \frac{1}{\mu l} \qquad (A3 - 10)$$

where $$\mu^2 = \frac{Gb}{t}\left(\frac{1}{E_1A_1} + \frac{1}{E_2A_2}\right) \qquad (A3 - 1)$$

and, as before, 2l = the length of wire bonded to the aluminium.

For the present resin system, the value of Q obtained for a maximum resin thickness of t = 0.002" were Q = 0.99325, 0.99797, 0.99980, for a breadth b = 0.001, 0.010, 0.500. The actual thickness of the resin layer applied was less than 0.002". For all intents and purposes, Q can be taken as unity and the strain in the wire as practically the same as that of the aluminium strip under load.

The Young's Modulus of the wire was quoted by the manufacturer as "of the order of 20 x 10^6lb/in^2 ", and using this value it has been seen that close agreement was obtained from the values of gauge factor quoted in Reference 24. However, Advance is an alloy of copper and nickel and the value of Young's Modulus for alloys is very dependent on composition. Reference values for the Young's Modulus of Cu - Ni resistance wires marketed under the trade names of Constantan, Advance etc. are given in Reference 25 and 26 as 16.24 x 10" dynes/cm^2 which is equivalent to a value of 23.6 x 10^6lb/in^2. This in turn would make the G.F. value 2.48 using the experimentally found value for the ratio $\frac{E}{GF}$ of 9.515 x 10^6lb/in^2. In turn this value of $\frac{E}{GF}$ used in conjunction with the experimentally found value of G.F. = 2.189 from the aluminium tests implies a value for the Young's Modulus of 20.92 x 10^6lb/in^2. for the wire.

Finally, there is the possibility of experimental errors for

the methods employed introduced by 1) the measurement of load, cross-sectional areas and Young's Modulus in each test. 2) the measurement of the lengths L_1 and 21 applied as a correction factor to the values obtained experimentally in the aluminium strip experiments. 3) the use of a wire wound resistor as a dummy gauge to balance the bridge circuit initially. From consideration of these factors, the accuracy of observation of the two methods detailed were estimated at not less than 3.4% for the unbonded wire tests and not less than 6.6% for the wire bonded to the aluminium strip, so that a difference of 4% between the two experimentally derived values is seen to lie within the range of experimental error.

In conjunction with the foregoing it is considered that the wire can be reliably used to measure the strain in the fibres of a composite material when wound into the structure as part of the roving band and because of the doubt concerning the accuracy of the value of Young's Modulus for the wire in case 1 and the larger thickness of resin applying in case 2 compared to case 3, the value of Gauge Factor employed has been taken as the mean of the two values determined, i.e. 2.145.

Where the wire is wound into a tube, it may be necessary to estimate the total effective length L_1 and the "active" gauge length'21' of the wire, although in most cases, the ratio of 'L_1' to'21' will be sufficiently close to unity to be treated as such.

Design of a Test Rig for the Tubes

In the analysis of a filament wound structure elastic modulii of the material along and transverse to the fibre are generally required. These modulii may be determined experimentally. In a circumferentially wound tube, the Young's Modulus along and transverse to the fibres and associated Poisson's ratios may be established by selected axial loadings and lateral pressure tests. The shear modulus may be determined separately from simple torsion tests.

If a circular cylinder is internally pressurised, a biaxial system of stress is induced where the circumferential load in the vessel wall is twice the value of that in the longitudinal direction. It will be possible to determine the modulus along the fibres E_L and the major Poissons ratio ν_{TL} for the tube provided that the longitudinal load component in the tube can be avoided. Therefore one of the functions of a test rig permitting the application of internal pressure loading to a cylinder will be to take up this stress component. Obviously, if the ends sealing the tube were restrained by infinitely rigid structures there would be no possibility of the pressure load on the ends being transmitted to the tube wall. As this is difficult to achieve in practise, the aim must be to so design the test rig that the ends are restrained as rigidly as possible and the method of pressure sealing is such that without loss of pressure the seals may slip along the tube inner surface through whatever small deflection of the end fixtures actually occurs or else deform under the shearing

action so that no longitudinal stress component is transmitted to the wall.

The rig is shown in Figure 18 and consists of two end assemblies which are restrained from relative movement under internal pressure loads by four shouldered tie rods. The end assemblies seat down onto the shoulders so that the weight of the end assemblies is carried by the rods and not the tube under test. These rods were made as large in diameter as possible consistent with overall dimensions of the rig to ensure the smallest possible elongation under load.

The tube is sealed against the internal pressure by 0.25" square neoprene sealing rings made to specification by Dunlop Ltd. The light compression pressure to initially effect a seal is manually applied to the rings whereafter the air pressure acts to compress the seals. To prevent over-compression at higher pressures the sealing ring sleeves are arranged so that they butt against the end plates before over-compression of the neoprene can occur. As an aid to achieving the design aims, the neoprene seals and tube inner wall are smeared with grease to facilitate the slipping of the neoprene rubber over the smooth PVC lining. The high degree of surface finish imparted to the PVC layer of the mandrel is beneficial in this context.

To enable accurate control and recording of the air pressure within the tube under test, a pressure control system was devised whereby the tube internal pressure might be increased by small controlled amounts. This was achieved by using a part of the

pressure line within the control system itself as a small pressure reservoir. The actual control system is shown in block form below.

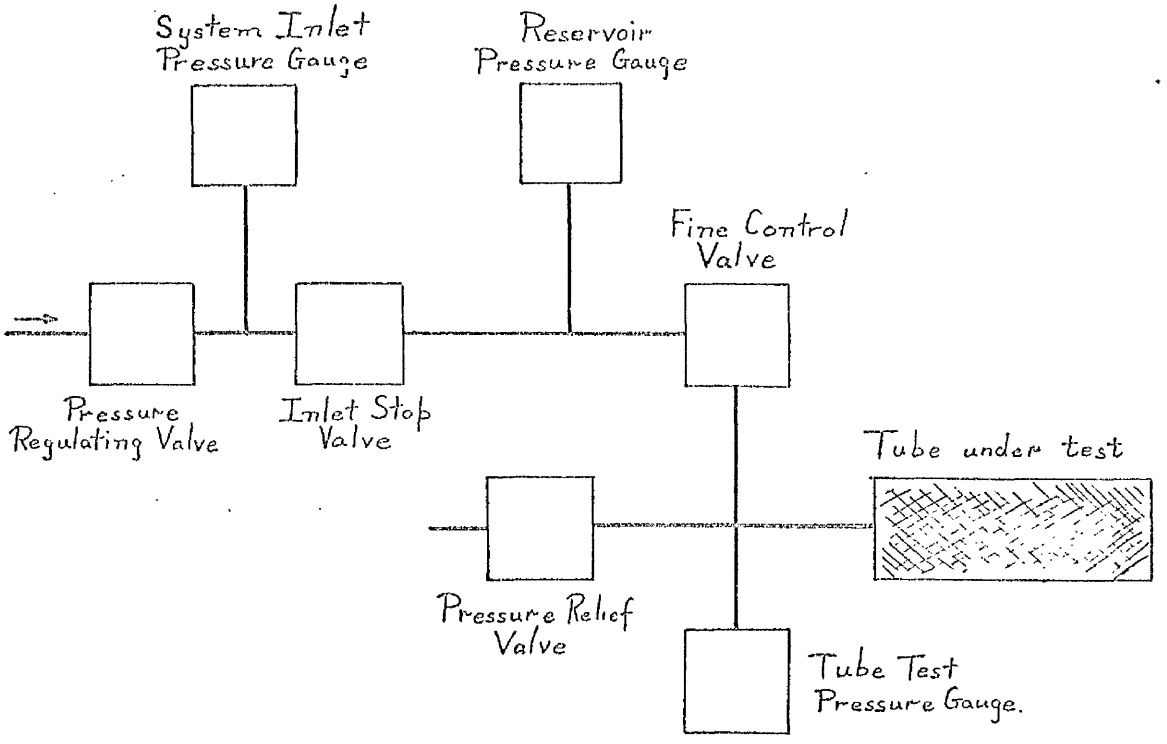

Pressure Control System

The system inlet pressure is controlled by the pressure regulating valve which has a variable outlet pressure capability of 300 - 2000psi. The portion of the line between the inlet stop valve and the fine control valve is used as the reservoir for the tube, and the reservoir pressure and tube test pressure are measured on identical large scale gauges. These have been calibrated as test gauges accurate to $\pm \frac{1}{4}\%$ full scale ($\pm$2.5psi.) and are protected from excess pressure by cutout valves.

During testing, the inlet stop valve is opened and air is admitted to the reservoir. This valve is then closed and the fine control valve opened whereupon pressure is slowly admitted

to the tube until either the tube reaches the desired test pressure or the pressure on either side of the valve equalises, when the valve is closed and the inlet stop valve opened once more to repeat the process. By this means, the test pressure within the tube can be incremented by small accurately controlled amounts. A normally closed stop valve is included in the tube test line to act as a pressure relief valve. To minimise the energy available should a seal fail or a tube burst during testing, a hardwood core is inserted within the tube. [This can be seen in the forefront of Figure 15].

In order to determine the Young's Modulus transverse to the fibres E_T and the minor Poisson's ratio ν_{LT}, the circumferential wound tube requires to be subjected to tensile or compressive axial loading. During the design of the rig just described, consideration was also given to the possibility of using the rig for compressive axial loading tests.

The flange faces of the end plates were machined flat and perpendicular to the axial centreline of the rig so that, with the four tie rods removed, face to face contact is achieved with the ends of the tube, square-formed by the rings mounted on the mandrel during winding (Figure 4.).

Compression platens for the ends were made at the same time. One platen is provided with a spherical recess to permit compressive loading to be applied through a steel ball at an accurately defined centre point. The other protects the pressure inlet tapping point from the compressive loading and thus provides the

ability to carry out compression testing of filament wound tubes on the rig with the stabilising effect of internal pressure, should this be required. However in the case of the determination of the modulii, internal pressure is not required during the application of compressive loading.

In order to determine the Young's Modulus E_T and Poisson's ratio ν_{LT} values under tensile loading and to determine the value of the Shear Modulus by the application of torsion, provision of a means of clamping the end of the tube on to the end assemblies would be required. While the rig has primarily been designed with the two loading conditions detailed above in mind, adaptation of the rig to the tensile and torsion loading conditions could be effected fairly readily without major modification.

Tube Experimental Tests.

Three hoop wound tubes 22" long and 4" internal diameter have been made on the machine to obtain the measurement of the longitudinal modulus E_L and major Poisson's ratio ν_{TL} of the material. Resistance wire was incorporated into several windings of the second and third tubes. Unfortunately all wires in the second tube were damaged prior to testing. However, in the third tube, consisting of 10 hoop layers, wires wound into layers 8 and 10 were successfully incorporated. All three tubes had one axially positioned and one circumferentially placed epoxy backed foil strain gauges (60mm. long) mounted on the tube exterior at mid length. Several windings of wire at different levels of the wall thickness are seen in the neighbourhood of the surface strain gauge in Figure 19.

At the time of winding, resin tensile test specimens were made from the resin mixes employed in the first two tubes and instrumented with foil gauges to determine the elastic modulus values of the resin while a block cast from the resin mix for the third tube was used to determine the density of the resin, both of which values are required in the analysis of the tubes.

a) Resin tests. Resin used was an Araldite MY 750 epoxy resin system formulated by CIBA Ltd., for wet winding applications. The resin mix used in all three tubes tested contained proportions of plasticiser and accelerator which were 15% and 3% of the resin weight respectively.

From the measured dimensions and weight of the block of resin cast from the mix for Tube 3, the density of the resin system was determined as 0.0436 lb/cu.in.

Tensile testing was carried out on two specimens of nominal $\frac{1}{2}$" x $\frac{3}{16}$" cross section, whose actual dimensions were measured in the course of the test. Miniature foil strain gauges were affixed on opposite sides of the specimens along and perpendicular to the line of action of the applied tensile force and strain measurements were made while the specimens were tensioned in a Hounsfield Tensometer. From these measurements, Young's Modulus and the Poisson's ratio for the resin was calculated.

From the two experimental observations,

mean value of Young's Modulus, $E_m = 0.462 \times 10^6$ lb/in^2

mean value of Poisson's ratio, $\nu_m = 0.343$.

From these values, the shear modulus $G_m = 0.1723 \times 10^6$ lb/in.^{2}

b) Tube tests. The tubes were internally pressurised in the test rig described earlier and the measurements of change of resistance recorded for the wire circuits and strain gauges as available. The overall test set-up is seen in Figure 20. The gauges were initially balanced by using dummy gauges. The resistance wire circuits in tube number 3 were balanced using wire wound variable resistors as employed earlier during the determination of the wire gauge factor value. The PVC layer on the inner face of the tube was found to effectively seal the tube against pressure loss due to seepage during testing. In the analysis of the tubes, this thin skin of PVC was assumed to act only as a pressure liner and to have negligible structural strength.

The following analysis was made for each tube to compare the experimental data with theoretically predicted values.

As the tubes consist of hoop windings only, the theoretical determination of the elastic constants may be performed for a unidirectional layer configuration, and the values of the longitudinal modulus E_L, the transverse modulus E_T and the Poisson's ratios ν_{TL} and ν_{LT} determined by the use of equations 2.8 to 2.11 where the volume fractions of the constituents and their elastic properties are known.

If v, E, ν are the volume fraction, Young's Modulus and Poisson ratio and subscripts f and m refer to the glass fibre and resin respectively, from Chapter 2,

$$E_L = v_f E_f + v_m E_m \quad (2.8)$$

$$E_T = 2\left[1-\nu_m-(\nu_f - \nu_m)v_f\right]\left[(1-C)\frac{K_f(2K_m + G_m) - G_m(K_f - K_m)(1 - v_f)}{(2K_m + G_m) + 2(K_f - K_m)(1 - v_f)}\right.$$

$$\left. + C\frac{K_f(2K_m + G_f) + G_f(K_m - K_f)(1 - v_f)}{2(K_m + G_m) + 2(K_f - K_m)(1 - v_f)}\right] \quad (2.9)$$

where K, G are defined in terms of E and ν and C is the contiguity factor assumed to be equal to 0.2, as is customary. Experimental determination of C would require photomicrographic study of sample coupons cut from the tubes, which was not possible at this stage.

$$\nu_{TL} = v_f \nu_f + \nu_m \nu_m \quad (2.10)$$

$$\nu_{LT} = \nu_{TL} \cdot \frac{E_t}{E_L} \quad (2.11)$$

The equation $\sigma_L = \frac{pr}{t}(1 + \varepsilon_L)$ (5.1)

relates the strain and stress induced by the internal pressure applied to the tube where 'p' is the pressure, 'r' the internal radius and 't' the mean wall thickness. The term $(1 + \varepsilon_L)$ accounts for the increase in tensile load carried by the cylinder wall due to the increase in cylinder size under load. Hence the circumferential strain in the tube may be determined as

$$\varepsilon_L = \frac{pr/tE_L}{(1 - pr/tE_L)} \quad (5.2)$$

and knowing the gauge factor of the gauges employed, a value of $\frac{\Delta R}{R}$ may be obtained for this strain to compare directly with the value recorded.

If the tube received zero longitudinal component of force when tested under internal pressure load in the test rig designed, then

$\sigma_T = 0$ and from equation 2.7, the strain component

$$\varepsilon_T = -\frac{\nu_{TL}\sigma_L}{E_L} \qquad (5.3)$$

and once again, knowing the gauge factor, it is possible to obtain a value of $\frac{\Delta R}{R}$ for direct comparison with that measured by the axially positioned gauge on the tube.

The experimental values of E_L and ν_{TL} may be calculated from the observations $(\frac{\Delta R}{R})_c$ and $(\frac{\Delta R}{R})_a$ of the circumferential and axially placed strain gauges, as

$$E_L = \frac{\sigma_L}{\varepsilon_L} = \frac{pr}{t} \cdot \frac{1+\varepsilon_L}{\varepsilon_L} \quad \text{where } \varepsilon_L = \frac{1}{G.F.}\left(\frac{\Delta R}{R}\right)_c$$

$$= \frac{pr}{t}\left(\frac{G.F. + (\Delta R/R)_c}{(\Delta R/R)_c}\right) \qquad (5.4)$$

$\nu_{TL} = \frac{\varepsilon_T}{\varepsilon_L}$ numerically, where $\varepsilon_T = \frac{1}{G.F.}\left(\frac{\Delta R}{R}\right)_a$

i.e. $\nu_{TL} = \frac{(\Delta R/R)_a}{(\Delta R/R)_c}$ (5.5)

The results have been calculated for an incremental pressure load p of 300 psi for all three tubes.

Tensile modulus:- glass fibre $E_f = 10.5 \times 10^6 lb/in^2$;

resin $E_m = 0.462 \times 10^6 lb/in^2$.

Poisson's ratio:- glass fibre $\nu_f = 0.23$;

resin $\nu_m = 0.343$.

Tube 1. A single pressure test to a maximum pressure of 400 psi. was carried out on this tube. A graph of the observations from the two surface foil strain gauges is plotted in Figure 21.

Radius r = 2.0"

Mean wall thickness (including a PVC layer 0.002" thick) = 0.115"

$\therefore$ mean composite wall thickness = 0.113"

Volume fraction:- glass fibre v_f = 66.33%; resin v_m = 33.66%

For this tube, the following calculated values may be obtained.

From equation (2.8) $E_L = 7.12 \times 10^6 lb/in^2$.

" " (2.9) $E_T = 2.06 \times 10^6 lb/in^2$.

" " (2.10) $\nu_{TL} = 0.2680$

" " (2.11) $\nu_{LT} = 0.0552$

For a pressure load of p = 300 psi from equations (5.2) and (5.3) the theoretically predicted value of longitudinal strain ε_L and transverse strain ε_T are

$$\varepsilon_L = 7.46 \times 10^{-4}$$

$$\varepsilon_T = 2.00 \times 10^{-4}$$

and hence, knowing the gauge factor to be 2.25, the following predicted values of gauge reading are obtained for the circumferential and axial gauges respectively

$$\left(\frac{\Delta R}{R}\%\right)_c = 0.1679$$

$$\left(\frac{\Delta R}{R}\%\right)_a = 0.0450$$

From the experimental observations, mean $\left(\frac{\Delta R}{R}\%\right)_c = 0.1743$

mean $\left(\frac{\Delta R}{R}\%\right)_a = 0.0289$

which are 104% and 64.2% respectively of the predicted values and hence, from equations (5.4) and (5.5) respectively, the longitudinal modulus $E_L = 6.859 \times 10^6 lb/in^2$ and $\nu_{TL} = 0.166$

Tube 2. Three pressure tests were performed on this tube, two to a maximum applied pressure of 400 psi and the third to a maximum of 900 psi. Graphs of the observed readings from the two surface foil strain gauges are plotted in Figures 22 and 23.

Radius r = 2.0"

Mean wall thickness (including a PVC layer 0.003" thick) = 0.121"

$\therefore$ Mean composite wall thickness t = 0.118"

Volume fractions:- glass fibre v_f = 58.62%; resin v_m = 41.35%

resistance wire v_w = 0.024%.

For this tube, the following calculated values may be obtained.

From equation (2.8) $E_L = 6.35 \times 10^6 lb/in^2$.

" " (2.9) $E_T = 1.677 \times 10^6 lb/in^2$.

" " (2.10) $\nu_{TL} = 0.2766$

" " (2.11) $\nu_{LT} = 0.0732$

For a pressure load of p = 300 psi from equations (5.2) and (5.3) the theoretically predicted value of longitudinal strain ε_L and transverse strain ε_T are

$$\varepsilon_L = 8 \times 10^{-4}$$
$$\varepsilon_T = 2.22 \times 10^{-4}$$

and hence knowing the gauge factor and hence, knowing the gauge factor to be 2.25, the following predicted values of gauge reading are obtained for the circumferential and axial gauges respectively.

$$\left(\frac{\Delta R}{R}\%\right)_c = 0.1803$$

$$\left(\frac{\Delta R}{R}\%\right)_a = 0.0499$$

From the experimental observations, close comparison was observed between the readings obtained from the first two tests.

In this case, mean $\left(\frac{\Delta R}{R}\%\right)_c = 0.1916$

$$\text{mean } \left(\frac{\Delta R}{R}\%\right)_a = 0.0274$$

which are 106.2% and 54.9% respectively of the predicted values

and hence from equations (5.4) and (5.5) respectively, the longitudinal modulus $E_L = 5.976 \times 10^6 lb/in^2$ and $\nu_{TL} = 0.143$. However, on the third run, the mean values from both gauges were different from the two previous runs.

Mean $(\frac{\Delta R}{R}\%)_c = 0.1845$ which is 102.5% of the predicted value and hence from equation (5.4), the longitudinal modulus

$E_L = 6.206 \times 10^6 lb/in^2$.

The previously noticed tendency of the graph of the readings from the axial gauge to exhibit a change of slope was very marked in this case and two distinct slopes were obtained, as seen in Figure 23, for the two ranges of pressure, $p \leq 400$ psi and $p \geq 400$ psi.

Below 400 psi, mean $(\frac{\Delta R}{R}\%)_a = 0.0260$

Above 400 psi, mean $(\frac{\Delta R}{R}\%)_a = 0.0410$

which are 52.0% and 82.0% respectively of the predicted values, and hence from equation (5.5) $\nu_{TL} = 0.141$ or 0.222 respectively for the two cases.

Tube 3. Three pressure tests in the range of pressure up to a maximum of 360 psi, were carried out on this tube in which were incorporated two windings of resistance wire as well as the surface foil gauges. Graphs of the observed readings from the wire and surface gauges are plotted in Figure 24.

Radius r = 2.0"

Total wall thickness (including PVC layer 0.0042" thick) = 0.0514"

$\therefore$ Mean composite wall thickness t = 0.0472"

Volume fraction:- glass fibre v_f = 58.4%; resin v_m 41.55%

resistance wire v_w = 0.0465%.

For this tube, the following calculated values may be obtained.

From equation (2.8) $E_L = 6.333 \times 10^6$

" " (2.9) $E_T = 1.668 \times 10^6$

" " (2.10) $\nu_{TL} = 0.277$

" " (2.11) $\nu_{LT} = 0.0738$

For a pressure load of p = 300 psi, from equations (5.2) and (5.3), the theoretically predicted value of longitudinal strain ε_L and transverse strain ε_T are

$$\varepsilon_L = 20.11 \times 10^{-4}$$

$$\varepsilon_T = 5.57 \times 10^{-4}$$

and hence, knowing the gauge factor to be 2.25, the following predicted values of gauge reading are obtained for the circumferential and axial foil gauges respectively.

$$\left(\frac{\Delta R}{R}\%\right)_c = 0.4525$$

$$\left(\frac{\Delta R}{R}\%\right)_a = 0.1253$$

In addition, the predicted value of gauge reading for the wire windings using the previously determined value of gauge factor of 2.145 is

$$\left(\frac{\Delta R}{R}\%\right)_w = 0.4313$$

From the experimental observations, all three tests showed close agreement between the observations. Considering the foil strain gauges first, the circumferential gauge exhibited a marked non-linear response initially. The mean $\left(\frac{\Delta R}{R}\%\right)_c$ = 0.3695 which is

only 81.6% of that predicted. Even if the effect of the non-linear portion is eliminated by calculation of the equivalent reading from consideration of the slope of the linear portion of the graph, the value obtained, $(\frac{\Delta R}{R}\%) = 0.4148$, is still only 91.6% of that predicted. The axial foil gauge gave rise to a mean value for $(\frac{\Delta R}{R}\%) = 0.1210$, which is 96.5% of the value predicted.

The circumferential wire windings wound into the tube along with the roving band indicated no such non-linear response however and the mean value obtained from these observations was

$$(\frac{\Delta R}{R}\%)_w = 0.4533 \text{ which is } 105\% \text{ of the value predicted.}$$

Hence, from equations (5.4) and (5.5) we may calculate the longitudinal modulus E_L and Poisson's ratio ν_{TL} to be (where for comparison the values obtained using the equivalent value of $(\frac{\Delta R}{R}\%)_c$ are given in parentheses) as

$$E_L = 7.745 \times 10^6 \text{lb/in}^2 \quad (6.90 \times 10^6 \text{lb/in}^2)$$

and $$\nu_{TL} = 0.328 \ (0.292)$$

The longitudinal modulus according to the wire windings may be calculated from equation (5.4) as $E_L = 6.027 \times 10^6 \text{lb/in}^2$.

A compilation of the results for all three tubes has been made in Table II.

Discussion

The measurements made by the surface gauges mounted on tubes 1 and 2 exhibited similar characteristics and will be discussed first.

TABLE II

Compilation of

Tube Theoretical and Experimental Results.

Tube No.	1		2				3		
No. of layers	30		26				10		
Radius r in.	2·0		2·0				2·0		
Thickness t in.	0·113		0·110				0·0472		
Glass Volume v_f	0·6633		0·5862				0·5840		
Total no. of tests	1		3				3		
Source of result	Theory	Experim.t	Theory	Experim.t	Experim.t	Experim.t	Theory	Experim.t	Experim.t
Test no.		1		1 & 2	3			1 ~ 3	
Max test pressure psi.		400		400	900 (<400 | >400)			360	
Gauge type		Foil		Foil	Foil	Foil		Foil	Wire
Gauge Factor		2·25		2·25	2·25	2·25		2·25	2·145
$E_L \times 10^{-6}$ lb/in^2	7·12	6·859	6·346	5·976	6·206		6·333	6·90	6·027
$E_T \times 10^{-6}$ lb/in^2	2·06		1·677				1·668		
$\nu_{TL} \times 10^2$	26·8	16·58	27·66	14·3	14·1	22·2	27·7	29·2	
$\nu_{LT} \times 10^2$	5·52		7·32				7·38		
Comparison between experimental observations and predicted values for a pressure increment of 300psi.									
$\epsilon_L \times 10^4$	7·46	7·75	8·02	8·51	8·20		20·11	18·44	21·13
$\epsilon_T \times 10^4$	2·00	1·285	2·22	1·219	1·156	1·822	5·57	5·38	
$\left(\frac{\Delta R}{R}\%\right)_c$	0·1679	0·1743	0·1803	0·1916	0·1845		0·4525	0·3695	
Percentage	100	104	100	106·2	102·5		100	81·6	
$\left(\frac{\Delta R}{R}\%\right)_a$	0·0450	0·0289	0·0499	0·0274	0·0260	0·0410	0·1253	0·1210	
Percentage	100	64·2	100	54·9	52·0	82·0	100	96·5	
$\left(\frac{\Delta R}{R}\%\right)_w$							0·4313		0·4533
Percentage							100		105

A basically linear response was obtained from the circumferential gauges throughout the ranges of testing and the values observed experimentally were in all tests less than 7% different from those predicted. The values observed were larger than predicted indicating a lower stiffness for the material but from the nature of the material, the strain measured by a surface gauge can only represent the resultant strain in the binder where the gauge is placed and so the difference between the observed and predicted values could reasonably be expected to indicate a lower material stiffness. This is corroborated by the results from tubes 1 and 2, where the values measured on tube 2 for the first two tests performed thereon gave consistent results with a difference from predicted values 2% greater than for tube 1. The wall thickness of these tubes are of the same order but tube 2 has a lower glass content and a much thicker resin-rich surface layer onto which the gauge was bonded. It is noteworthy that very good agreement obtained between measured and predicted values of strain for tube 2 in the third test when quite long surface cracks in the axial direction were visible in this resin outer layer in the vicinity of the circumferential gauge and it is possible that these cracks were permitting the reinforcement to be more efficient in resisting the internal pressure induced hoop stresses.

The observations obtained from the longitudinally positioned gauges for tubes 1 and 2 were however in very poor agreement (of the order of 50 - 70%) with the predicted values of $\left(\frac{\Delta R}{R}\%\right)_a$. A tendency to change slope was exhibited by the plots of these values

against applied pressure, and in the third test on tube 2, where the pressure was increased above the region of 400 psi. at which all other tests were terminated, two distinct slopes were apparent. This graph has been re-plotted in Figure 23 with an enlarged scale for change of resistance $\frac{\Delta R}{R}\%$ to demonstrate this more clearly. No such change of slope was apparent for the circumferential gauge readings during this test. The lack of agreement between the predicted and measured values for the longitudinal gauges and the sudden change of slope apparent in Figure 23 at pressures of the order of 375 - 400 psi. combine to indicate that the longitudinal force component of the internal pressure loading is not being reacted solely by the test rig as desired but is being transmitted through the sealing rings so that the tube is also carrying a certain amount.

It is unfortunate that all other tests performed on tubes 1 and 2 were arbitrarily terminated in the region of 300 - 400 psi. internal pressure, which is the region of transition of slope in the high pressure test on tube 2, (run 3), so that comparable results are not available. However the following study may be made.

Where ε_T and ε_L are the compressive longitudinal and tensile hoop strains induced in the tube by the internal pressure if a hoop component of force only is being applied to the tube as required, and ε_x is the tensile longitudinal strain due to whatever longitudinal force component actually being applied to the tube by the test rig, (and treating as small the strain induced in the hoop direction by this longitudinal force component), then

$$\text{theoretical } (\nu_{TL})_t = -\frac{\varepsilon_T}{\varepsilon_L}$$

and the experimentally derived $(\nu_{TL})_e = \dfrac{\varepsilon_x - \varepsilon_T}{\varepsilon_L} = \dfrac{-(\Delta R/R\%)_a}{(\Delta R/R\%)_c}$

Hence, $\varepsilon_x = \left[(\nu_{TL})_e + \dfrac{\varepsilon_T}{\varepsilon_L}\right]\varepsilon_L$

which in terms of observed values of $\frac{\Delta R}{R}\%$,

$$= \left[-\frac{(\Delta R/R\%)_a}{(\Delta R/R\%)_c} - (\nu_{TL})_t\right]\left[\frac{(\Delta R/R\%)_c}{100(G.F.)}\right]$$

Now if we let p' be the equivalent internal pressure that would induce this amount of longitudinal force component in the tube, ε_x may be expressed as

$$\varepsilon_x = \frac{p'r}{2tE_T}$$

and hence $p' = \dfrac{2tE_T\varepsilon_L}{r}\left[(\nu_{TL})_e - (\nu_{TL})_t\right]$

where r, t, E_T and $(\nu_{TL})_t$ are the radius and mean composite wall thickness, transverse modulus and major Poisson's ratio respectively, where E_T and $(\nu_{TL})_t$ are calculated as before from equations (2.9) and (2.10).

These pressures p' were calculated for tubes 1 and 2 and plotted against applied internal pressure p in Figure 25. It is seen that, following an initial sharp increase in the pressure p'

as the end seals are compressed manually to effect the seal, the longitudinal force steadily increases with only an occasional fluctuation as the internal pressure is increased up to the region of 360 psi. The next increment of pressure to 400 psi. is accompanied by a sharp check in the value of p', and it is in this region that the change of slope occurs in the plot of the response of the longitudinal gauge. This would indicate that in the region of these fluctuations and especially at the increment of internal pressure from 360 to 400 psi., a certain amount of slip of the neoprene rings over the PVC surface has occurred. During the remainder of the test, up to the maximum of 900 psi. internal pressure, a much lower rate of increase of equivalent pressure p' being applied to the tube in the longitudinal direction obtains, together with several more marked fluctuations in its value indicating that, at these higher pressure levels, slip of the rings over the PVC is occurring more readily.

From the foregoing, it would appear the test rig is failing to eliminate, by deformation or slip of the neoprene sealing rings, the longitudinal force component in the tube due to the internal pressure until relatively high pressure levels are reached when a certain amount of slip takes place. This partially reduces the induced force component causing the change in slope shown in Figure 23 and thereafter a sufficient degree of slip is occurring to improve the comparison between the experimental and theoretical values of Poisson ratio ν_{TL} by nearly 30%.

There appear to be several contributory factors to this phenomenon. In the design of the rig, more than adequate provision was made for sealing ring compression in anticipation of the tubes being a poorer fit over the end plugs of the rig than has actually been achieved. The use of the Melinex layer has made it possible to manufacture tubes that are a tight sliding fit over the uncompressed rings and this, together with the high surface finish imparted by the Melinex to the tube interior should be beneficial to the design aim of low clamping pressures at the sealing rings of the test rig. However, the Melinex has in its turn caused a sealing problem.

If the Melinex is not wrapped sufficiently tightly around the mandrel or its edges do not butt closely together before the PVC lining is brushed onto its surface, under the clamping action of the glass windings, a well-defined ridge may be formed in the PVC lining. Sealing of the tube against pressure leaks then requires much greater compression of the neoprene rings to eliminate leaks in the region of this blemish than would be required otherwise. These ridges were present on the inside of tubes 1 and 2 and post-cure action to effect their removal proved only partially successful and so, the initial sealing compression manually applied to the rings during the tests of these tubes was much higher than is desirable. Three regions where the rings had to be compressed to effect a seal in this way are clearly visible in the increase in value of p' between 40 psi and 60 psi, and 160 - 180 psi for tube 1 and 80 - 100 psi for tube 2 in Figure 25.

On recognition of this problem, a new Melinex liner, cut to much closer tolerances was made for the manufacture of tube 3. This eliminated the ridge to the extent that the slight lines left on the PVC surface by the self-adhesive tape locating the Melinex, are of the same order of size. As will be noted presently in the discussion of the results from tube 3, there was no sign of a similar occurrence to tubes 1 and 2 in this case. With the ridge on the inside of the tubes eliminated, it may be expected that less compression of the rings will be required to effect a seal and that the range of sealing ring compression available will now be excessive.

As a result of this, it will be probable that the internal pressure load on the faces of the ring sleeves will force the neoprene into contact with the tube wall with greater pressure than required to maintain a pressure seal. This will again reduce the possibility of slip being able to occur. This may be remedied easily by restriction, by means of packing discs, of the 0.015" movement available before the ring sleeve comes into contact with the face of the end plate in each end assembly of the rig, so that only sufficient compression of the neoprene to effect a seal throughout the range of testing occurs.

The importance of control of the impregnation and tensioning of the glass reinforcement in the filament winding process is clearly demonstrated by tubes 1 and 2, where although the number of layers wound is less, the wall of tube 2 is in fact thicker than

that of tube 1 because of the excess resin present in this tube. Tube 2 on curing possessed a thick resin - rich layer over its outer surface. This was partly squeezed out from within the windings by the higher tension level employed in the winding of this tube and partly was excess resin, picked up in the impregnation bath by the roving, during attempts to incorporate resistance wire into the windings. From the lessons learnt from these attempts, although the same resin content was used in tube 3, the impregnation and tension were controlled more efficiently and only the normal thin resin layer is present on the surface.

Tube 3 was the only tube in which resistance wire was successfully incorporated along with the windings for use as a strain gauge. The response of the wire wound into the eighth and tenth layers of this tube was linear throughout the range of testing and the consistency of the results as well as the linearity from all three tests can be clearly seen from Figure 24. The measured strains are in agreement with the predicted strains to within 5% throughout the whole loading range. Although the two circuits of wire were wound in different layers, no consistent difference in response due to position within the wall was detectable for this thin tube but further investigation using tubes of various thickness might be rewarding.

The experimental results obtained from the foil gauge, on the other hand, do not agree so well, either in comparison with the wires in this tube or the circumferential gauge results in the other two tubes. The measured discrepancy between theoretical and

predicted strains are of the order of 19% and even if the curves are shifted sideways so that the extension of their linear portion presses through the origin at zero pressure, there is still a discrepancy of 10% - 12% between the measured and predicted values. The non-linear characteristic of the results from this gauge at low pressure levels is disturbing and whether this portion of the response can be eliminated by such manipulation is open to question. It is possible that the resin layer on top of the filaments does not respond to straining in quite the same way as the stronger sub-layers in the structure but if this is the case, then this characteristic should have been also apparent in the response of the gauge in a similar position on tube 2 where the resin layer at the surface was very much thicker. Two other possibilities present themselves. If slight ovality of the tube is present in the region of the gauge, this thin walled tube may be initially deforming to a circular cross-section under the internal pressure and a compressive strain component in the hoop direction could be induced to produce this initial curved portion of the response. Or, since in a composite material, the matrix acts as a load transmitting medium and the surface strain gauge measurement only represent the resultant local strain in the binder, if the gauge is mounted over a region where the fibres are undertensioned for whatever reason, low strain levels would be recorded until such time as these fibres too are fully load carrying. Possible reasons for this would lie in poor winding process control of factors such as impregnation or tensioning.

Much better agreement between predicted and measured strain values was obtained in this tube 3 for the longitudinally placed gauge than had been previously obtained for the other two tubes and although the strain levels induced were of the same order as that induced in tube 2 by the final test to 900 psi. maximum internal pressure, no tendency for the response of this gauge to indicate a change of slope was detected, and measured and predicted values of the transverse strain were within 3.5% of each other. As noted earlier, this is considered to be due to the application of much lower clamping pressures on the seals of the test rig to effect a pressure seal because of the almost complete elimination of the blemish on the PVC lining surface caused by the Melinex release layer on the mandrel.

Conclusion

In the introduction to this work, filament winding was stated to be a fabrication technique for forming reinforced plastic parts of high specific strength, carried out on specially designed machines on which may be achieved the precise control of the winding pattern and direction of the filament orientation required to take full advantage of the remarkable high strength properties exhibited in tension by filamentary materials.

In a review of the methods of analysis for this type of material, it has been shown how, for all configurations of winding, the elastic properties can be related to the properties and relative quantities of the constituents and the orientation of the reinforcement within each layer of the structure. Accordingly, the design and use of any winding equipment must be appraised with regard to these considerations.

The helical winding machine designed and put into operation in the course of this study has shown itself capable of winding cylindrical tubes 22" long x 4" dia. using 12-end E-glass roving as the reinforcement phase and a hot setting epoxy resin system as matrix. A feature of this machine was its use of separate motor drives to the mandrel and leadscrew shafts, thus permitting the setting of a wide range of shaft speed ratios, upon which quantity the angle of wind depends. Control of this ratio has been shown to be capable of maintenance within a maximum 1° variation of the angle of wind at a setting of 45°. With this facility, any angle of wind from the low

helix angles required for polar winding to that required for hoop winding may be rapidly set on the associated control console, the design of which was also part of this present work.

The provision of automatic traversing of the reinforcement final laying-on guide together with timed delay periods at either end of the traverse by the use of two electro-mechanical timing units interconnected in a way evolved by the writer, has worked well. When winding open ended cylindrical tubes at other than hoop angles of wind, the build-up of tube wall thickness at either end during the timed delay period there can serve to disrupt the accuracy of the winding pattern in that region and as winding progresses, the effect of this disruption may extend further along the tube. A method of calculating the most suitable time delay to be applied to the moving carriage at either end of the traverse to minimise this problem has been derived. This takes into account both the requirement to locate the roving on the cylinder surface at the end before recommencing the next traverse and the requirement for optimum strength of the end item that the reinforcement be evenly applied over the mandrel surface in each layer.

In a further area of study of the winding process and its associated procedures, the design of a braking system to provide a constant tension in the roving as it is being drawn from the cheese has been considered. This has proved effective in providing the low level of constant back tension required during the wet winding of the tubes fabricated in this initial study. Provision of much higher

tension levels, up to a maximum of 1 lb per end for use with dry pre-impregnated roving, is possible within the range of adjustment designed into these units.

The problem of guiding the roving from the cheese to the mandrel surface without reducing the strength through handling and the problem of ensuring adequate impregnation within the limited space available on this compact machine has received attention and the present combined impregnation bath and laying-on guide mounted on the carriage have proved adequate. In the limited amount of winding performed during this work, a study of the relation between back-tension levels and the winding speeds on the final tube composition and the performance of the impregnation bath was not attempted. Modification of the resin trough drip feeder above the impregnation bath has improved the ease of control of the resin flow rate but provision of a means of automatic cut-off of resin supply to the bath during halts in the winding, for example during incorporation of the 0.001" dia. resistance wire into the roving band, would be advantageous from the point of view of operational ease.

The commercial roving used in this study has proved to contain large numbers of broken fibres of short length. These have been removed from the roving by the rods and scrapers in the bath but in the process tend to accumulate and can be troublesome. The provision of a suction head adjacent to the filament band prior to its entry into the bath so that all loose ends were removed, would, it is considered, be a further source of improvement to the equipment.

Some difficulty was experienced in the course of this work in the area of removal of the mandrel from within the finished tube after curing, the winding tension in the roving after passing through the impregnation bath being sufficiently high to cause the tube to bind onto the split mandrel despite the use of normal release agents such as aluminium foil, silicon lubricant etc. This has been completely overcome by the use of Melinex film as a release layer and mandrel liner combined. A side benefit to the use of Melinex has been the high surface finish imparted to the tube inner wall. The use of room temperature curing PVC solution to provide a sealing layer on the interior of the tube has also proved very successful, the PVC releasing very easily from the Melinex on removal of the mandrel. The PVC was also a very effective liner, sealing the tube against pressure loss due to seepage through resin cracks developed during the internal pressure tests.

These tests, on three hoop wound tubes to determine the modulus along the fibre direction and the major Poisson's ratio of the material have been discussed very fully in Chapter 5. Results for the longitudinal modulus were found to agree within 4% with the values predicted by consideration of the tube composition but the results for the major Poisson's ratio were initially poor. Investigation of the cause indicated that the pressure test rig, which was designed as part of this present work, was not in fact eliminating as desired the longitudinal force component due to the internal pressure in the tube. High compression of the neoprene rubber pressure seals at either end

of the tube to eliminate small pressure leaks in the region of ridges formed in the PVC lining by the butt joint of the Melinex wrap was determined as a major contributory factor. Steps were taken to eliminate this problem area and as a result the correlation between predicted and experimentally obtained values for a subsequent tube was improved by several orders of magnitude.

A major field of study in the course of this work has been the assessment for use as a strain measuring device of fine electrical resistance wire wound into a filament wound vessel along with the reinforcement. This was undertaken because of doubt about the significance of results from ordinary bonded strain gauges on filament wound structures. In an initial part of this study close agreement with referenced values was obtained experimentally for the value of the Gauge Factor of the wire when used either in the unbonded state or when bonded to a strip of aluminium alloy as a basic material. The rather tricky handling procedures associated with the integral winding of this wire (0.001" dia.) in a tube were evolved and the wire incorporated into two layers of a tube for testing under internal pressure. The results were compared with those from foil gauges bonded on the tube outer surface. From consideration of the consistent linear results from both windings of wire, at all times within 4% of the calculated values, in comparison with the surface gauge response which displayed a non-linear characteristic at low pressure levels and were in poor agreement with calculated values, it is concluded that this method makes it possible to take meaningful strain measurement along the fibre direction with satisfactory results.

Summary

In the course of this work, following a review of filament winding and the analysis of filament wound composites, the design of a helical winding machine to be capable of use over a large range of winding angles has been undertaken. The machine and its control unit have been built. Detailed study has been made of important areas of the winding process.

Test apparatus to be used in the determination of some of the elastic modulii of the composite was designed and built. In an initial experimental study, the machine has been used to make hoop wound cylindrical tubes using E-glass roving and epoxy resin. The tubes have been tested in the apparatus under internal pressure to determine certain elastic properties.

Fine electrical resistance wire incorporated in the roving band during winding has been shown experimentally to provide a method of taking strain measurements along the fibre direction with satisfactory results.

References

1. Fibre Composite Materials - papers presented at a seminar of the American Society for Metals, October, 1964. American Society for Metals, 1965.

2. Rosato D.V. & Grove C.S. (1964) Filament Winding Interscience Publishers 1964.

3. Holliday L.(Editor) (1966) Composite Materials Elsevier Publishing Co. 1966.

4. Morley J. (1968) The Development of New Structural Materials - paper presented at a symposium on "The Mechanical Reliability of Turbo-machinery Blading" at Derby and District College of Technology April 1968.

5. Rosato D.V. (1967) Reinforced Plastics - What they can do for you in the next ten years S.A.E. Trans. Vol. 75 Paper 660643 1967.

6. Hofeditz J.T. (1963) Structural Design Considerations for Glass Pressure Vessels. Engineering Paper 1415, Douglas Aircraft Company Inc. 1963.

7. Wong H.Y. (1968) Structural Considerations of Filament Wound Cylindrical Shells' Report No. 8604 University of Glasgow - Department of Aeronautics & Fluid Mechanics 1968.

8. Tsai S.W. (1964) Structural Behaviour of Composite Materials. NASA CR-71 1964.

9. Card M.F. (1965) Experiments to Determine Elastic Moduli for Filament Wound Cylinders. NASA TN D-3110 1965

10. Hashin Z;Rosen B.W. (1964) Elastic Moduli of Fibre Reinforced Materials. J.App. Mech.,June 1964 Trans. ASME

11. Greszczuk L.B.(1965) Elastic Constants and Analysis Methods for Filament Wound Shell Structures. Report No. SM-45849 Missile and Space Systems Div.,Douglas Aircraft Co.Inc. Jan. 1965.

12. Tsai S.W. (1965) Strength Characteristics of Composite Materials. NASA CR-224 1965.

13. Anon. Design of Wood Aircraft Structures - ANC-18 Bulletin, Second Edition, Munitions Board Aircraft Committee, U.S.Dept. of Defence June 1951.

14. Von Karman T. and Tsien H.S. (1941) Buckling of Thin Cylindrical Shells under Axial Compression
J.Ae.Sc. Vol. 8 June 1941

15. Card M.F. (1966) Experiments to Determine the Strength of Filament Wound Cylinders Loaded in Axial Compression
NASA TN D-3522 1966.

16. Herring H.W;Baucom R.M. and Pride R.A. (1968) Mechanical Behaviour of Boron Epoxy and Glass Epoxy Filament Wound Cylinders under Various Loads
NASA TN D-5050 (1968).

17. Ambartsumyan S.A.(1964) Theory of Anisotropic Shells
NASA TT-F-118 1964.

18. Dow N.F. & Rosen B.W. (1966) Structural Efficiency of Orthotropic Cylindrical Shells Subjected to Axial Compression.
AIAA Journal Vol. 4 No. 3 1966.

19. Donnell L.H. (1933) Stability of Thin Walled Tubes under Torsion.
NACA Report No. 479 1933.

20. Batdorf S.B., Stein M. and Schilderout, M. (1943) Critical Stress of Thin-Walled Cylinders in Torsion
NASA TN D-4878 1943.

21. Crate, H., Batdorf S.B. and Baab, G.W. (1944) The Effect of Internal Pressure on the Buckling Stress of Thin Walled Circular Cylinders under Torsion. NACA ARR NO. L4E27 (1944).

22. Zender G.W. and Dexter H.B. (1968) Compressive Properties and Column Efficiency of Metals Reinforced on the Surface with Bonded Filaments. NASA TN D-4878 1968.

23. Timoshenko S.P.(1944) Theory of Plates and Shells McGraw-Hill Book Company Inc. 1944.

24. Hetényi M. (1950) Handbook of Experimental Stress Analysis Wiley & Sons Inc. 1950.

25. Smithells C.J. Metals Reference Book Volume III Butterworths. 1967.

26. Kaye G.W.C. & Laby T.H. Tables of Physical and Chemical Constants. Longmans 1959.

Appendix 1 Cheese Braking Unit

The design requirement of the brake unit is to provide a constant tension in the rovings as they are drawn from the cheese.

The glass cheese together with a brake drum is keyed to a shaft free to rotate under the pull of the tension in the roving as it is unwound from the cheese

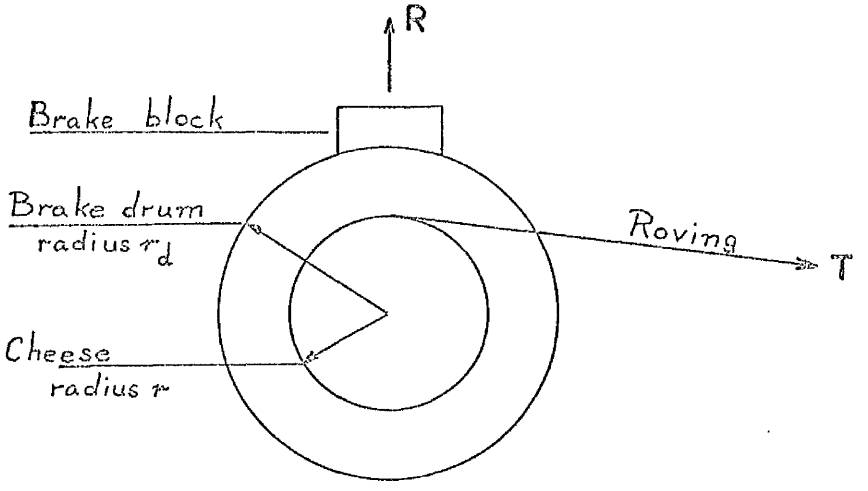

Notation

r_o = initial radius of cheese.

r = radius of cheese at any instant of time.

r_d = radius of brake drum.

T = tension in roving.

R = normal reaction at brake block.

F = brake torque: spring force.

μ = brake coefficient of friction.

Considering this system, the equation of motion is

$$Tr - F = I\ddot{\theta} \qquad (A1 - 1)$$

where I is the moment of inertia and $\ddot{\theta}$ is the angular acceleration. As $I\ddot{\theta}$ is very small in the present case, equation A1 - 1 may be

written as

$$Tr = F = \mu R r_d \qquad (A1\text{-}2)$$

For the design requirement of constant tension T, we have, therefore

$$R = \frac{T}{\mu} \cdot \frac{r}{r_d} \qquad (A1 - 3)$$

Initially, where $r = r_o$, the normal reaction at the brake block is

$$R = R_o = \frac{T}{\mu} \frac{r_o}{r_d} \qquad (A1 - 4)$$

and as glass is unwound, at any subsequent instant from equation A1 - 3 we have

$$R = \frac{T}{\mu} \cdot \frac{r_o}{r_d} - \frac{T}{\mu} \frac{(r_o - r)}{r_d}$$

$$= R_o - \frac{T}{\mu} \frac{(r_o - r)}{r_d} \qquad (A1 - 5)$$

Therefore, to maintain a constant tension T in the filaments, a force $\frac{T}{\mu} \frac{r_o - r}{r_d}$ must be applied at the brake mechanism to diminish R_o as the radius of the cheese, r diminishes.

A linkage system is arranged for this purpose.

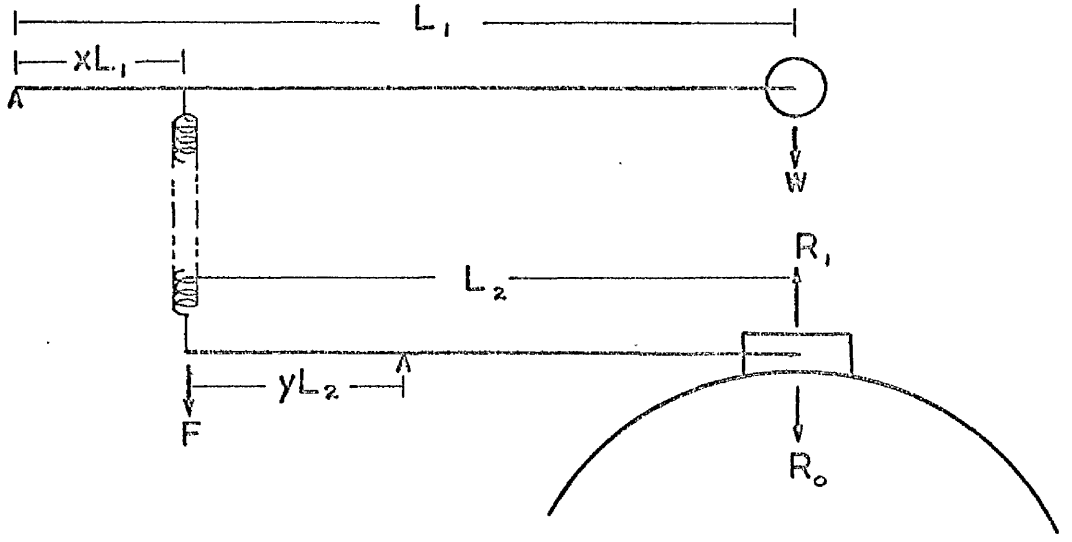

A roller of weight, w rests on the surface of the glass cheese at all times and is connected through the levers, of length L_1 and L_2 to the brake block. R_1 is the force applied through the linkage to the brake block by the roller at the instant when the radius of the cheese is r. Accordingly,

$$R_1 (1 - y) = Fy \qquad (A1 - 6)$$

where F is the force transmitted from the roller lever arm to the block lever arm.

If this force F is applied by a compression spring $F = k_s \Delta$ where k_s is the spring constant and Δ is the deflection of the roller arm at the spring.

Since the commencement of winding, the roller has lowered a distance $(r_o - r)$, therefore

$$\Delta = (r_o - r)\, x$$

$$\text{and} \quad F = k_s (r_o - r)\, x \qquad (A1 - 7)$$

Hence from A1 - 6, $R_1 = k_s \cdot \frac{x\, y}{1 - y} (r_o - r)$ (A1 - 8)

From equation A1 - 5, to provide a constant tension T, R_1 must equal $\frac{T}{\mu} \left(\frac{r_o - r}{r_d}\right)$ and hence $k_s = \frac{T}{\mu r_d} \cdot \frac{1 - y}{xy}$ (A1 - 9)

The required value of k_s can now be determined from equation A1 - 9.

To ensure that the roller stays in contact with the surface of the glass cheese at all times, its weight w must be greater than or equal to the maximum force reacted by the spring. This occurs when r is equal to the inner (or spool) radius r_i of the cheese. Thus we must have, ignoring the weights of the levers and spring, which are small in comparison,

$$w L_1 \geq k_s (r_o - r_i) x . x L_1$$

i.e. $$w \geq k_s (r_o - r_i) x^2 \qquad (A1 - 10)$$

A similar arrangement can be made with a tension spring in the place of the compression spring. In this case, the values of R_o and w have to be increased by amounts $\frac{f y}{1 - y}$ and f x respectively to provide the spring initial tension load f and apply net forces of R_o and w at the brake and cheese as before.

The requirement for an interconnecting spring between the lever arms may be shown by consideration of an inextensional link in place of the spring. In this case, as before

$$R_1 (1 - y) = Fy \qquad (A1 - 6)$$

but F is determined by the relation

$$w = F x \qquad (A 1 - 11)$$

Hence for a constant value of T, from equation A1 - 5, 6 and 11,

$w = \frac{T}{\mu} \frac{(r_o - r)}{r_d} \frac{x}{y} (1 - y)$ would have to vary with r, a much more involved arrangement to be made feasible in practice.

From equations A1 - 9 and A1 - 10, and geometrical considerations, the values of k_s, y and $\frac{L_2}{L_1}$ may be expressed in terms of x or alternatively, for any one spring constant k_s and tension T,

$$x \leq \sqrt{\frac{w}{(r_o - r_i)k_s}}$$

$$\frac{L_2}{L_1} \geq 1 - x = 1 - \sqrt{\frac{w}{(r_o - r_i)k_s}}$$

$$y \geq \frac{T}{T + \mu r_d \sqrt{\frac{w k_s}{r_o - r_i}}}$$

A linkage mechanism of this form using an extension spring was designed and fitted to the six cheese shafts on the machine. The mechanism is visible in Figure 26. On the machine

$L_1 = 4"$

$L_2 = 3.2"$

$r_d = 3"$

$k_s = 10.615$ lb/in

$(w + fx) = 1$ lb

The initial brake block load ($= R_o + \frac{f\,y}{1 - y}$) is applied by a compression spring, manually adjustable for initial tension loading of the roving. The pivot point on the roller arm may be adjusted between the positions where $y = 0.15$ and $y = 0.75$. A constant value of T may then be obtained in the range 0.75lb to 12.25lb. For the 12 end roving used, this permits the application of up to 1lb of tension per end.

Appendix 2 A Study of the Winding Pattern at the Ends of Carriage Traverse to Determine Total Time Delay.

Apart from any initial delay period at the end of the mandrel at the start of the winding process required to "anchor" the ends of the roving band before commencing to wind helically at an angle α_o in each direction of travel, the delay times for each end will be equal and depend on the angle of wind α_o and various machine dimensions. The desired delay will be that sufficient to lock the wind just finished and to position the rovings correctly for the next wind so that the desired pattern is achieved without undue build-up of wall thickness at each end of the tube. As can be seen from the diagram of the idealised pattern,

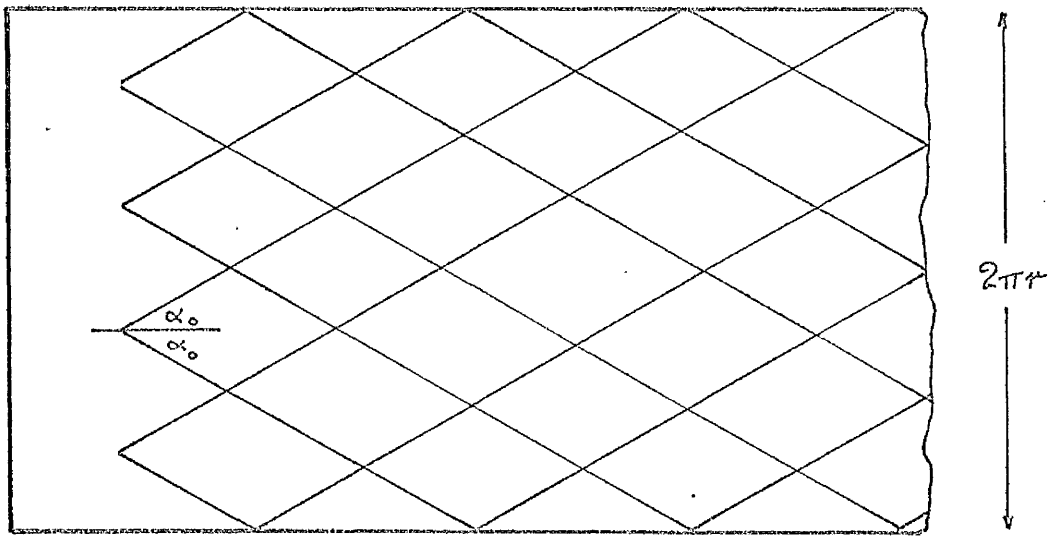

Fig. 1

the sudden change of angle from $+\alpha_o$ to $-\alpha_o$ without a delay time will cause slippage of the roving. The required delay time is that with which the roving, on returning from the end of the tube, will be laid alongside the previous wind as shown overleaf.

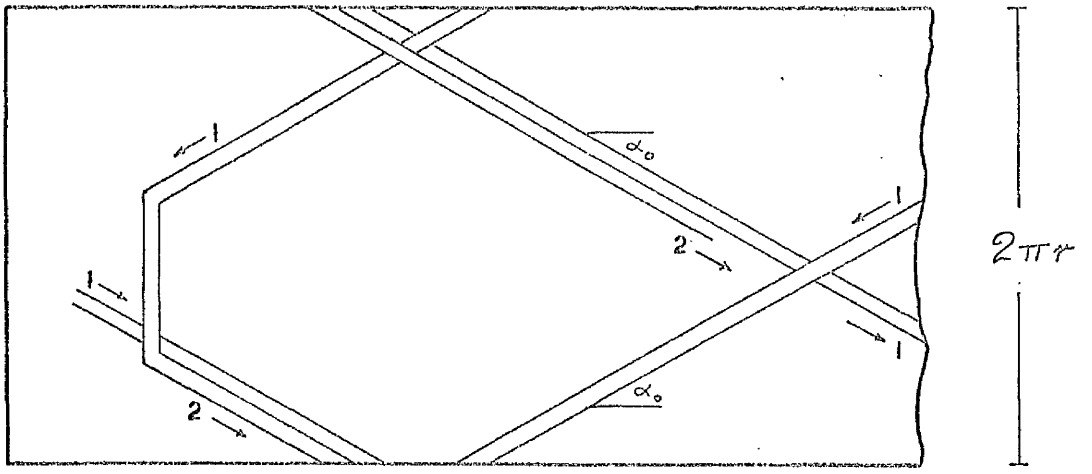

Fig. II

The delay will be made up of two parts.

When the carriage reaches the end of its travel, it will have a lead over the point of contact of the roving on the mandrel surface. During the first part of the delay T_1, the instantaneous value of the angle of wind α will increase from α_o to $\frac{\pi}{2}$ while the roving follows a path over the mandrel surface to eliminate the carriage lead and bring the point of contact in line with the centre-line of the impregnation bath and the end of the mandrel. The second part of the delay, T_2, holds the carriage stationary while the mandrel rotates through the further angle required to bring the point of contact of the roving band to the correct position for the start of the return pass.

Notations

a	distance in X - direction between final guide and point P_1 on mandrel surface.
l	mandrel length.
m	number of mandrel revolutions wound at helical angle α_o.
n	integer number of traverses of carriage.
n_m	mandrel speed (r.p.m.)
r	mandrel radius.

w	roving band width.
z	distance in Z direction between instantaneous points P and P_2.
Z_o	distance in Z direction between points P_1 and P_2.
D	circumferential delay distance.
N	integer number of mandrel revolutions.
P	instantaneous point of contact of roving band on mandrel surface between points P_1 and P_2.
P_1	instantaneous point of contact of roving band on mandrel surface at end of winding at $\alpha = \alpha_o$.
P_2	instantaneous point of contact of roving band on mandrel surface at end of mandrel when $\alpha = \frac{\pi}{2}$.
T	total delay time.
T_1	delay time during which angle of wind increases from $\alpha = \alpha_o$ to $\alpha = \frac{\pi}{2}$.
T_2	delay time required to hold roving pattern at end and place in position for the start of the carriage return pass.
X,Y,Z	axis directions.
α	angle of wind at any instant during delay T_1.
α_o	desired helical angle of wind on mandrel.
Δ	small increment.
ϕ	rotational angle turned through by mandrel.
θ	small angle defined in text.

Part 1. To determine T_1

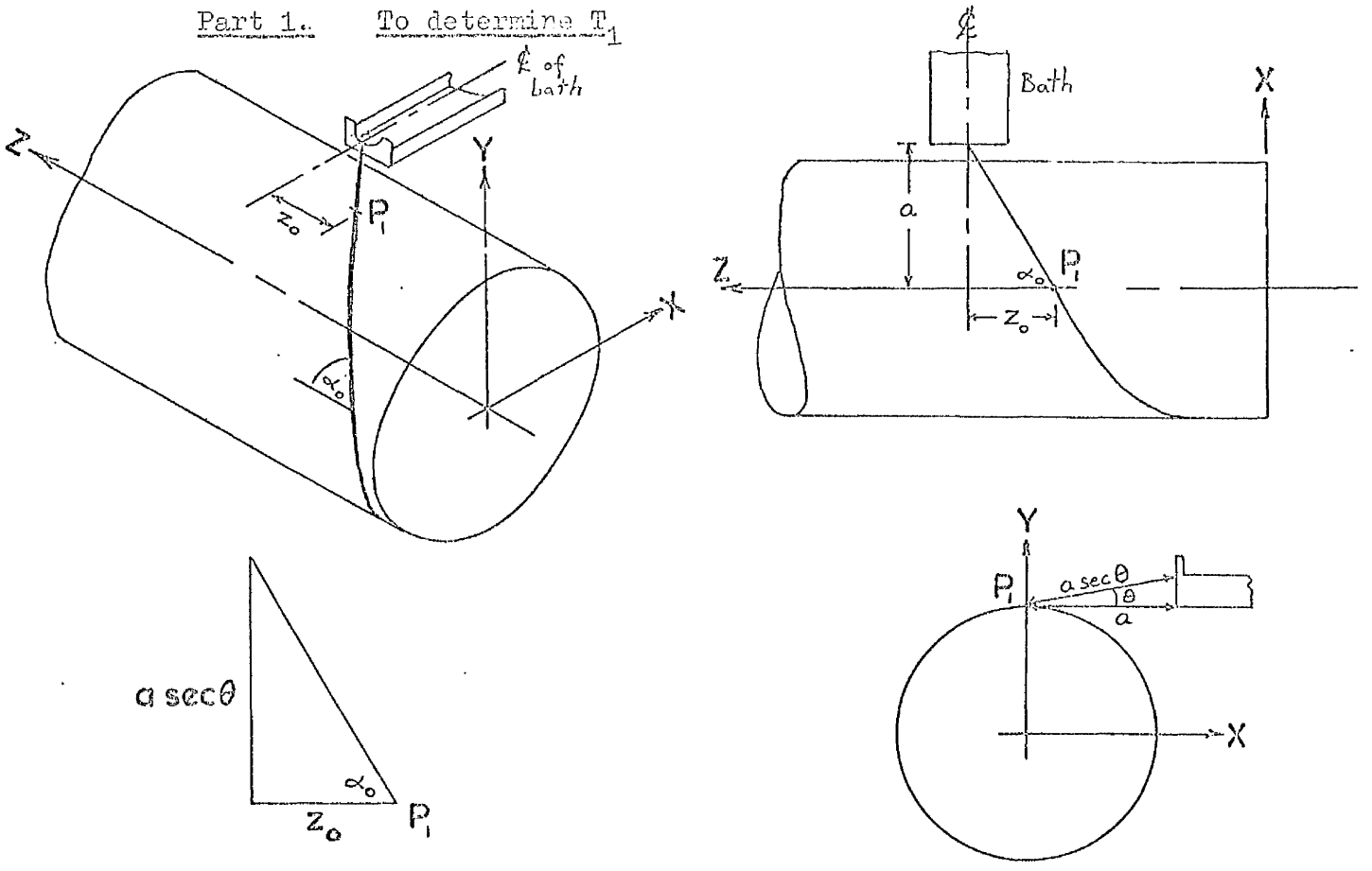

Fig III

Let the final guide lie at a distance 'a' in the X - direction from the line parallel to the Z - axis through the instantaneous point of contact of the rovings on the surface of the mandrel. Let θ be the small angle between the final guide and the plane Y = r through the point of contact (which may be assumed to lie vertically above the mandrel axis (Z axis) since θ is small). Let z_o be the carriage lead distance, i.e. the distance along the mandrel axial (Z -) direction between the final guide centreline and the point of contact of the rovings on the mandrel surface. Let α_o be the angle of helical winding on the mandrel. Then when the

carriage reaches the end of its travel, it will be the distance z_o ahead of the point of contact P_1 as shown in figure III where

$$z_o = a \sec\theta \cot\alpha_o \qquad (A2 - 1)$$

During the delay T_1, while the mandrel rotates through an angle ϕ_1, this lead distance z_o is eliminated by the roving band following a path on the mandrel such that the angle of wind α increases from the value α_o at point P_1 to the value $\frac{\pi}{2}$ at the point P_2 in line with the centreline of the final guide where the roving band lies tangential to the end of the mandrel.

Using a co-ordinate system $r\phi$ and Z on the surface with "zero point" at P_2, this roving path over the surface of the mandrel takes the form shown in figure IV.

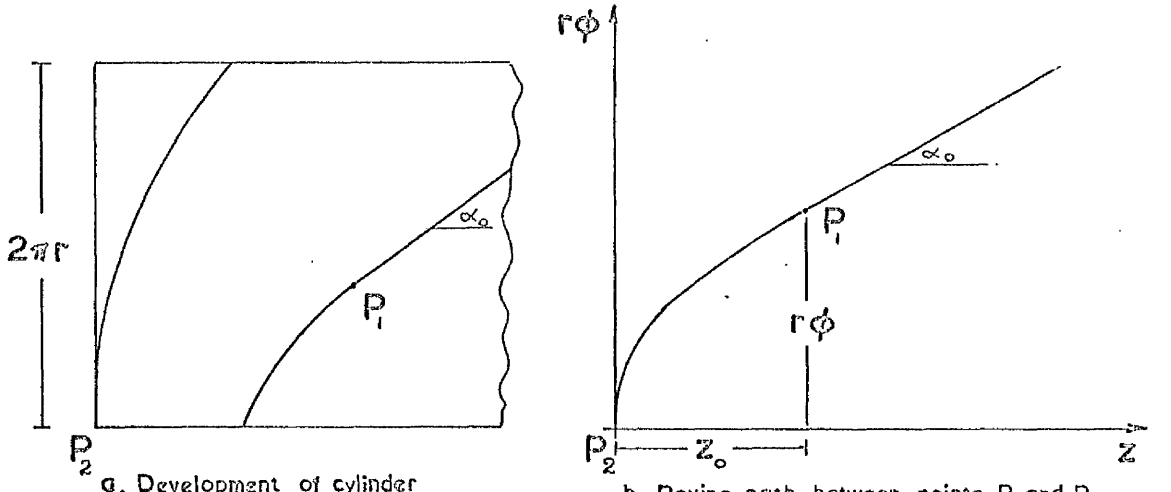

a. Development of cylinder

b. Roving path between points P_1 and P_2

Fig. IV

Where n_m and r are the mandrel rotational speed and radius respectively,

$$r\phi_1 = 2\pi r \frac{n_m}{60} \cdot T_1 \qquad (A2 - 2)$$

where delay time T_1 is measured in seconds.

Consider plot of $r\phi$ vs. z between P_1 and P_2 for any angle of helical wind α_o. Figure IV b below.

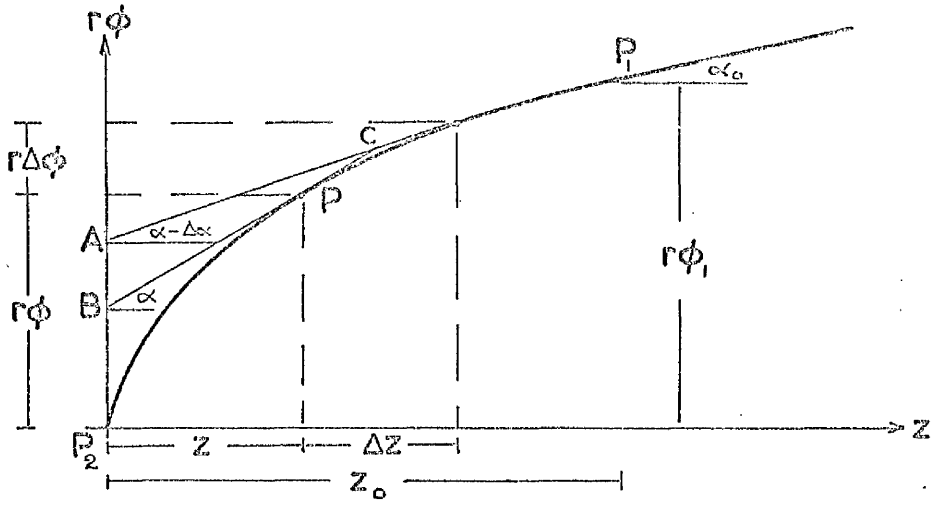

Fig. IV b (Enlarged)

At any instant when roving point of contact is P $(r\phi, z)$ when the instantaneous value of the angle of wind is α.

$$r = P_2B + z \tan \alpha.$$

An increment $r\Delta\phi$ (r constant for a cylinder) later,

$$r(\phi + \Delta\phi) = P_2B + BA + (z + \Delta z) \tan (\alpha - \Delta\alpha)$$

Now at point P, from equation A2 - 1; $z = a \sec \theta \cot \alpha$

$$\therefore \quad r\phi = P_2B + a \sec\theta$$

and similarly $(z + \Delta z) = a \sec \theta \cot (\alpha - \Delta\alpha)$

$$\therefore \quad r(\phi + \Delta\phi) = P_2B + BA + a \sec\theta$$

$$\therefore \quad r\Delta\phi = BA$$

Considering the triangle ABC for small increments tending to 0, the following relation holds, $\dfrac{BA}{\sin \Delta\alpha} = \dfrac{BC}{\sin [90 + (\alpha - \Delta\alpha)]}$

where BC tends to the value $\dfrac{z}{\cos \alpha}$ as Δz tends to zero.

Hence $\Delta\phi = \dfrac{z}{r} \dfrac{\sin \Delta \alpha}{\cos \alpha \cos(\alpha - \Delta\alpha)}$

$$= \frac{a \sec \theta \cot \alpha \sec^2 \alpha \, \Delta\alpha}{r\,(1 + \tan \alpha \, \Delta\alpha)} \qquad (A2 - 3)$$

making the usual approximation for small angles that $\tan \Delta\alpha = \Delta\alpha$.

A plot may be made of ϕ using equation A2 - 3 starting with the known value of $\phi = 0$ when $\alpha = \frac{\pi}{2}$ and using the value of $\tan \alpha$ at $\alpha = 89.999^{\circ}$ to generate the initial value for $\Delta\phi$. Rest of the points on the graph may be found by a step by step method. Figure 27.

Using the value of ϕ obtained in this way for any angle of wind $\alpha = \alpha_o$, the delay time T_1 may be calculated using equation A2 - 2.

Part 2 To determine T_2

It is required to estimate the delay necessary so that at the end of each traverse, the commencement of the next traverse positions the rovings alongside the previous wind as shown in figure II. This implies that at the start of any traverse (other than the first), mandrel has rotated $(N + \frac{w \sec \alpha_o}{2\pi r})$ revolutions since the commencement of the $(n - 1)^{th}$ traverse, where N is an integer number of revolutions and $\frac{w \sec \alpha_o}{2\pi r}$ is that part of a revolution necessary to effect a shift of one band width 'w' in the placing of the rovings.

Consider now the traverse of the carriage, where by 'traverse' we mean one complete to and fro movement along the mandrel length. (i.e. 1 traverse ≡ 2 passes). In the pass in one direction, rotational angle passed through by mandrel is $\phi_1 + 2m\pi + \phi_1$ where ϕ_1 is defined earlier in part 1, and m is number of revolutions

wound at α_o given by $m = \frac{l - 2z_o}{2\pi r} \tan \alpha_o$ where l is mandrel length and z_o is the carriage lead distance applicable to angle of wind α_o, as defined in Part I. Then the delay T_2 occurs with the carriage held stationary still to position the rovings correctly for the return pass, while during this the mandrel rotates through an angle $\frac{D}{r}$. The carriage then commences return pass, during which, assuming return pass is also winding at angle α_o, the mandrel rotates a further $(\phi_1 + 2m\pi + \phi_1)$ radians, after which a second delay T_2 occurs during which mandrel rotates $\frac{D}{r}$. Note that if a pattern was being wound with unequal values of α_o on outward and return passes, these expressions would have to be $(2\phi_1 + 2m_1\pi r)$ radians, followed by a delay $\frac{D_1}{r}$ radians, on the outward leg and then $(2\phi_2 + 2m_2\pi r)$ radians followed by a delay $\frac{D_2}{r}$ radians, on the return leg. Beyond introducing additional terms, analysis is the same as for the equal angle of wind case detailed.

Thinking in terms of the circumferential distance $(r\phi)$, rather than the rotational angles 'ϕ' turned by the mandrel, and taking commencement of first wind as 'zero' on the developed circumferential $r\phi$ scale, the start of the return pass is at the point $(r\phi)_{11} = 2(r\phi_1) + 2\pi mr + D$. The start of the 2nd traverse is at point $(r\phi)_2 = 4\, r\phi_1 + 4\pi mr + 2D$ and so on. Thus all points of the wind can be calculated in this manner and if the starting points of the outward passes are denoted by a single suffix and those of the return passes by a double suffix we have, in general terms,

$$(r\phi)_n = (4n - 4)\, r\phi_1 + (4n - 4)\pi mr + (2n - 2)D$$

$$(r\phi)_{nn} = (4n - 2)r\phi_1 + (4n - 2)\pi mr + (2n - 1)D$$

The circumferential distance between the starting points of the n^{th} and $(n-1)^{th}$ traverse at each end of mandrel is thus

$$4r\phi_1 + 4\pi mr + 2D \quad \text{for } n \geq 2 \quad m \geq 2. \qquad (A2-4)$$

In a similar manner, for unequal wind angles, the circumferential distance would be

$$2r\phi_1 + 2\pi m_1 r + 2r\phi_2 + 2\pi m_2 r + D_1 + D_2 \qquad (A2-4a)$$

Now, we have seen that at the start of each pass, for the roving to be laid alongside the previous start and to lock the previous band in position, the mandrel must have rotated $(N + \frac{w \sec \alpha_o}{2\pi r})$ revolutions, i.e. a circumferential scale distance of $(2\pi rN + w \sec \alpha_o)$.

Thus $4r\phi_1 + 4\pi rm + 2D = N.2\pi r + w \sec \alpha_o$

where N is first integer such that $2\pi rN - \{(r\phi)_n - (r\phi)_{n-1}\}$ is positive.

$$\therefore D = \pi r(N + \frac{w \sec \alpha_o}{2\pi r} - \frac{2\phi_1}{\pi} - 2m)$$

and expanding m,

$$= \pi rN + \frac{w}{2} \sec \alpha_o + 2a \sec\theta - 2r\phi_1 - l \tan \alpha_o$$

where N is first integer $> \frac{1}{\pi}(2\phi_1 + \frac{l}{r} \tan \alpha_o - \frac{2a}{r} \sec \theta)$.

$\therefore$ Time delay T_2 to be added to that required to eliminate carriage lead over roving tangent point, T_1, is given by

$$T_2 = \frac{D}{2\pi r} \times \frac{60}{n_m} \text{ seconds where } n_m \text{ is mandrel r.p.m.}$$

Now it is obvious that on many occasions the calculated value of D will not be an optimum value in practise, although it is the value ensuring a single start pattern. Two cases are possible. If the tangent point P_2 is too near the desired starting point of

the next traverse, D would be inadequate to ensure a lock on the previous wind is obtained (where experience suggests minimum required of order $\frac{D}{r} = \frac{\pi}{2}$ radians). In this case a submultiple 2n of a revolution can be added where n is the integer number of traverses necessary to regain initial start position. The calculated value of D should however be diminished by $\frac{n-1}{n} \cdot \frac{w \sec \alpha_o}{2}$ so that the start point of each traverse advances $(N + \frac{1}{n}) 2\pi r + \frac{w \sec \alpha_o}{n}$ and hence after n traverses, the start point has advanced $(n \times N + 1)2\pi r + w \sec \alpha_o$ and roving is laid alongside the original path.

Similarly if the delay is too large, so that excessive build-up of the wall thickness occurs at each end of the travel, a sub-multiple 2n of a revolution can be subtracted but 'D' in this case should still be diminished by $\frac{n-1}{n} \cdot \frac{w \sec \alpha_o}{2}$ so that each start point now advances $(N - \frac{1}{n})2\pi r + \frac{w \sec \alpha_o}{n}$. Thus after n traverses, start point is advanced $(n \times N - 1)2\pi r + w \sec \alpha_o$ so that roving is laid alongside original path.

For example: suppose D proves too small, then where $D = \pi r N + \frac{w \sec \alpha_o}{2} - 2r\phi_1 - 2\pi rm + \frac{1}{2n} \cdot 2\pi r - (\frac{n-1}{n}) \frac{w \sec \alpha_o}{2}$

the start points $(r\phi)_\eta$ and $(r\phi)_{\eta\eta}$ at either end of the travel are given by:-

$$(r\phi)_1 = 0$$

$$(r\phi)_{11} = \pi rN + \frac{\pi r}{n} + \frac{w \sec \alpha_o}{2} \cdot \frac{1}{n}$$

$$(r\phi)_2 = 2\pi r \left(N + \frac{1}{n}\right) + w \sec \alpha_o \cdot \frac{1}{n}$$

$$(r\phi)_{22} = 3\pi r \left(N + \frac{1}{n}\right) + \frac{3 w \sec \alpha_o}{2} \cdot \frac{1}{n}$$

$$(r\phi)_3 = 4\pi r\left(N + \frac{1}{n}\right) + 2\ w \sec \alpha_o \cdot \frac{1}{n}$$

$$(r\phi)_{33} = 5\pi r\left(N + \frac{1}{n}\right) + \frac{5}{2}\ w \sec \alpha_o \cdot \frac{1}{n}$$

Generally, $(r\phi)_{\eta+1} = 2\eta\pi r\left(N + \frac{1}{n}\right) + \frac{\eta}{n}\ w \sec \alpha_o$

$$(r\phi)_{(\eta+1)bis} = (2\eta + 1)\ \pi r\left(N + \frac{1}{n}\right) + \frac{2\eta + 1}{2n}\ w \sec \alpha_o$$

When $\eta = n$

$$(r\phi)_{n+1} = 2n\ \pi r\left(N + \frac{1}{n}\right) + w \sec \alpha_o$$

$$(r\phi)_{(n+1)bis} = (2n + 1)\pi r\left(N + \frac{1}{n}\right) + \frac{(2n+1)}{2n} \cdot w \sec \alpha_o$$

both of which are $2n.\pi r\left(N + \frac{1}{n}\right) + w \sec \alpha_o$ advanced on the start positions at each end of first traverse. Now this, as n and N are integers, still gives the desired result, after n starts, of a pattern being laid that is placed alongside that previously laid.

From parts 1 and 2, the total delay time T is now seen to be

$$T = T_1 + T_2$$

$$= \frac{30\,\phi_1}{\pi\, n_m} + \frac{30\ D}{\pi r\ n_m} \quad \text{seconds}$$

$$= \frac{30}{\pi\, n_m}\left(\phi_1 + \frac{D}{r}\right) \text{ seconds}$$

A logarithmic plot of delay time against mandrel rotational speed may be made for each angle of wind α_o. In conjunction with Figure 13, this may be used to aid selection of a suitable winding rate.

An example of such a plot has been made for a few angles α_o for the two cases of a $\frac{1}{4}$ revolution and $\frac{1}{2}$ revolution locking rotation at each end, for the case of a 22" long tube of 2" radius and a roving band width of $\frac{5}{32}$" Figure 28(a) and (b).

APPENDIX 3 A Study to Determine the Strain Difference Between a Bonded Resistance Wire and the Basic Material.

Assuming that the resin layer carries no load, the strain is transferred into the wire by the transfer of shear through the resin layer, and the following study may be made.

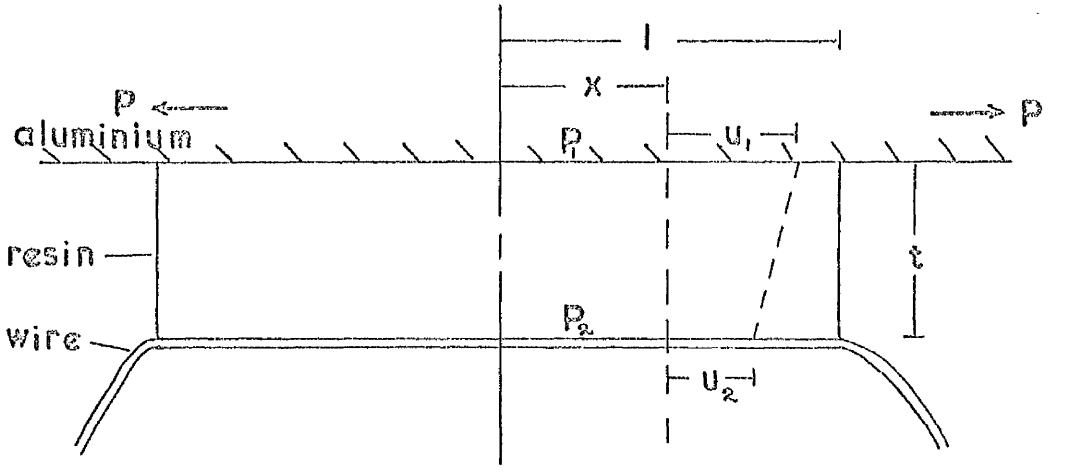

Let subscripts 1 and 2 refer to the aluminium and wire respectively.

Let P be the applied tensile load

τ the shear stress in the resin

G the shear modulus of the resin

E Young's Modulus

A cross sectional area

b the effective breadth of the resin layer in shear

d the wire diameter

2l length of wire bonded to the aluminium

u displacement

x distance

ε the tensile strain.

Considering the aluminium under an applied tensile load P, the theoretically calculated strain $\varepsilon_1 = \frac{P}{A_1 E_1}$. This is the strain the resistance wire is required to measure. If the wire records a resistance change $\frac{\Delta R}{R}$ representing an average strain ε_2, where $\frac{\varepsilon_2}{\varepsilon_1} = Q$ say, then the apparent gauge factor G.F.' of the wire will appear to be G.F.' $= \frac{\Delta R/R}{\varepsilon_2}$ while the true gauge factor G.F. relating this observed value of $\frac{\Delta R}{R}$ to the calculated strain in the aluminium ε_1 wil be G.F. $\frac{\Delta R/R}{\varepsilon_1}$. It is readily apparent that G.F.' $= \frac{1}{Q} \cdot$ G.F. It is the size of this ratio Q we require to estimate for a resin layer thickness t and shear modulus G.

$$\frac{dP_1}{dx} = \tau b \quad ; \qquad \frac{dP_2}{dx} = -\tau b$$

where $P_1 = E_1 A_1 \frac{du_1}{dx}$; $\qquad P_2 = E_2 A_2 \frac{du_2}{dx}$.

$$\tau = \frac{G}{t}(u_1 - u_2).$$

$$\frac{d^2\tau}{dx^2} = \frac{G}{t}\left(\frac{d^2u_1}{dx^2} - \frac{d^2u_2}{dx^2}\right) = \frac{G}{t}\left[\frac{1}{E_1A_1}\frac{dP_1}{dx} - \frac{1}{E_2A_2}\frac{dP_2}{dx}\right]$$

$$= \frac{Gb}{t}\left(\frac{1}{E_1 A_1} + \frac{1}{E_2 A_2}\right)\tau$$

i.e. $\frac{d^2\tau}{dx^2} - \mu^2\tau = 0$ where $\mu^2 = \frac{Gb}{t}\left(\frac{1}{E_1 A_1} + \frac{1}{E_2 A_2}\right)$ (A3 - 1)

solution is of form $\tau = C_1 \cosh \mu x + C_2 \sinh \mu x$.

Boundary conditions.

at $x = 0$, $\tau = 0$, $\therefore C_1 = 0$ and $\tau = C_2 \sinh \mu x$.

at $x = l$, $P_2 = 0$, $P_1 = P$

$$\therefore \frac{d\tau}{dx} = C_2 \mu \cosh \mu x = \frac{G}{t}\left(\frac{du_1}{dx} - \frac{du_2}{dx}\right) = \frac{G}{t}\left(\frac{P_1}{E_1A_1} - \frac{P_2}{E_2A_2}\right)$$

$$\therefore C_2 \mu \cosh \mu l = \frac{G P}{t E_1 A_1}$$

and hence $$\tau = \frac{G P}{\mu t E_1 A_1} \cdot \frac{\sinh \mu x}{\cosh \mu l} . \qquad (A3 - 2)$$

$$P_1 = \int \tau b \, dx = \frac{G P b}{\mu^2 t E_1 A_1} \cdot \frac{\cosh \mu x}{\cosh \mu l} + C_3 .$$

at $x = l$, $P_1 = P$ and so $$P_1 = P\left[\frac{G b}{\mu^2 t E_1 A_1} \left(\frac{\cosh \mu x}{\cosh \mu l} - 1\right) + 1 \right] \qquad (A3 - 3)$$

$$P_2 = -\int \tau b \, dx = -\frac{G P b}{\mu^2 t E_1 A_1} \cdot \frac{\cosh \mu x}{\cosh \mu l} + C_4 .$$

at $x = l$, $P_2 = 0$ $\qquad \therefore C_4 = \frac{G P b}{\mu^2 t E_1 A_1}$

$$\therefore P_2 = P \left[\frac{G b}{\mu^2 t E_1 A_1} \left(1 - \frac{\cosh \mu x}{\cosh \mu l}\right) \right] \qquad (A3 - 4)$$

and $P = P_1 + P_2$ as required by assumption that resin layer carries no end load. This assumption demands that the same breadth b be applied to the equilibrium equations for the aluminium and wire to permit $P = P_1 + P_2$ to be satisfied for all x.

$$u_2 = \int \frac{P_2}{E_2 A_2} dx = \frac{G b P}{\mu^2 t E_1 A_1 E_2 A_2} \left[x - \frac{\sinh \mu x}{\cosh \mu l} \right] + C_5 .$$

At $x = 0$, $u_2 = 0$ $\qquad \therefore C_5 = 0$

$$\therefore u_2 = \frac{G b P}{\mu^2 t E_1 A_1 E_2 A_2} \left[x - \frac{\sinh \mu x}{\cosh \mu l} \right] \qquad (A3 - 5)$$

$$\text{for } x = l; \quad u_2 = \frac{G b P}{\mu^2 t E_1 A_1 E_2 A_2} \left[l - \frac{\sinh \mu l}{\cosh \mu l} \right] . \qquad (A3 - 6)$$

$$u_1 = \int \frac{P_1}{E_1 A_1} dx = \frac{P}{E_1 A_1} \left[\frac{G b}{\mu^2 t E_1 A_1} \left(\frac{\sinh \mu x}{\mu \cosh \mu l} - x \right) + x \right] + C_6 .$$

At $x = 0$, $u_1 = 0$ $\therefore$ $C_6 = 0$

$$\therefore \quad u_1 = \frac{P}{E_1 A_1} \left[\frac{G\,b}{\mu^2 t E_1 A_1} \left(\frac{\sinh \mu x}{\mu \cosh \mu l} - x \right) + x \right] \qquad \text{(A3 - 7)}$$

$$\text{for } x = l, \quad u_1 = \frac{P\,G\,b}{\mu^2 t E_1 A_1} \left[\frac{\sinh \mu l}{\mu \cosh \mu l} - l \right] + \frac{P\,l}{E_1 A_1} . \qquad \text{(A3 - 8)}$$

Now the average strain in the wire $\varepsilon_2 = \dfrac{\text{extension } u_2 \text{ at } x = l}{\text{length } l}$

$$\therefore \varepsilon_2 = \frac{u_2}{l} = \frac{G\,b\,P}{\mu^2 t E_1 A_1 E_2 A_2} \left(1 - \frac{\sinh \mu l}{\mu l \cosh \mu l} \right)$$

$$= \frac{P}{E_1 A_1 + E_2 A_2} \left(1 - \frac{\tanh \mu l}{\mu l} \right). \qquad \text{(A3 - 9)}$$

As (μl) increases, $\tanh (\mu l)$ tends to unity, therefore since l is large and A_1 is large compared with A_2,

$$\varepsilon_2 = \frac{P/A_1}{E_1 + E_2 A_2 / A_1} \left(1 - \frac{\sinh \mu l}{\mu l \cosh \mu l} \right)$$

$$\doteq \frac{P}{E_1 A_1} \left(1 - \frac{1}{\mu l} \right) = \varepsilon_1 \left(1 - \frac{1}{\mu l} \right)$$

$$\therefore Q = \frac{\varepsilon_2}{\varepsilon_1} = \left(1 - \frac{1}{\mu l} \right) \qquad \text{(A3 - 10)}$$

Similarly, the average strain in the plate $= \dfrac{u_1}{l}$ may be shown to be

$$= \frac{P}{E_1 A_1} + \frac{P}{E_1 A_1} \cdot \frac{1}{1 + \dfrac{E_1 A_1}{E_2 A_2}} \left(\frac{\sinh \mu l}{\mu l \cosh \mu l} - 1 \right) \doteq \frac{P}{E_1 A_1} \qquad \text{(A3 - 11)}$$

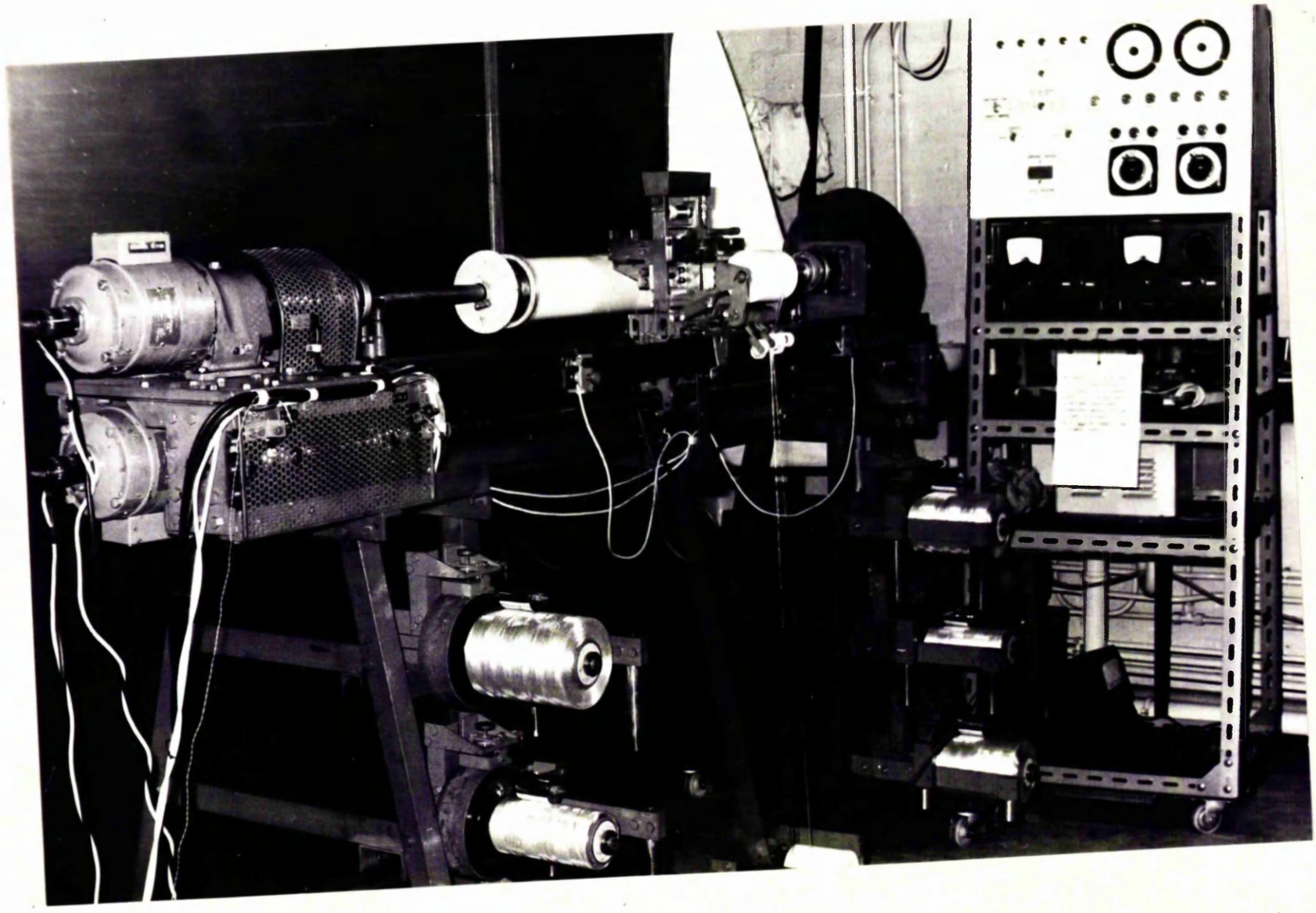

Figure 1: General View of Winding Machine and Control Console.

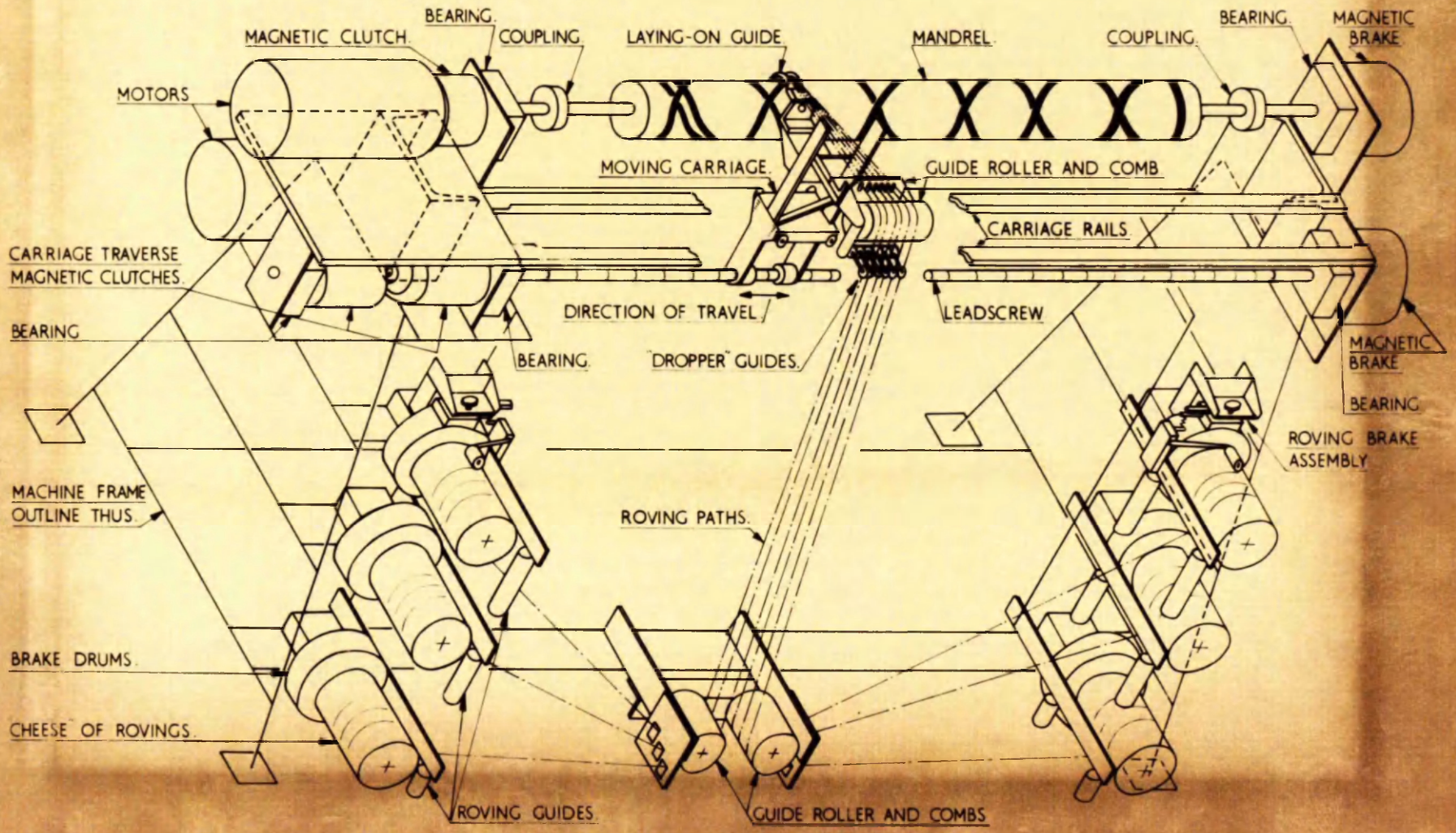

Fig. 2 FILAMENT WINDING MACHINE.

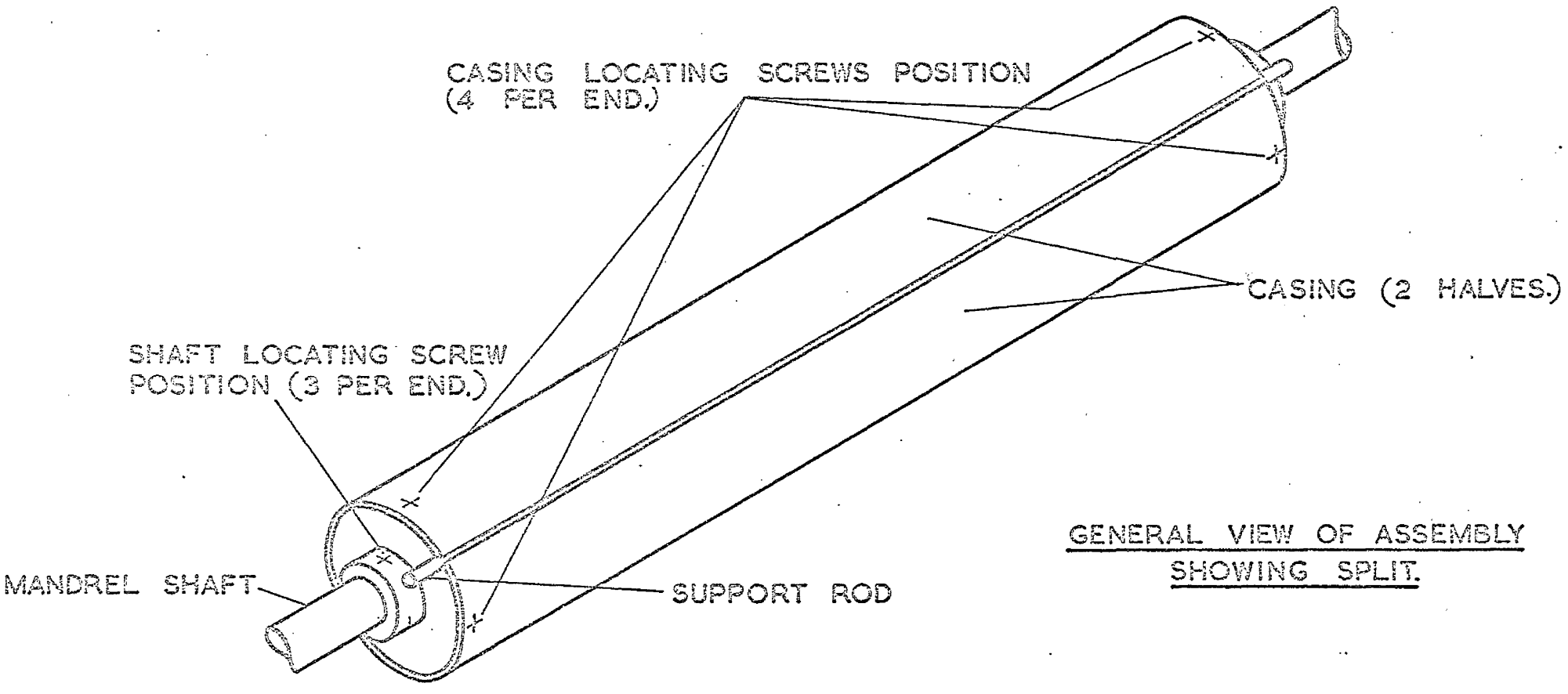

Fig.3a. SPLIT MANDREL ASSEMBLY.

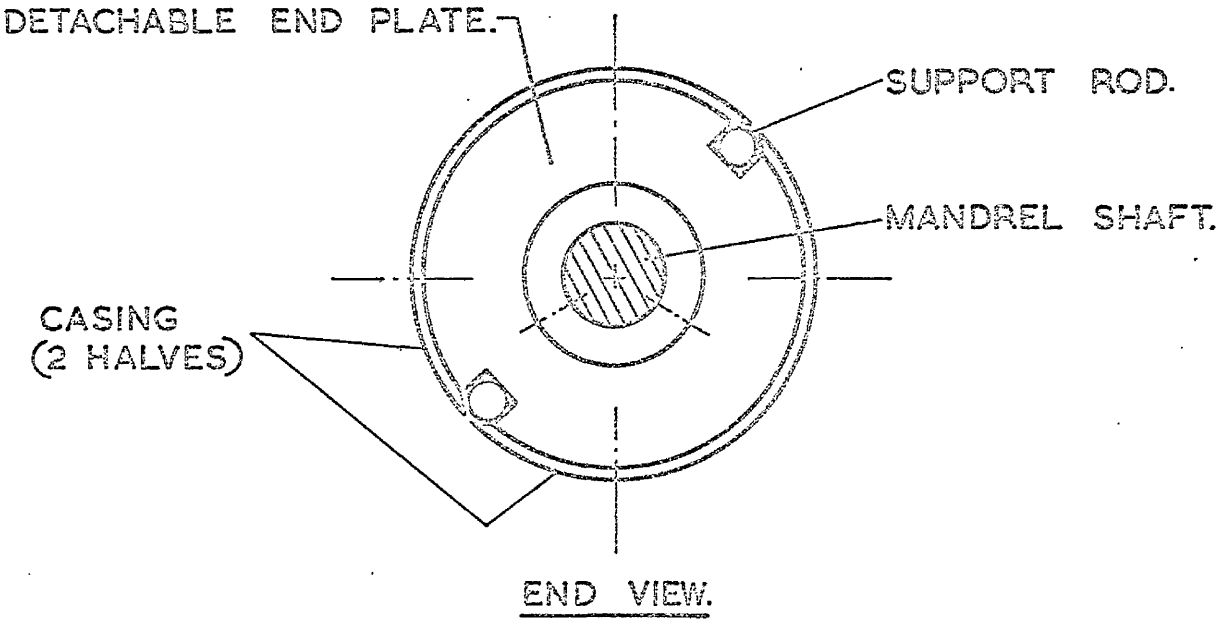

Fig.3b. SPLIT MANDREL ASSEMBLY.

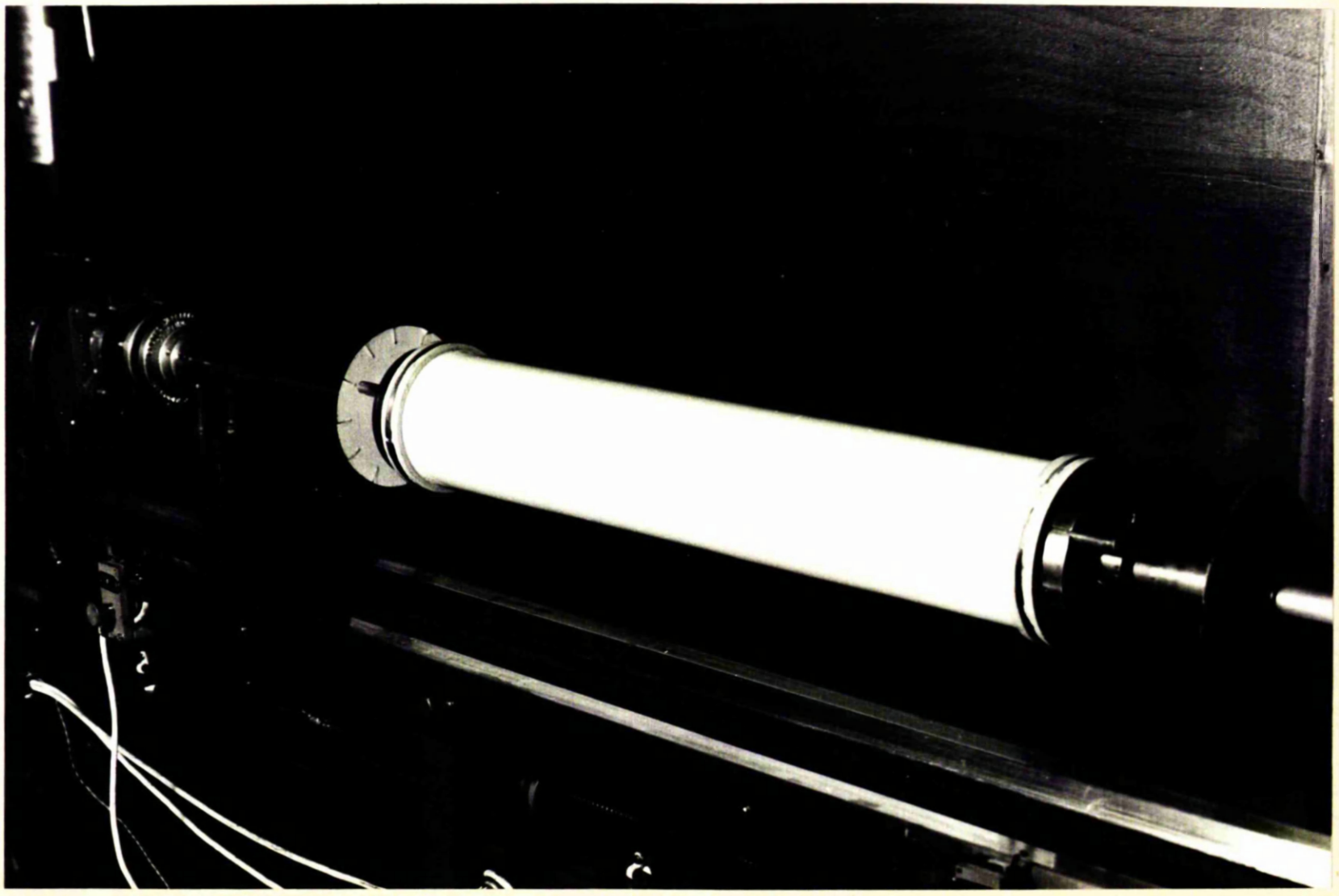

Figure 4: Mandrel Assembly with Melinex Layer and End Rings.

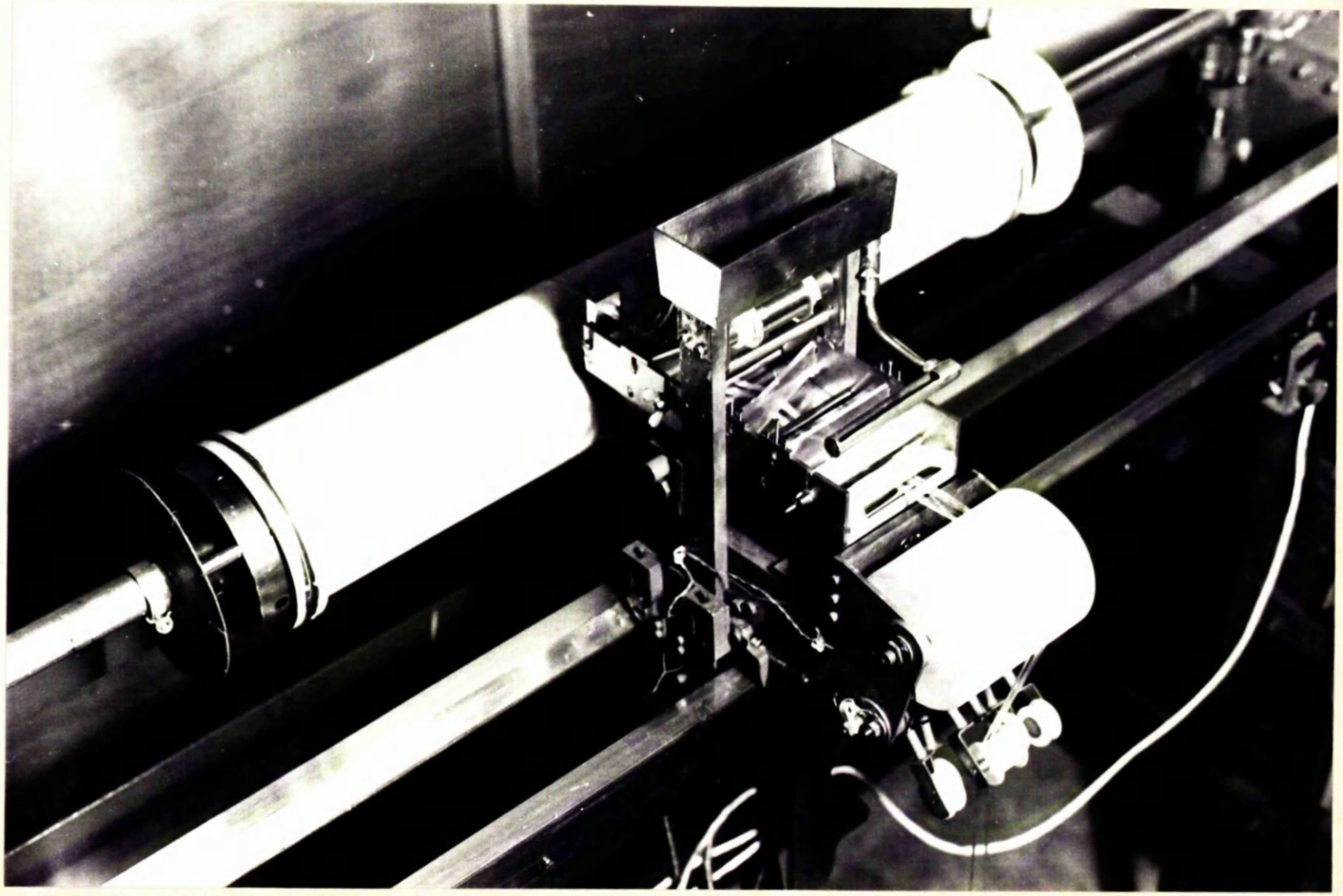

Figure 5: Close-up of Carriage Assembly showing Roving Path.

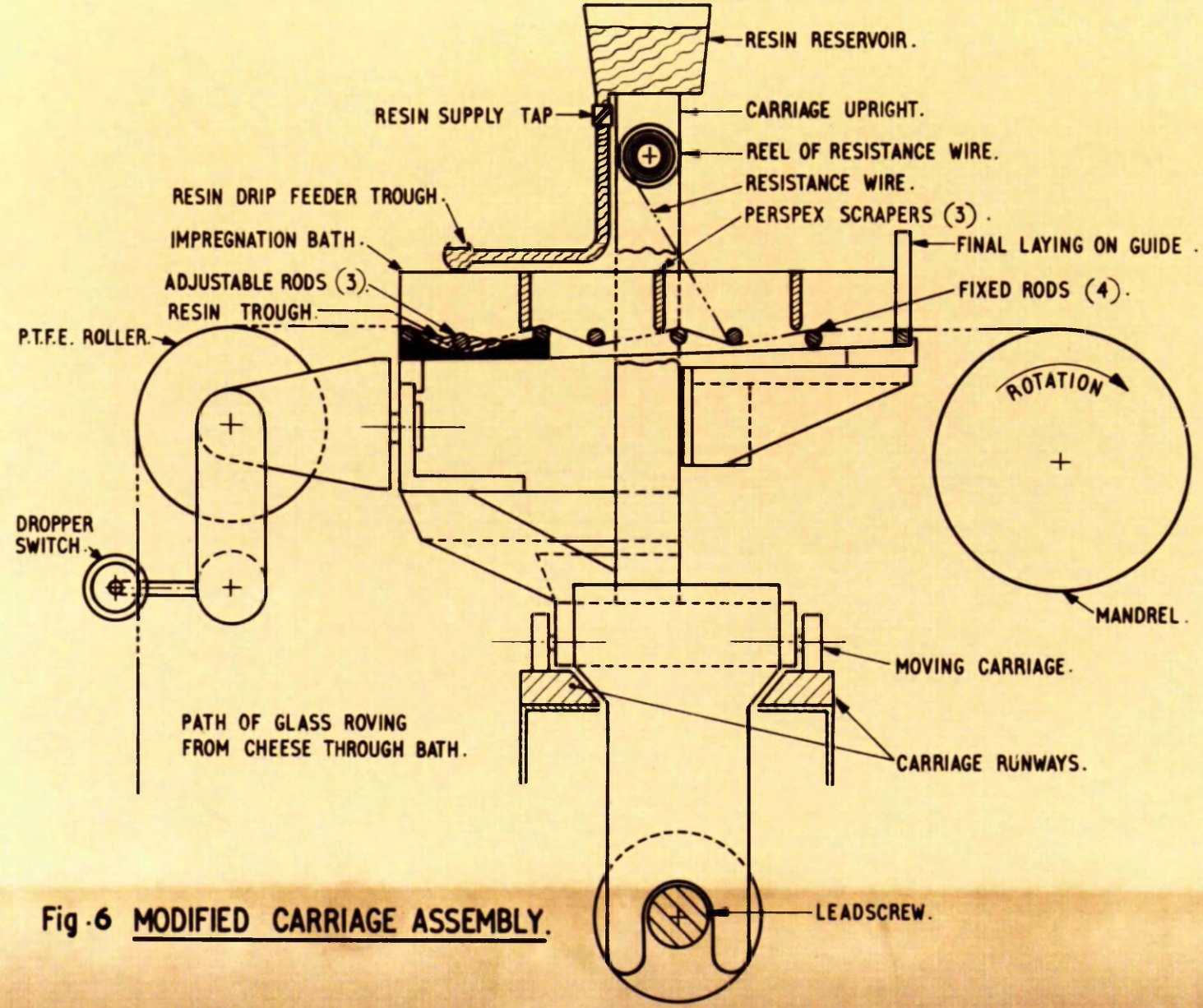

Fig.6 MODIFIED CARRIAGE ASSEMBLY.

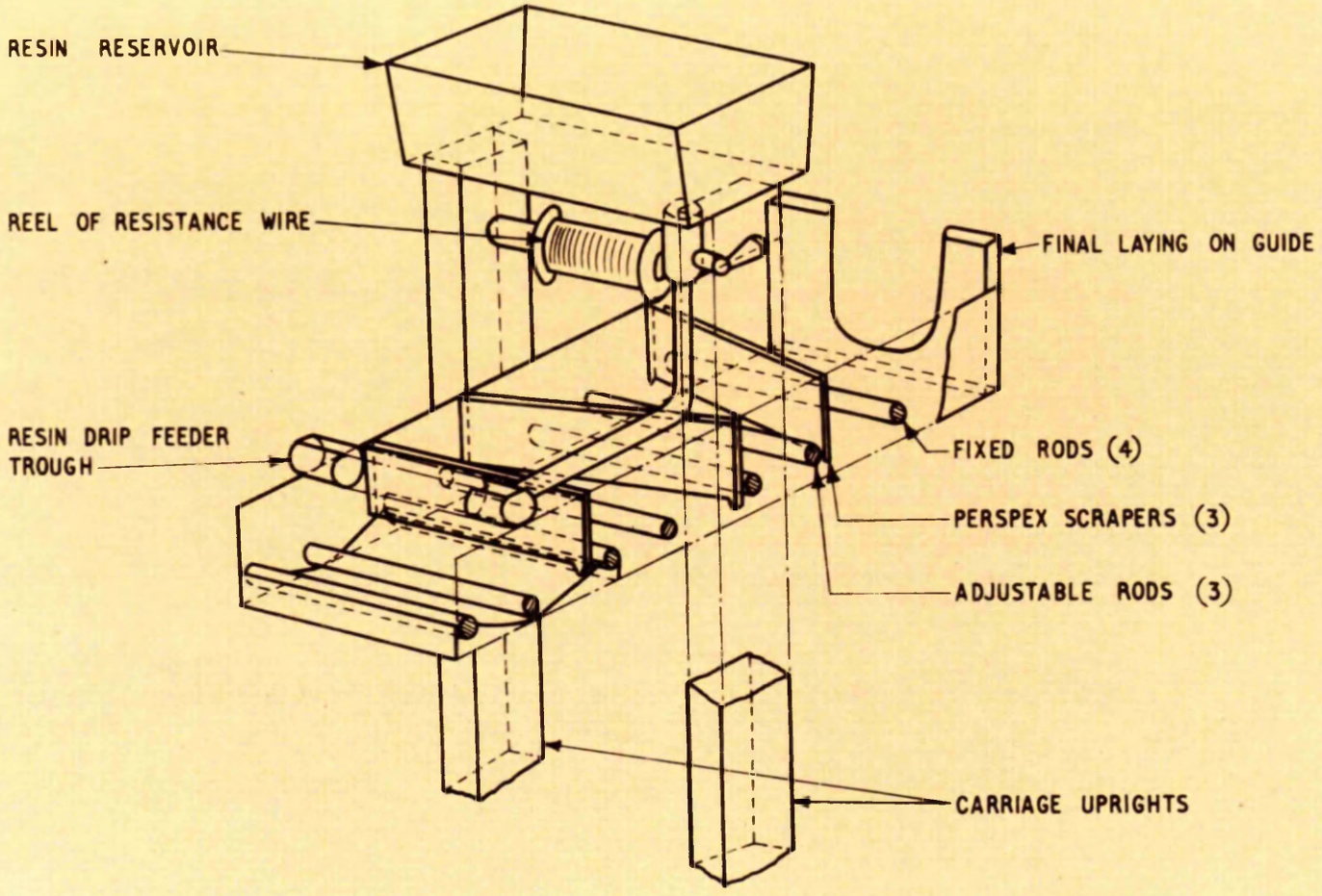

Fig. 7 PICTORIAL VIEW OF COMBINED IMPREGNATION BATH AND LAYING-ON GUIDE.

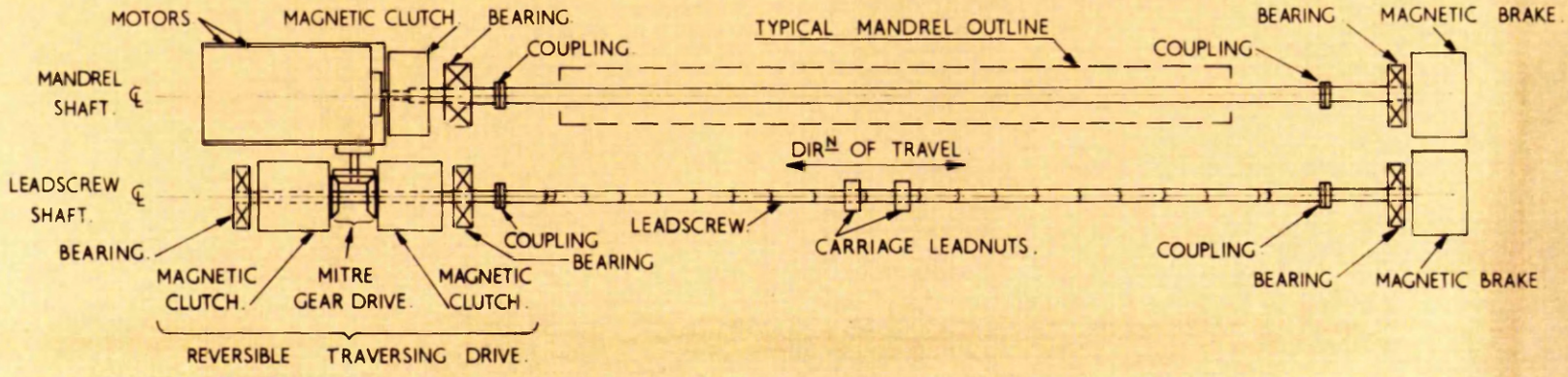

Fig. 8 LAYOUT PLAN OF MANDREL AND LEADSCREW DRIVES.

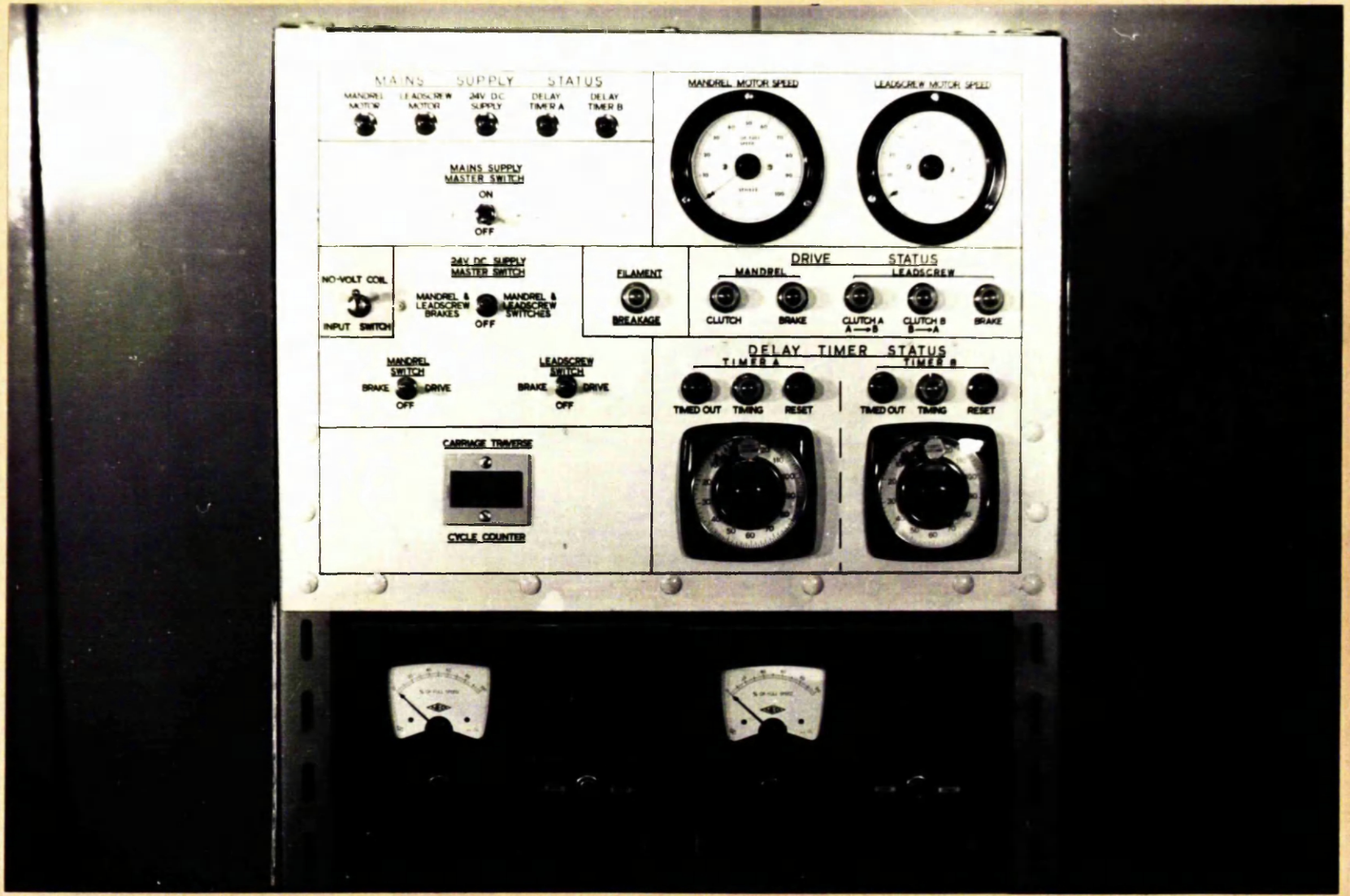

Figure 9: Close-up of Control Panel and Motor Controllers.

DRAWING NUMBER
AER/177/14

DO NOT SCALE DRAWING
IF IN DOUBT—ASK.

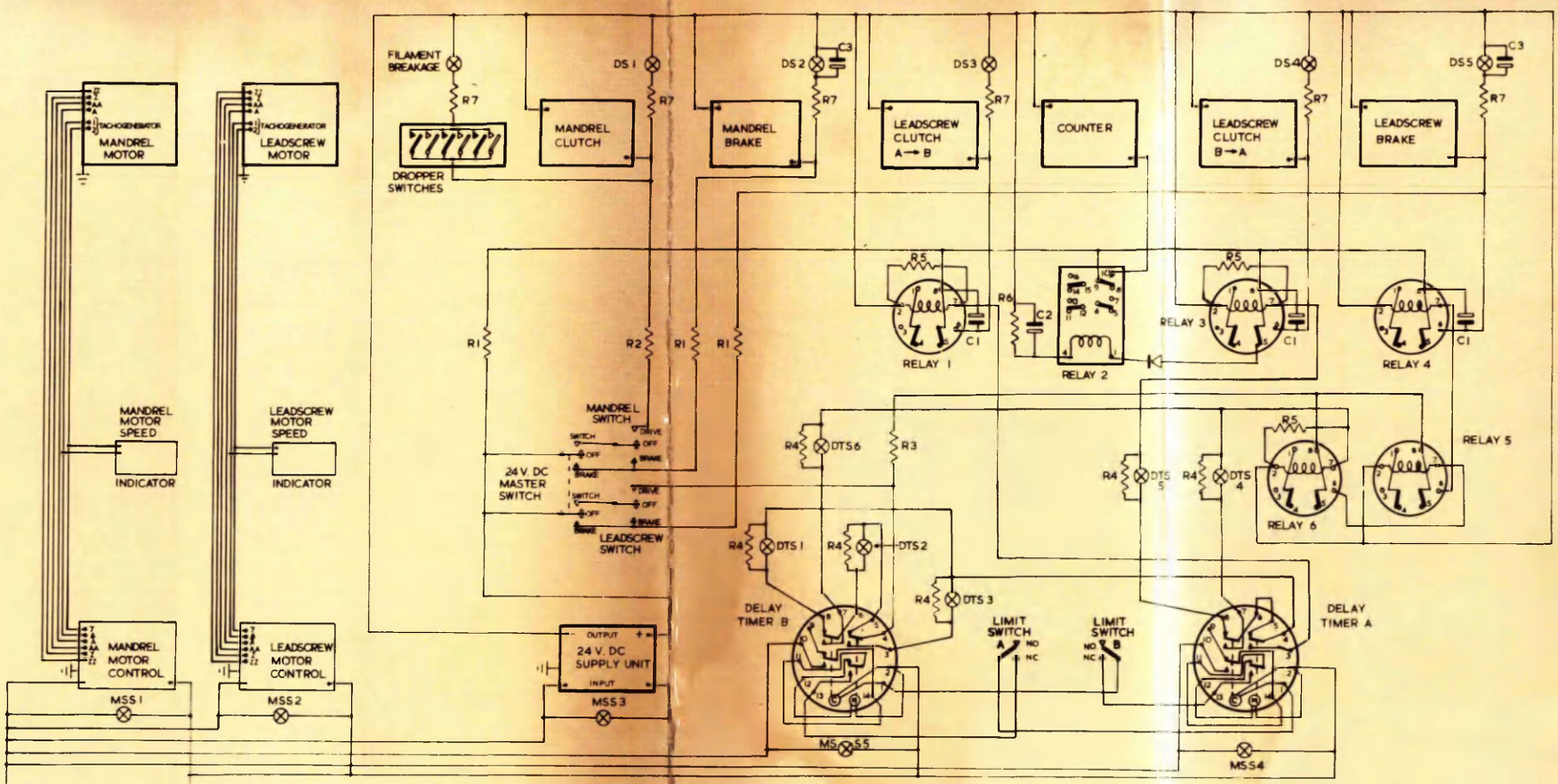

Fig. 10 Control Circuit Diagram

DIAGRAM KEY (DIAGRAM SHOULD BE READ IN CONJUNCTION WITH AER/177/11, /12)

PILOT LAMPS (12V. 0.1A)			
DELAY TIMER STATUS		DRIVE STATUS	
DTS 1	TIMER B RESET	DS 1	MANDREL CLUTCH
DTS 2	" A TIMED OUT	DS 2	" BRAKE
DTS 3	" B " "	DS 3	LEADSCREW CLUTCH A→B
DTS 4	" A TIMING	DS 4	" " B→A
DTS 5	" A RESET	DS 5	" BRAKE
DTS 6	" B TIMING		FILAMENT BREAKAGE

PANEL NEONS (250V. AC)	
MAINS SUPPLY STATUS	
MSS 1	MANDREL MOTOR
MSS 2	L/SCREW "
MSS 3	24 V. DC SUPPLY
MSS 4	DELAY TIMER A
MSS 5	DELAY TIMER B

RELAYS		
RELAY 1	L/SCREW CLUTCH A→B	12V.
RELAY 2	COUNTER	24V.
RELAY 3	L/SCREW CLUTCH B→A	12V.
RELAY 4	" BRAKE No 3	24V.
RELAY 5	" " No 2	24V.
RELAY 6	" " No 1	12V.
NO-VOLT RELAY		230V. AC

RESISTORS	
R 1	4.7Ω 10W
R 2	3.3Ω 10W
R 3	150Ω 3W
R 4	270Ω 3W
R 5	390Ω 3W
R 6	10K 0.5W
R 7	202Ω 3W

CAPACITORS	
C 1	64V. 0.64 μF
C 2	25V. 50 μF
C 3	25V. 40 μF

ITEM	No. OFF	DESCRIPTION	MATL	REMARKS

UNIVERSITY GLASGOW
ENGINEERING LABORATORIES

TITLE OF DRAWING:— ELECTRICAL CIRCUIT DIAGRAM

TITLE OF PROJECT:— TORSIONAL STRENGTH OF FILAMENT WOUND STRUCTURE

DEPARTMENT:— AERONAUTICS AND FLUID MECHANICS

PROJECT No.	AER/177
DRAWN BY	R.H. Gordon
TRACED BY	
CHECKED BY	
APPROVED BY	
DATE DRAWN	23/6/67
SCALE	—
	AER/177/14
No. OF SHEETS	1
SHEET No.	1

NOTE:- THIS DRAWING IS A PRIVATE AND CONFIDENTIAL COMMUNICATION AND THE PROPERTY OF THE UNIVERSITY OF GLASGOW IT MUST NOT BE COPIED OR LOANED WITHOUT THE WRITTEN CONSENT OF THE UNIVERSITY AND MUST BE RETURNED IMMEDIATELY ON COMPLETION OF TENDER OR CONTRACT.

A ORIGL LETTER OF ISSUE

DIMENSIONS MUST NOT BE TAKEN OFF THIS DRAWING BUT FIGURED DIMENSIONS ONLY TO BE WORKED TO FINISHED DIMENSIONS GIVEN IN ALL CASES
MACHINE SYMBOLS MARKED THUS:
MACHINE SMOOTH MACHINE
ROUGH MACHINE GROUND FINISH

ALL UNTOLERANCED DIMENSIONS IN DECIMALS TO BE WITHIN THE FOLLOWING LIMITS
HOLES AND INTERNAL SURFACES .010"
SHAFTS AND EXTERNAL SURFACES .010"
CENTRES OF HOLES AND CENTRES TO FACE .005"
FRACTIONAL DIMENSIONS 64"

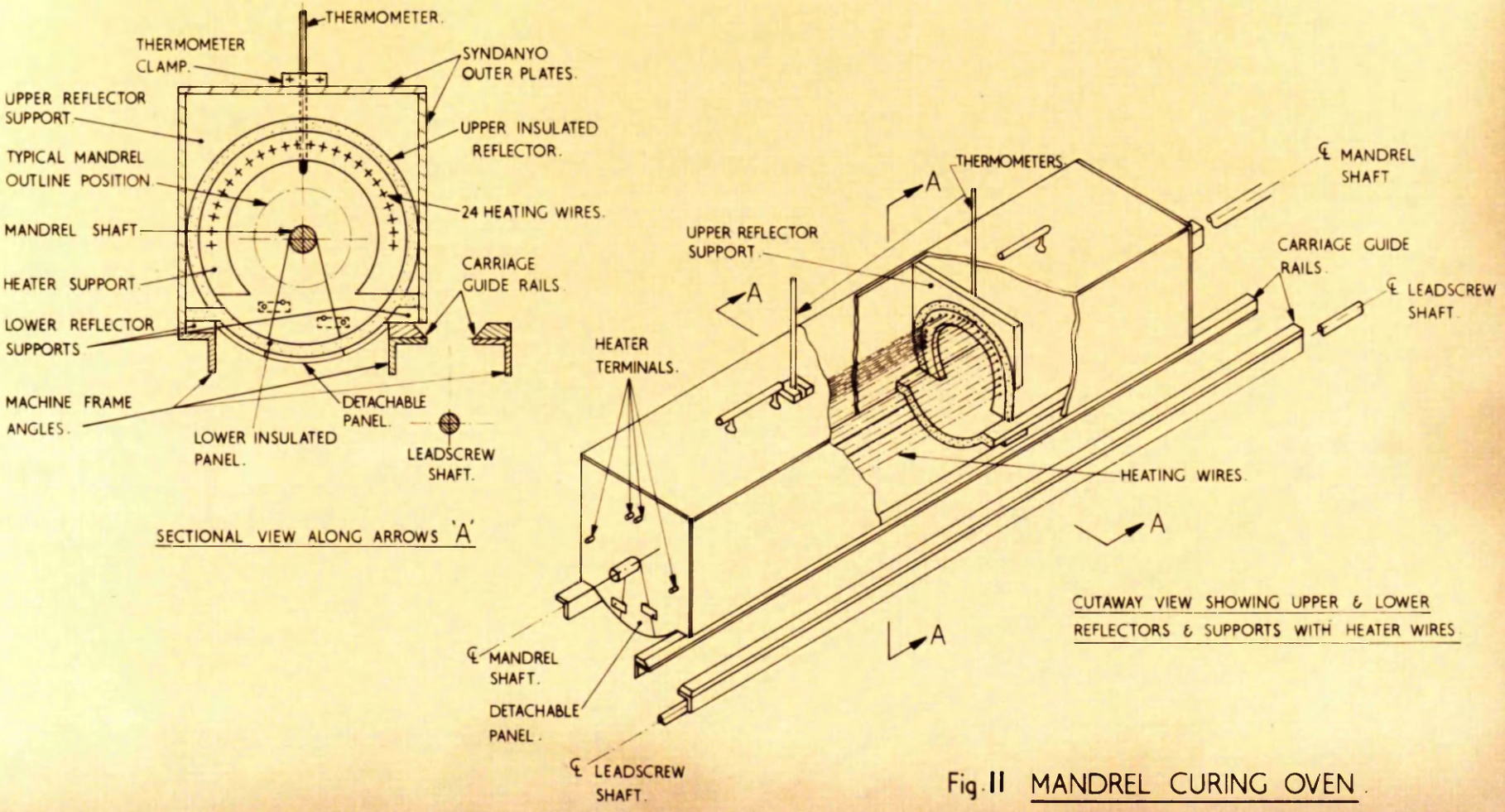

Fig. 11 MANDREL CURING OVEN.

Fig. 12

ROVING IMPREGNATION RIG.

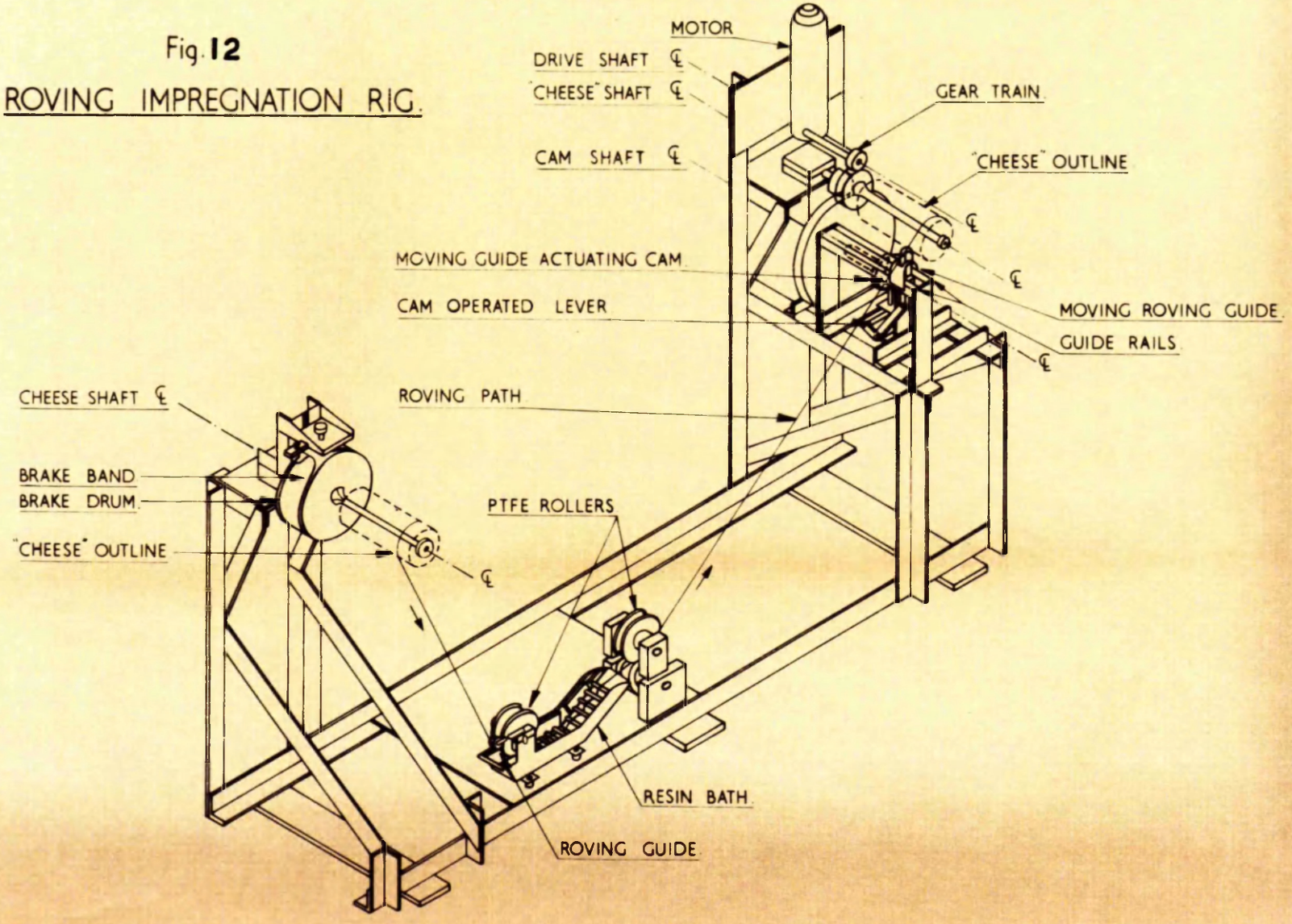

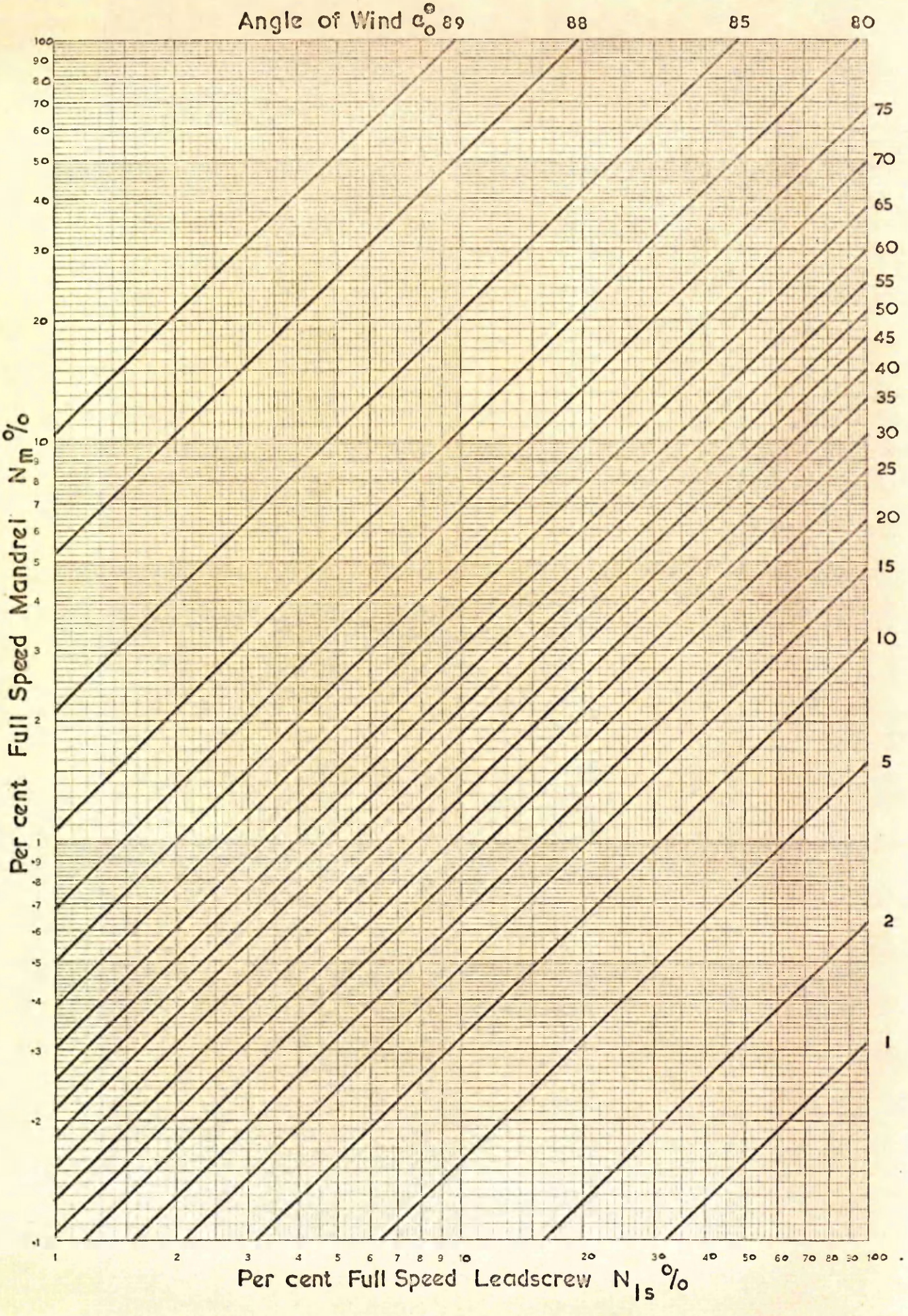

Fig 13 Motor Speed Settings for Angles of Wind a_o°

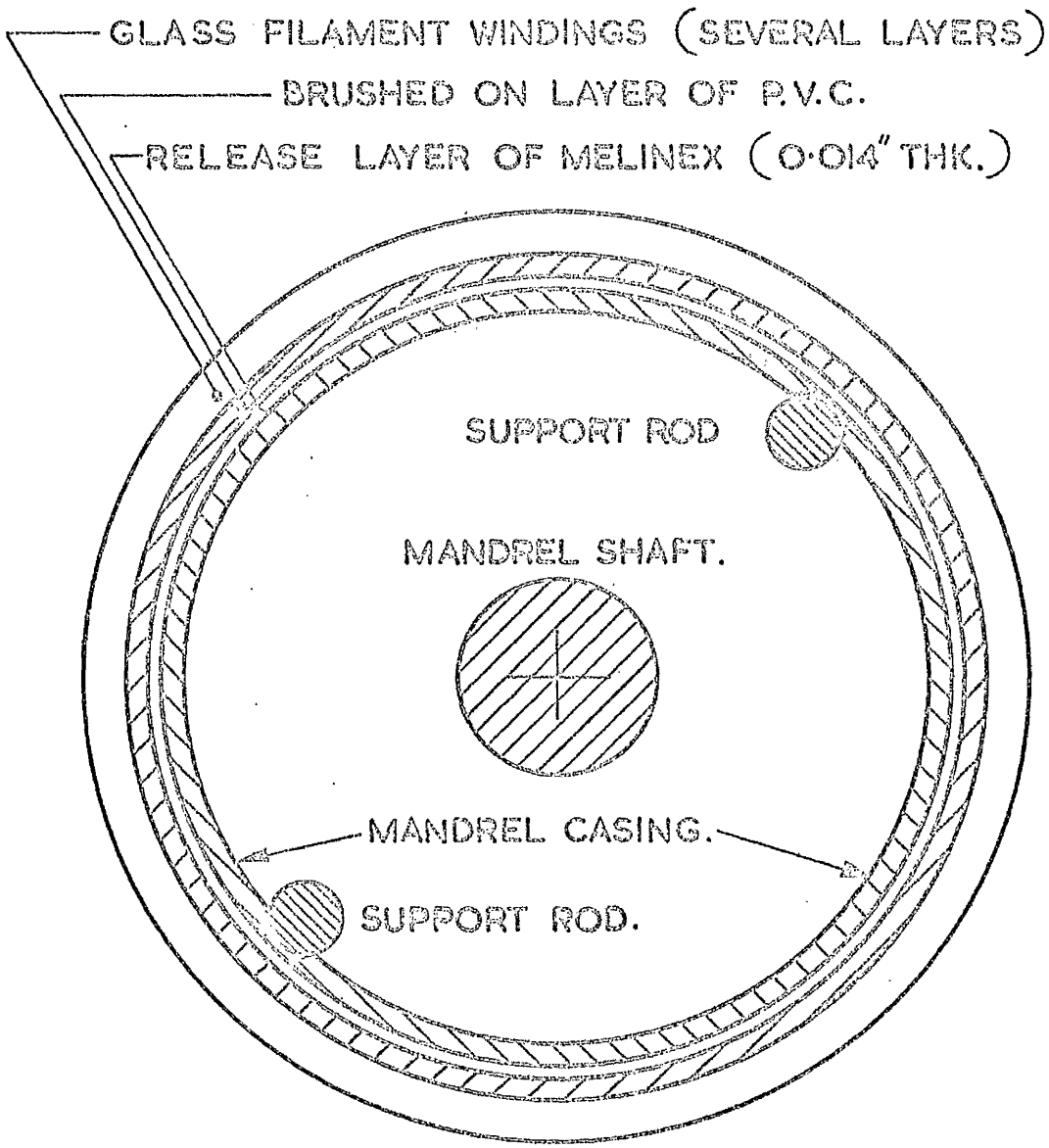

Fig.14 TYPICAL MANDREL BUILD-UP.

NOT TO SCALE.

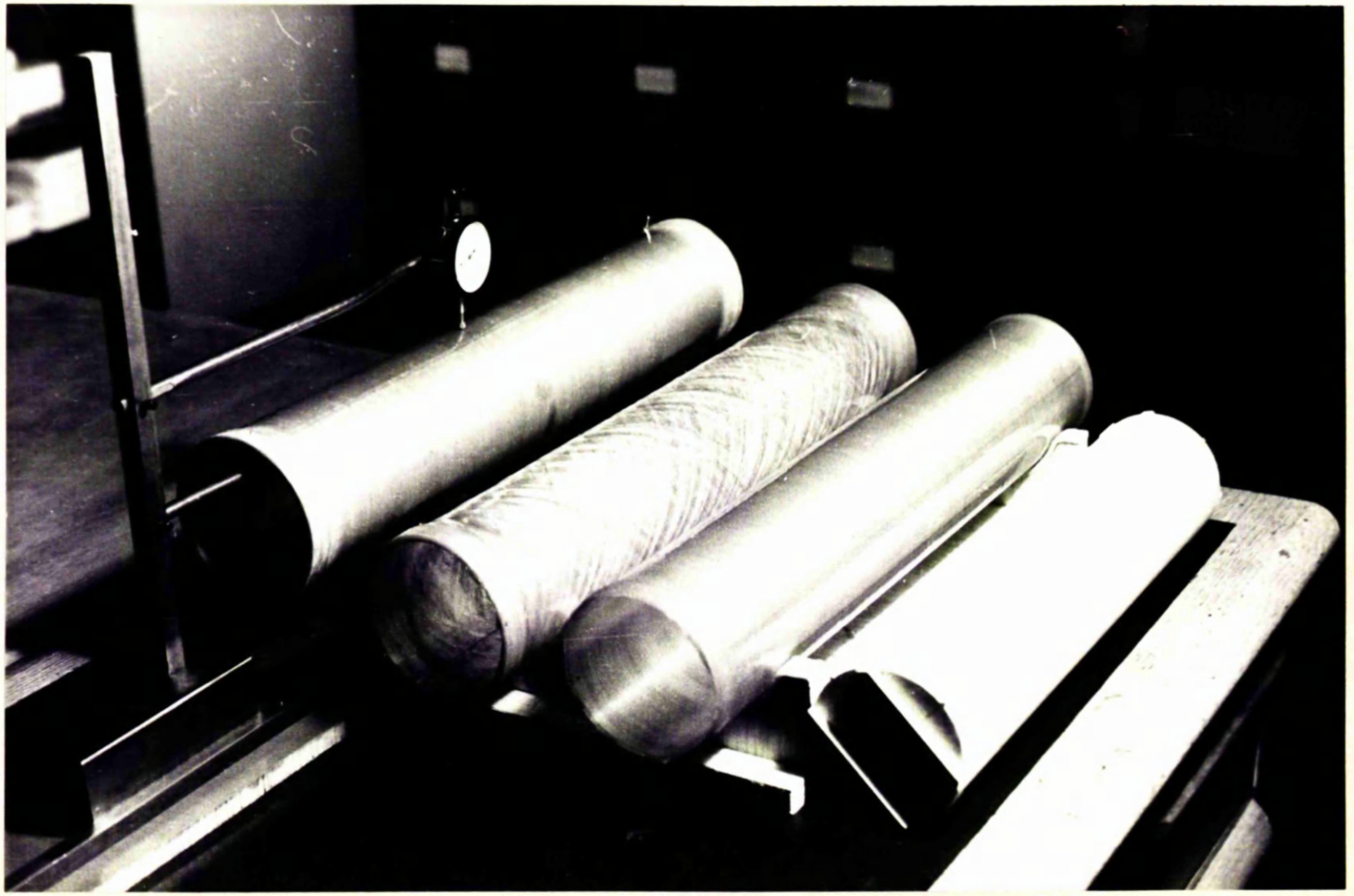

Figure 15: View of Filament-wound Tubes showing the Hardwood Insert and Wall Thickness Measuring Device.

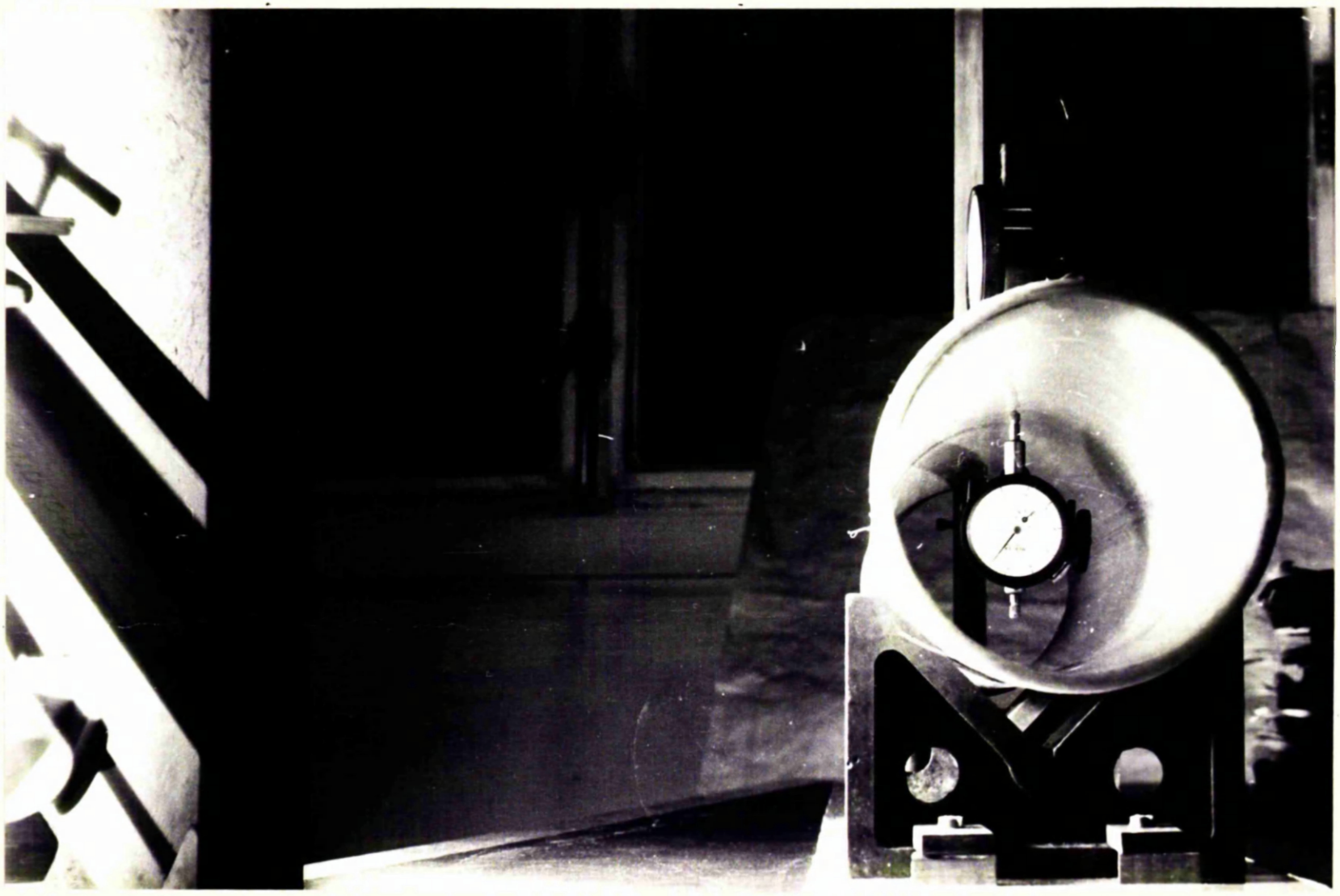

Figure 16: Close-up of Tube mounted on the Wall Thickness Measuring Device, showing the interior Dial Gauge and the High Surface Finish of the PVC Lining.

Figure 17. Distribution of values for $\frac{\Delta R}{R}$ due to a load of 0·5 gm. on 0·001" dia. advance wire.

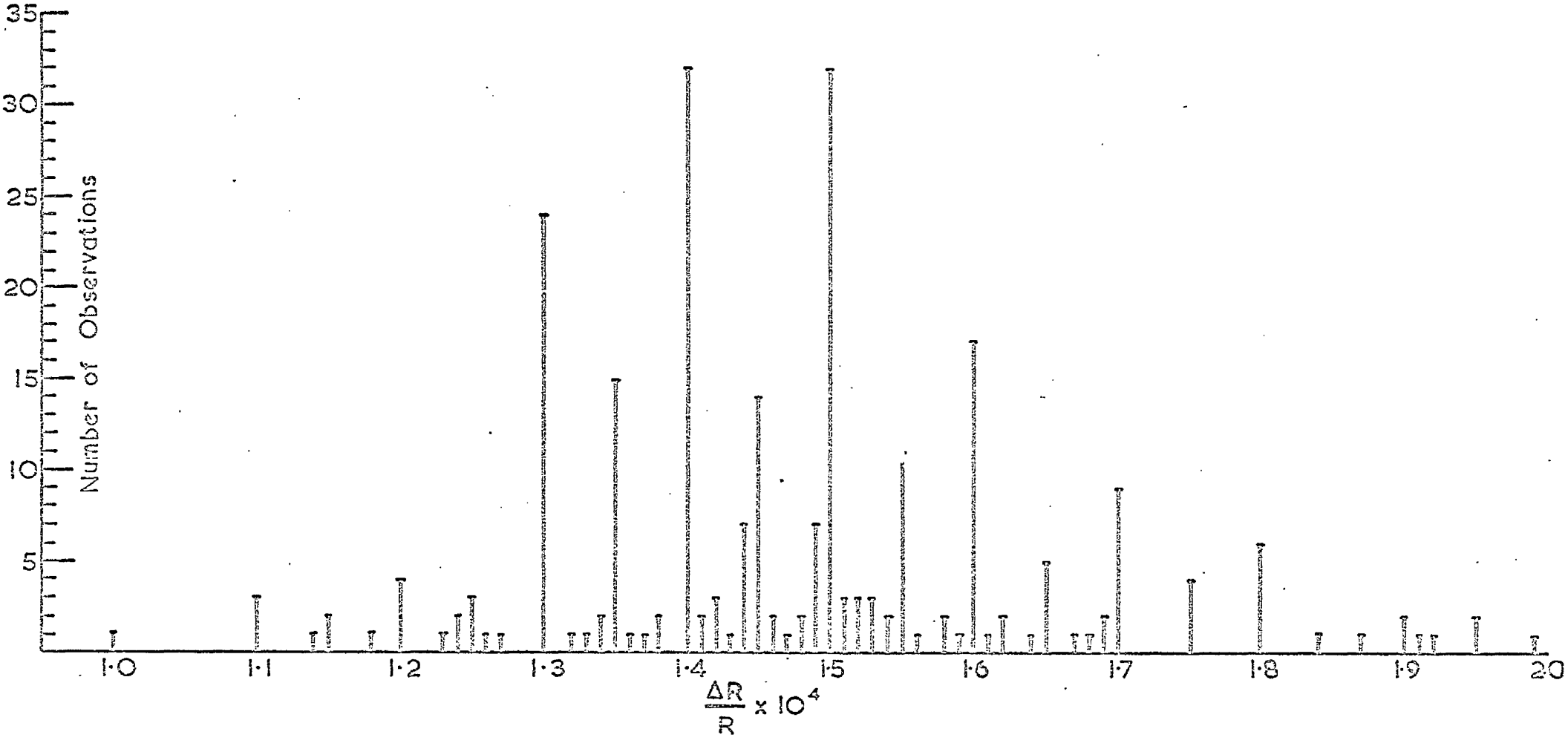

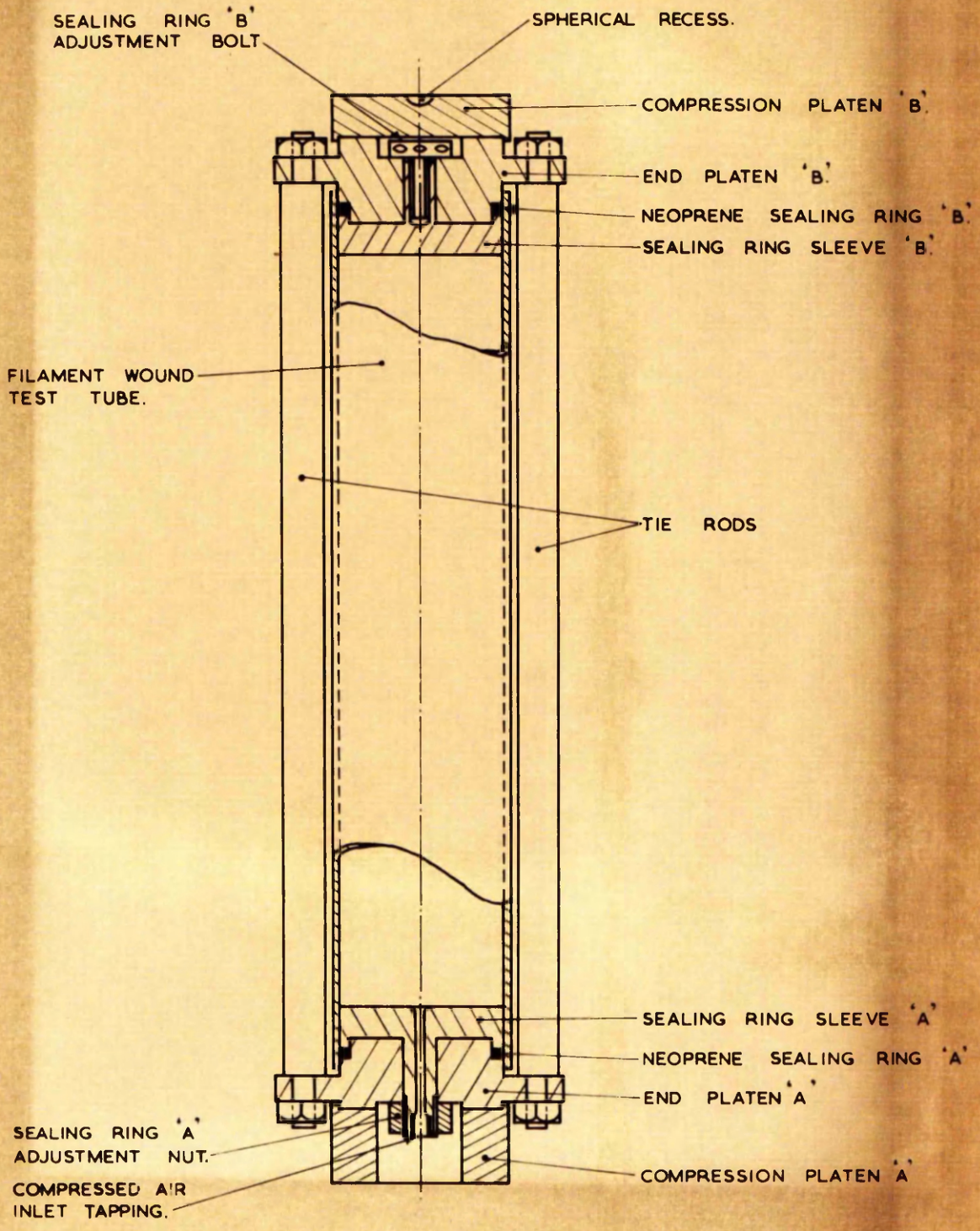

Fig.18 TEST RIG ASSEMBLY.

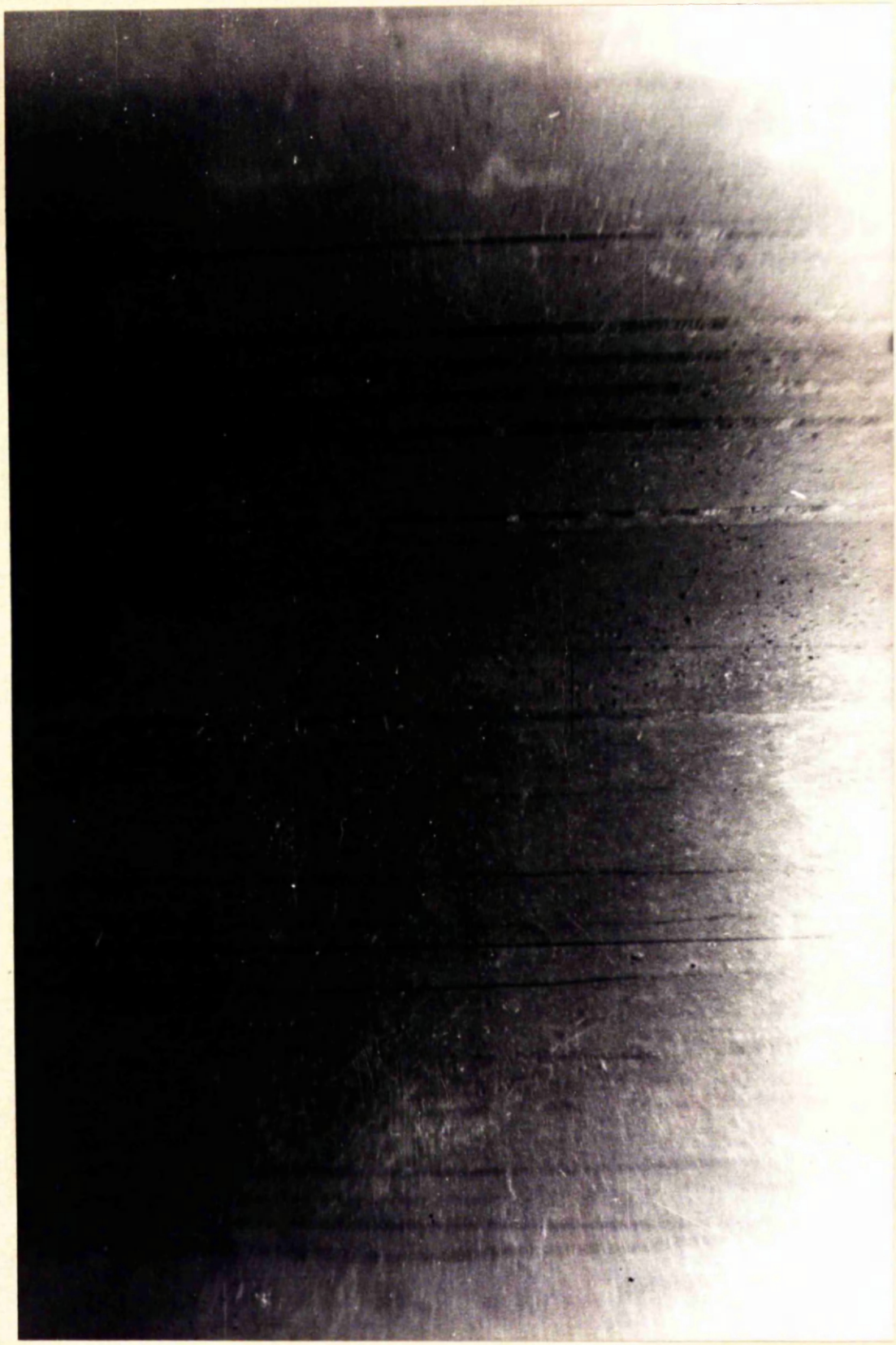

Figure 19: Close-up of 'Advance' Wires in Tube Wall in the vicinity of the surface foil strain gauge.

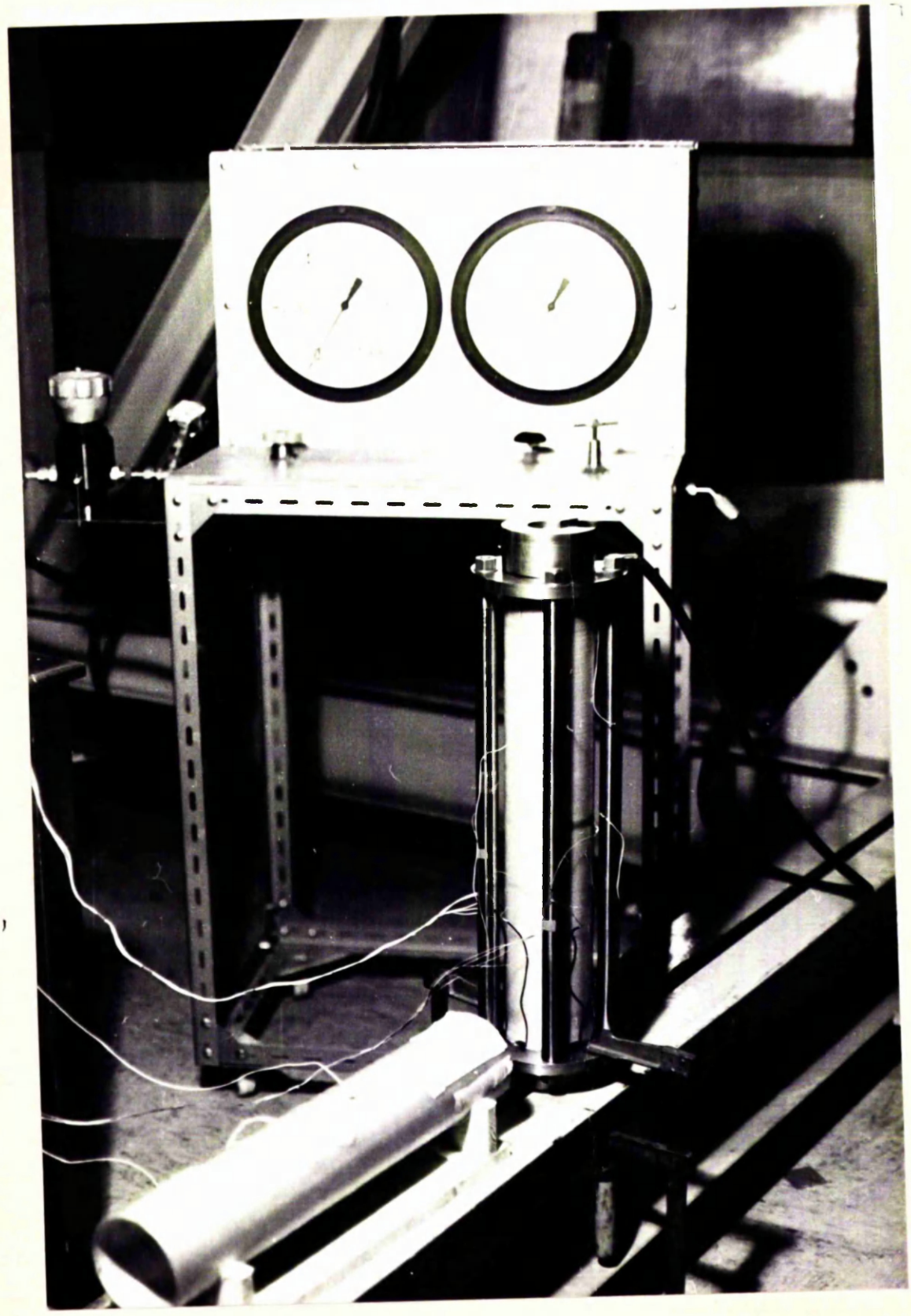

Figure 20: Tube in Test Rig with Pressure Control Unit in background.

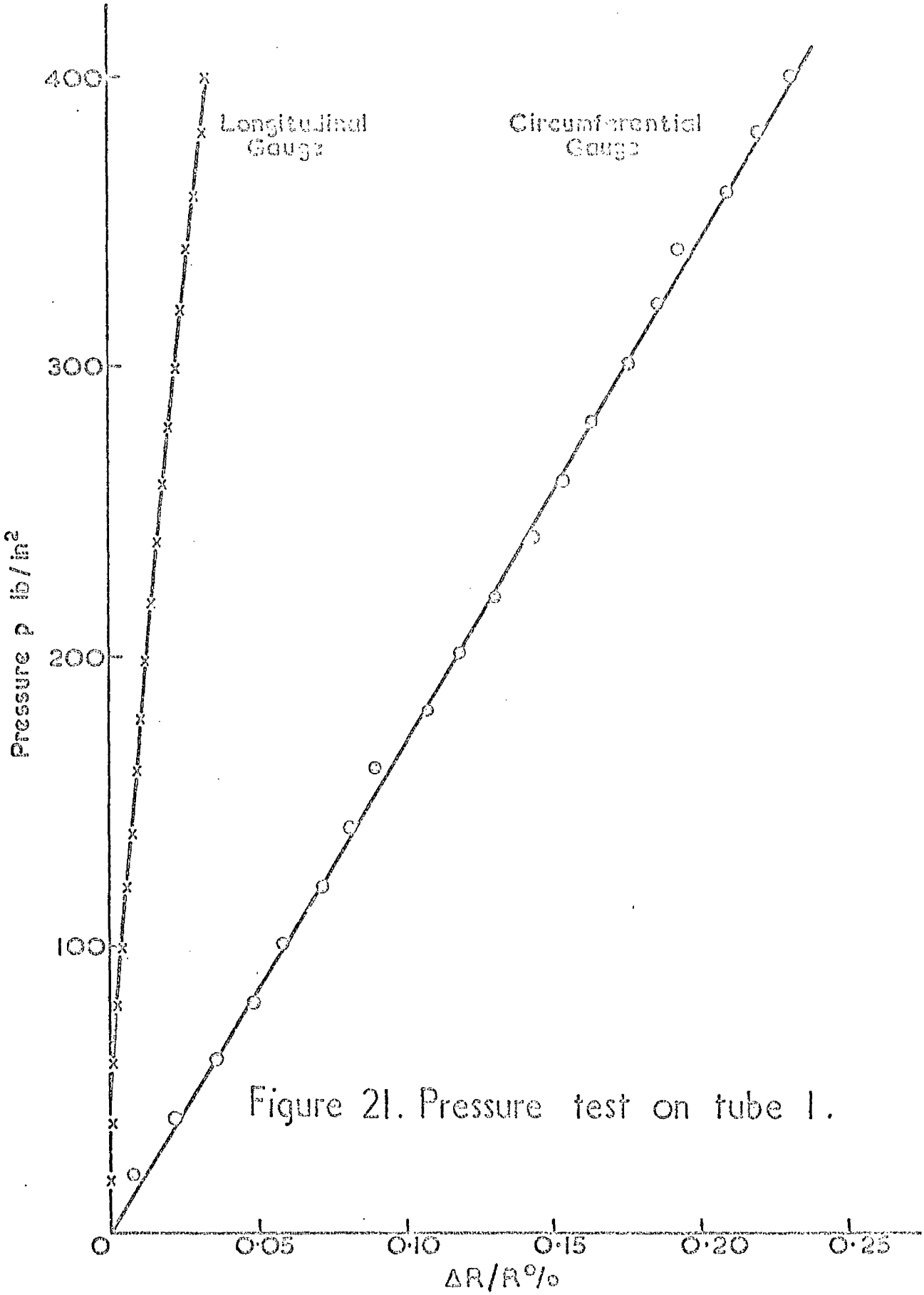

Figure 21. Pressure test on tube 1.

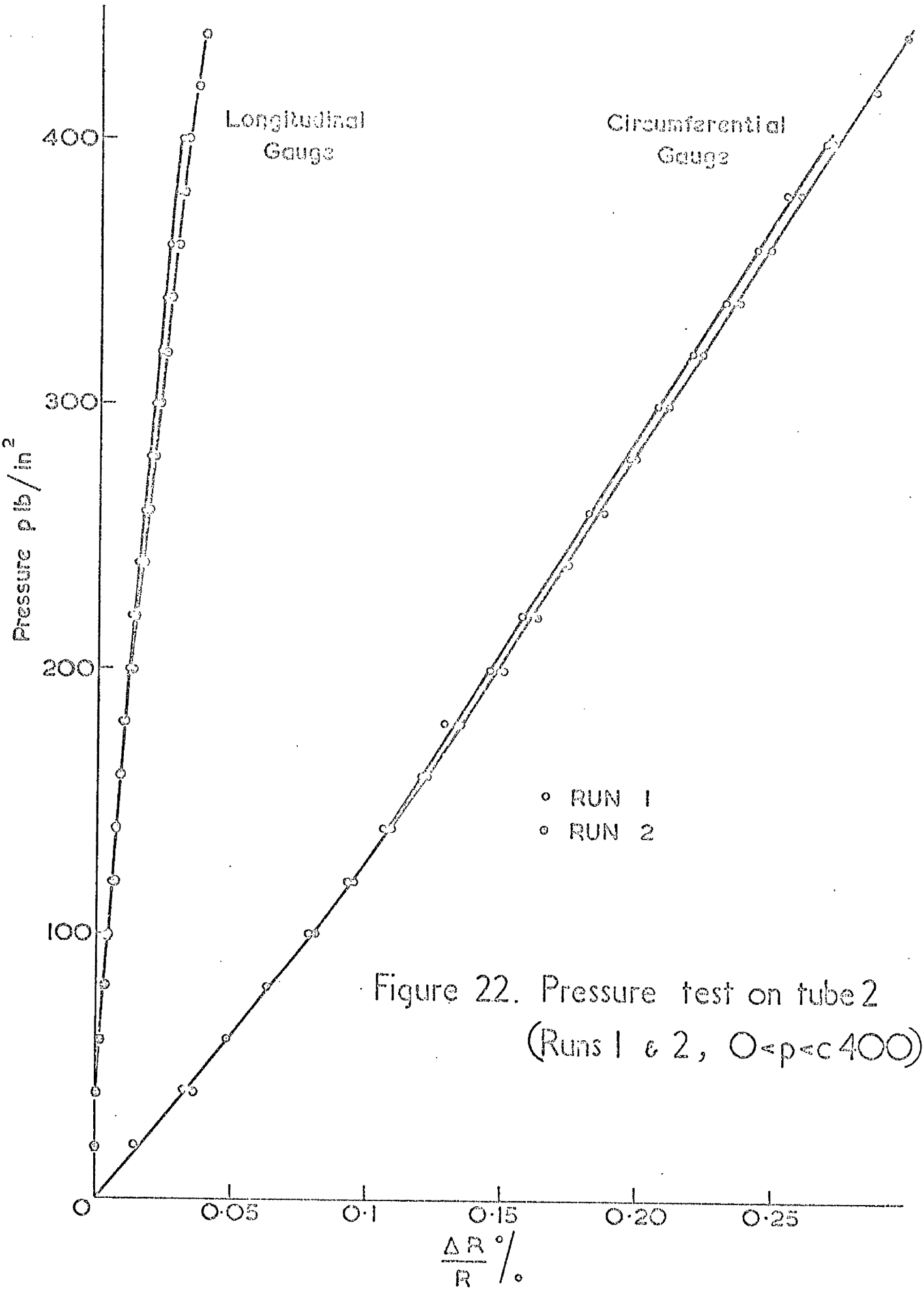

Figure 22. Pressure test on tube 2
(Runs 1 & 2, $0 < p < 400$)

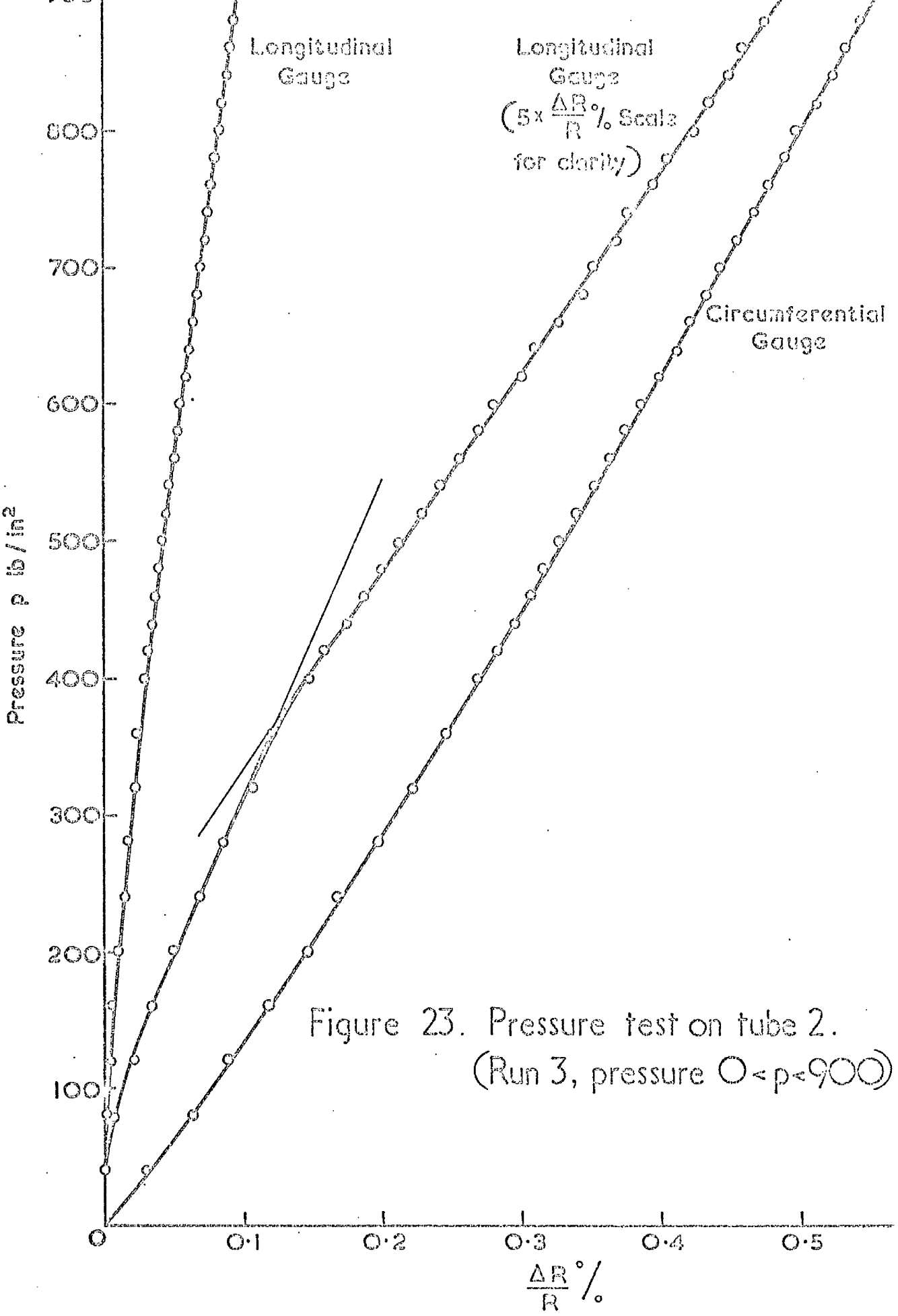

Figure 23. Pressure test on tube 2.
(Run 3, pressure $0 < p < 900$)

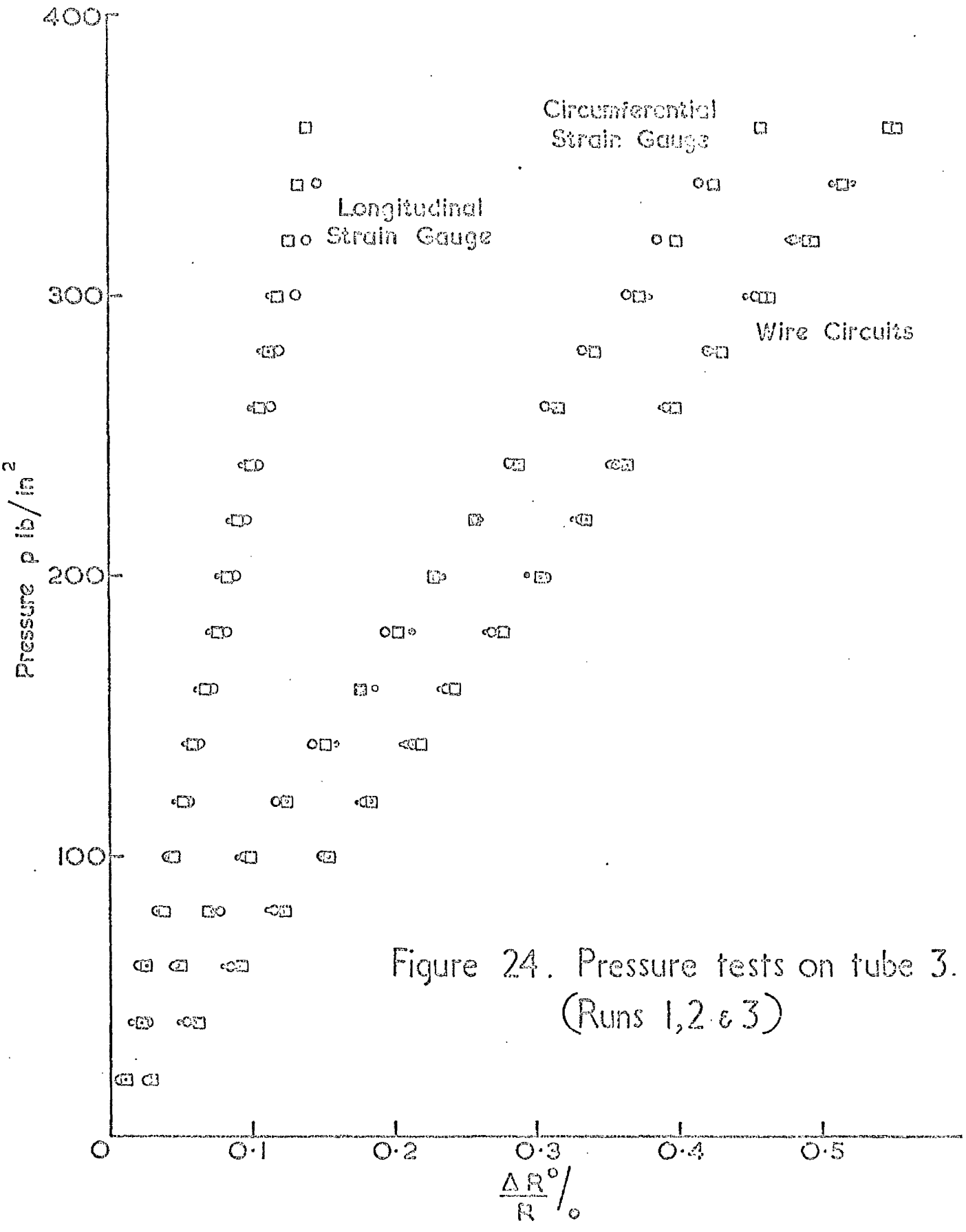

Figure 24. Pressure tests on tube 3. (Runs 1, 2 & 3)

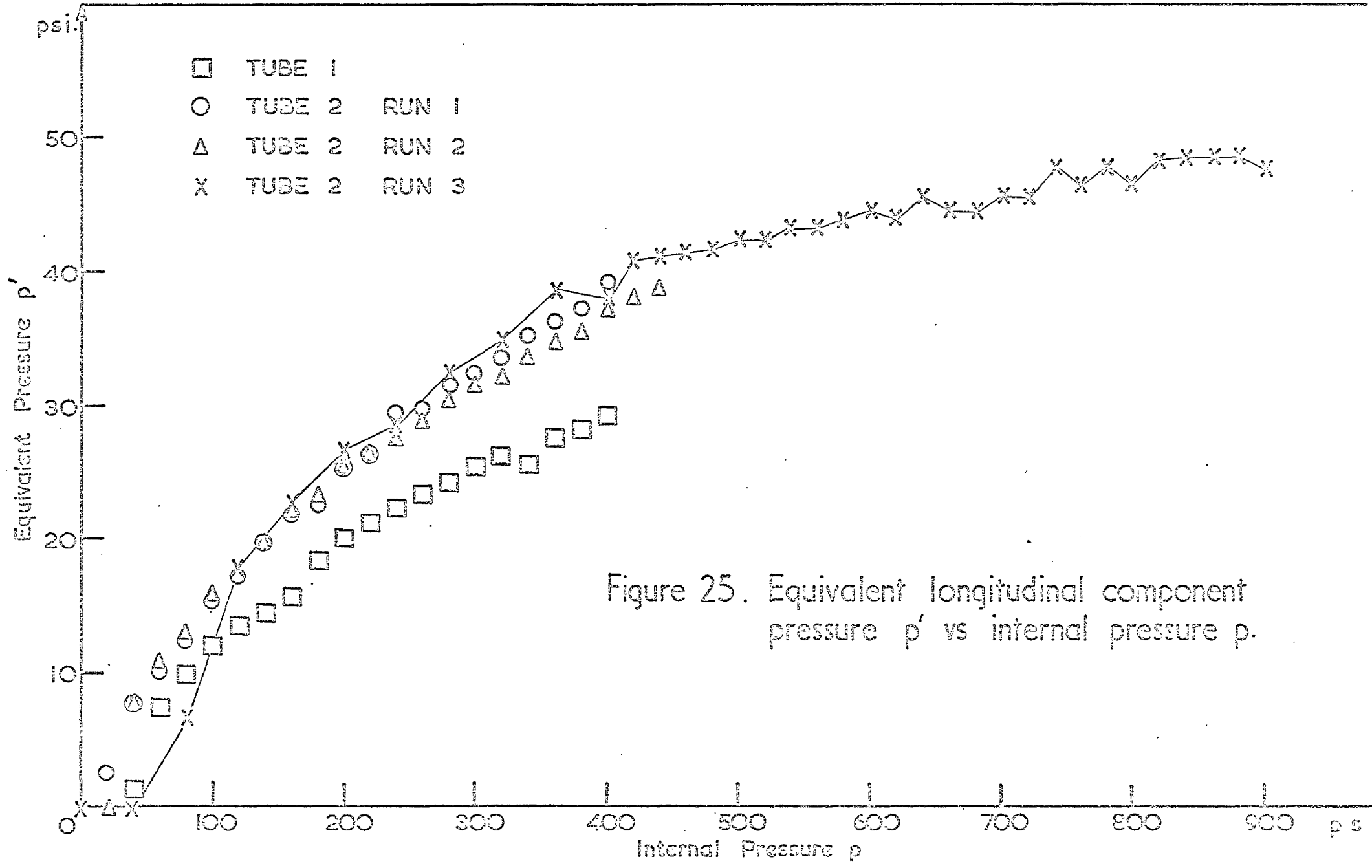

Figure 25. Equivalent longitudinal component pressure p' vs internal pressure p.

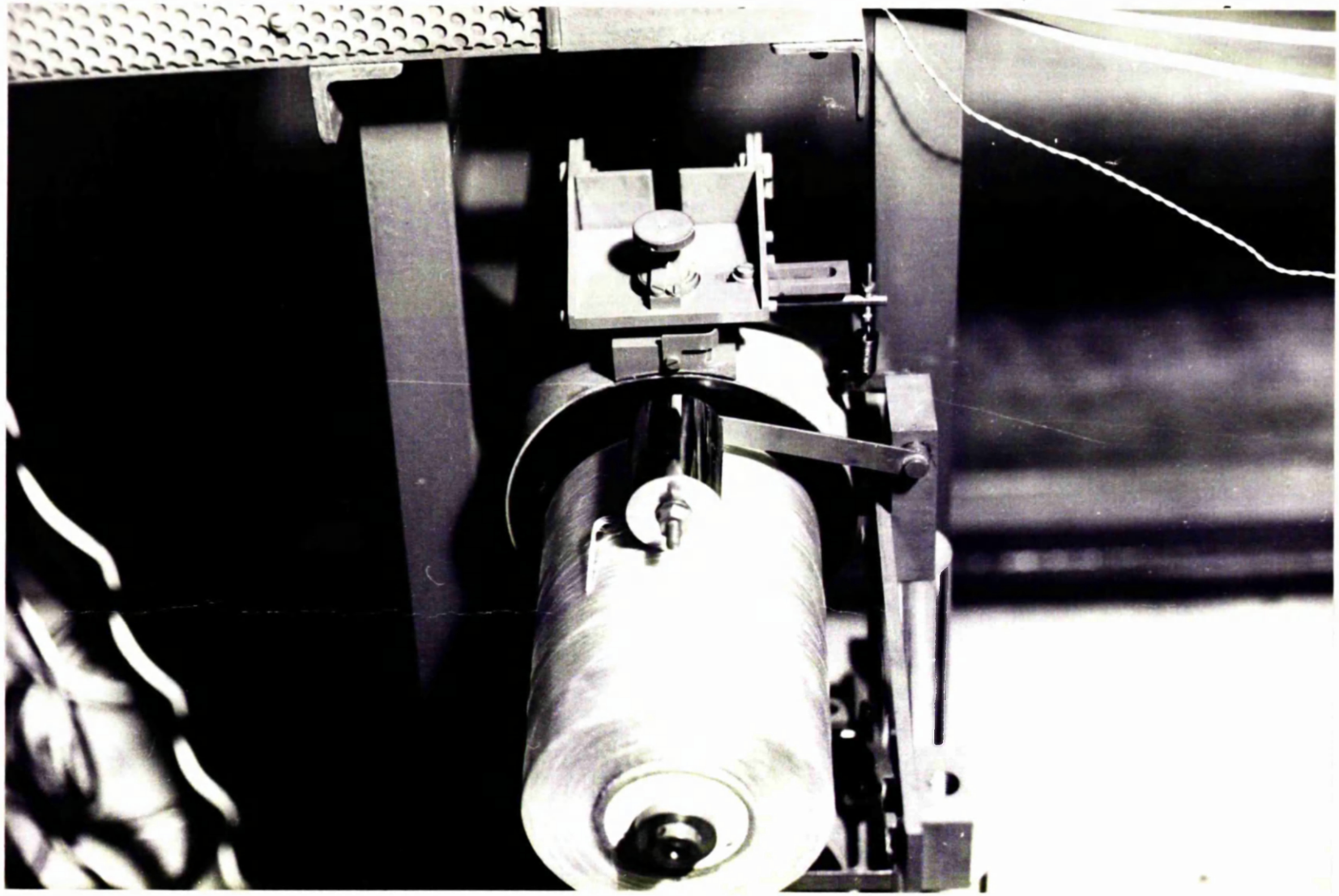

Figure 26: Close-up of Cheese Brake Assembly.

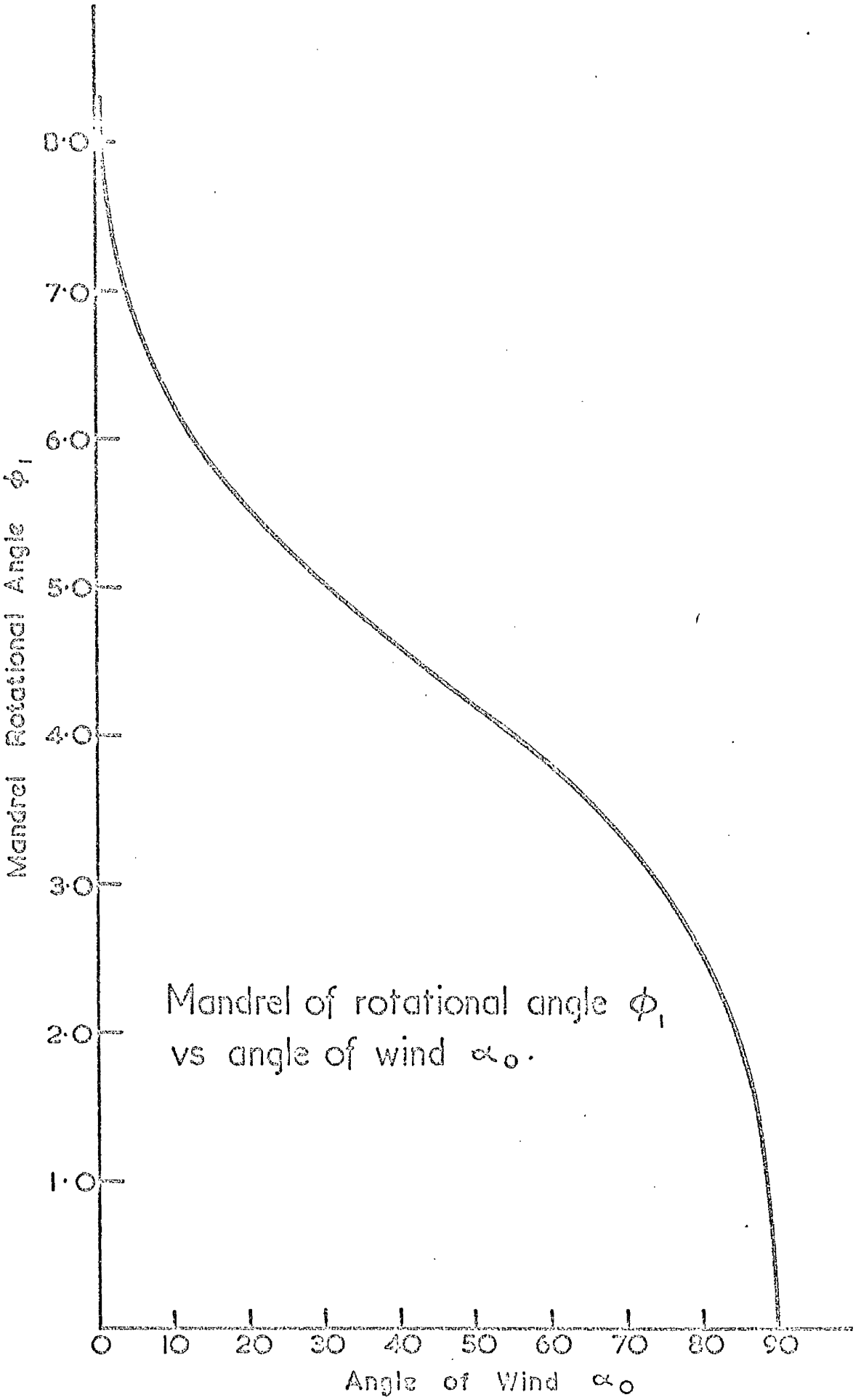
Mandrel Rotational Angle ϕ_1
8·0
7·0
6·0
5·0
4·0
3·0
2·0
1·0
0
10
20
30
40
50
60
70
80
90
Angle of Wind α_0
Mandrel of rotational angle ϕ_1
vs angle of wind α_0.

Figure 27.

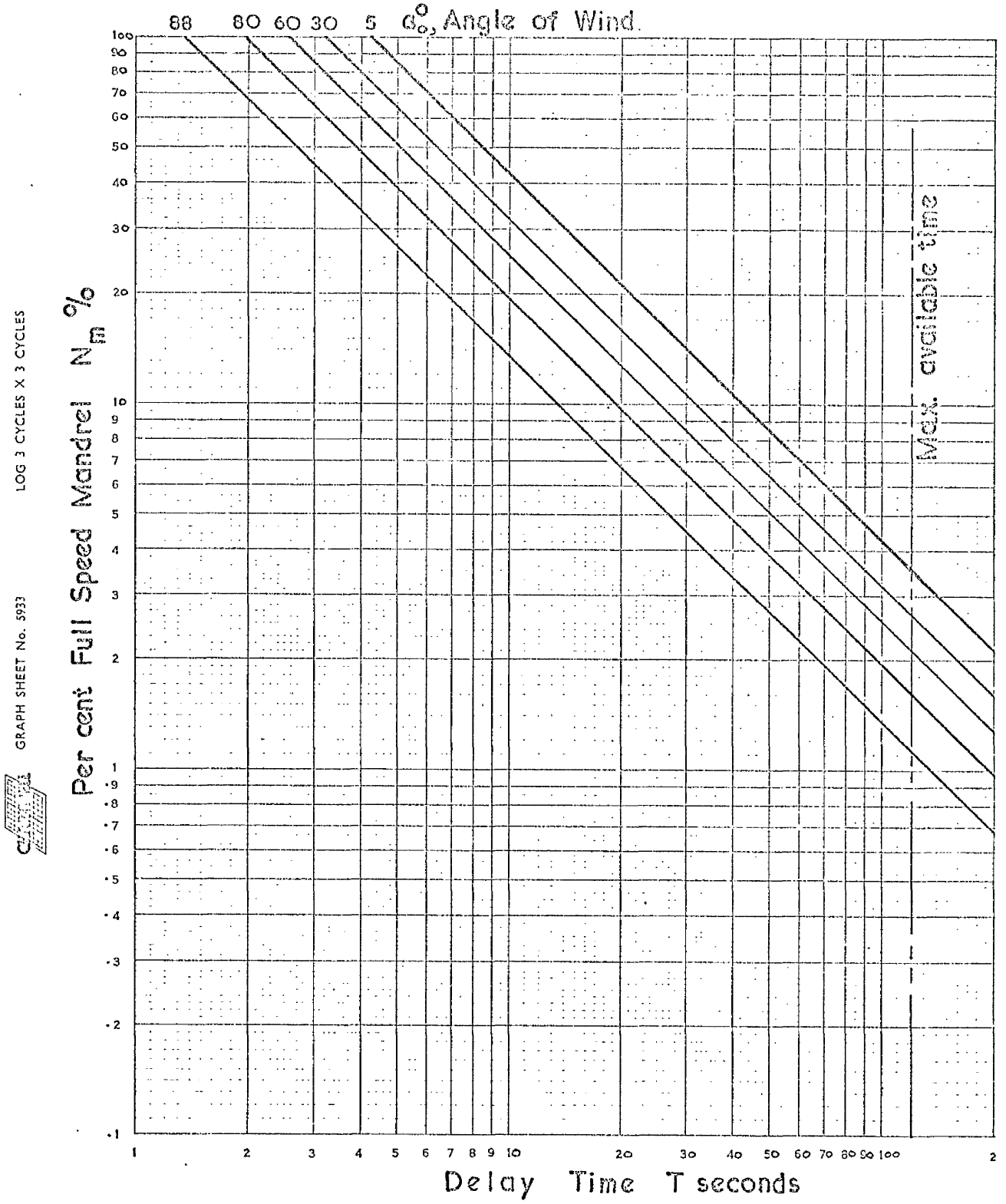

Fig. 28 a. Time Delay at end of carriage traverse vs. Mandrel Motor Speed for Angle of Wind a_o (1/4 Rev. Locking Turn)

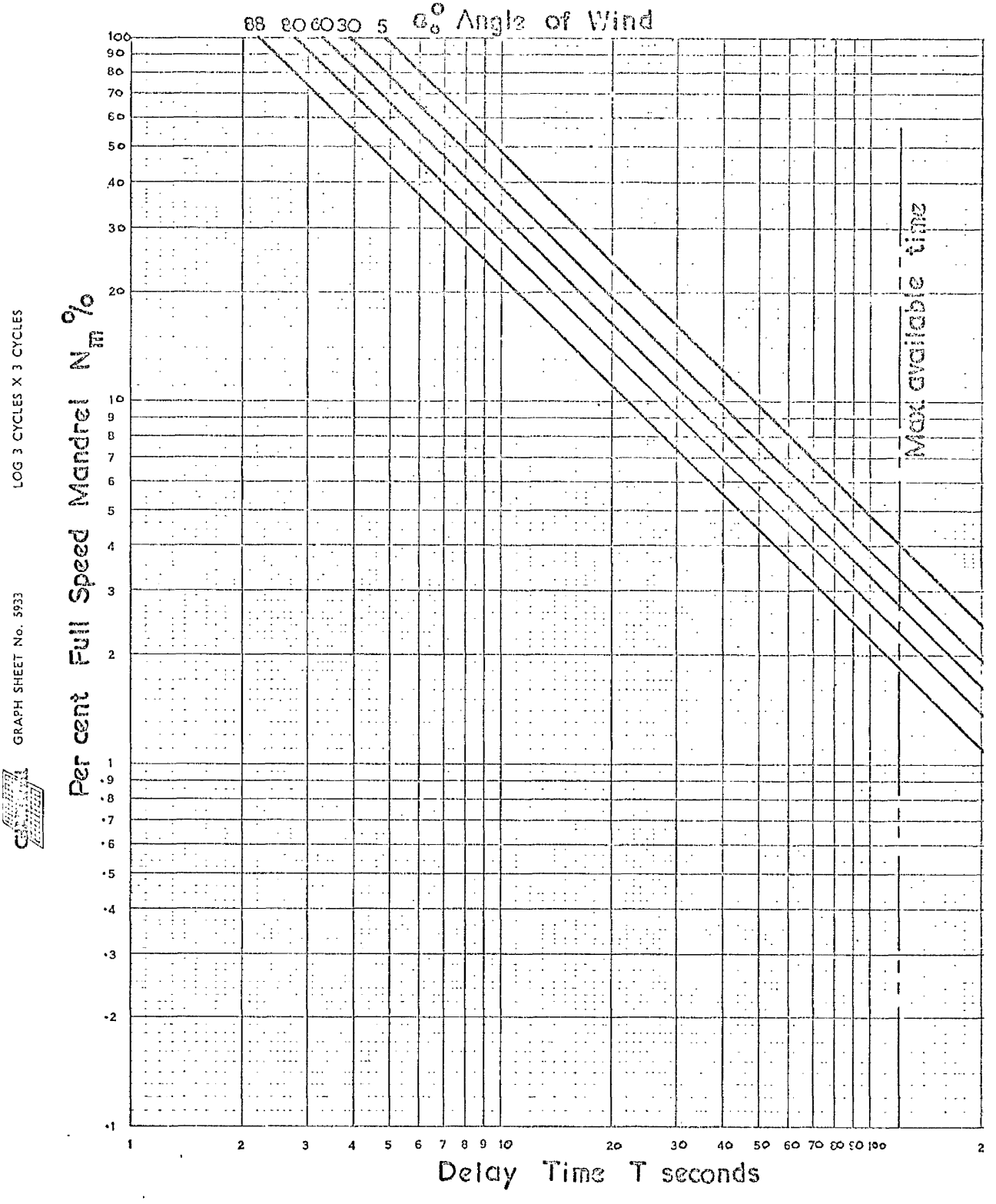

Fig. 28 b. Time Delay at end of carriage traverse vs. Mandrel Motor Speed for Angle of Wind α_o (½ Rev. Locking Turn)